Material-Mediated Tissue Induction; Geometrical, Surgical & Material Parameters

Sabah Oghazian

Faculty of Dental Medicine and Oral Health Sciences

Division of Biomaterials and Bone Tissue Engineering

Supervisor: Dr. Jake E Barralet

McGill University

Montreal, Quebec, Canada

A thesis submitted to McGill University in partial fulfillment of the requirement of the degree of M.Sc. in Dental Sciences

Table of Contents

Abstract

INTRODUCTION: Marrow transplantation or even extramedullary marrow formation is known to often result in new bone formation. Extramedullary marrow may form as a result of haematological diseases. However, it has also been reported to occur following injury such as surgery or other trauma. The implantation of biomaterials often results in a sterile inflammation and extramedullary hematopoietic tissue is occasionally reported as an incidental finding. The simplest system reported to pre-clinically induce extramedullary marrow and ectopic bone was an open-ended glass tube. This study recreates this early report for the first time and determines if the tissue induced by this bioinert material had any regenerative potential. **METHODS:** We conducted this pre-clinical study by placing glass and silicone open-ended tubes subcutaneously and subperiosteally in the cranial region. We maintained periosteum either over or under the implants in all experimental groups except one. In this group, the periosteal flap was removed to allow direct contact between the tube, skin and bone. Moreover, to assess the effect of decortication, several mono-cortical holes were created in the calvarial bone in one of the groups. Tubes were either 3 mm or 6 mm in height and 9 mm in diameter. To assess the efficacy of this method in healing bony defects, we also placed the tubes over 6mm-diameter skull defects. Five weeks postoperatively further analyses including gross examination, micro-CT analysis, and histological evaluation were conducted. **RESULTS**: Macroscopic examination of the specimens revealed a central cord connecting the skin to the basal connective tissue over the skull. This cord appeared thinner in the silicone tube group compared to the shorter and thicker cords observed in the other groups. Micro-CT evaluation indicated osseous features were present in all glass tubes but not in silicone tubes placed under skin. Among the groups without bony defects, the

highest amount of bone formation was found in shorter glass tubes which were placed under periosteum, followed by subperiosteal 6 mm-height glass implants. Surprisingly removal of periosteum and decortication was not correlated with a significant difference in the amount of bone formed within the tubes. Although the highest defect closure was observed in the 6mm high glass tubes, the difference compared to the control group was not statistically significant (ANOVA, $p < 0.05$; Tukey's post hoc test). Histological examination confirmed vascularization in all samples' central tissue cords. In subcutaneous silicone group, basal tissues comprised adipose tissue and a distribution of fibroblasts and inflammatory cells, with no evidence of bone formation. Subcutaneous glass tubes shared the same pattern of tissue formation with additional islands of intramembranous bone formation. Ectopic lamellae of bone were found encircling the central cord in short glass tubes, whereas the cord showed no peripheral bone in other groups. The newly formed bone connected to the skull showed evidence of hematopoietic tissue. Thirteen out of fifteen samples placed over the defect, showed an additional osseous structure on top extending to the basal plate. **CONCLUSIONS:** Our study suggests that physical stimuli alone, not related to the physicochemical properties of the biomaterial could induce bone formation. This is highly important since it suggests that some tissue regeneration observed in biomaterials can be attributed in part to the foreign body reaction. Deliberate manipulation of this phenomenon would appear a new and underappreciated route to materials mediated tissue regeneration.

Résumé

INTRODUCTION: La transplantation de moelle osseuse ou même la formation de moelle extramédullaire est souvent connue pour entraîner une nouvelle formation osseuse. La moelle extramédullaire peut se former à la suite de maladies hématologiques. Cependant, il a également été rapporté qu'elle peut survenir après une blessure telle qu'une chirurgie ou un autre traumatisme. L'implantation de biomatériaux entraîne souvent une inflammation stérile et du tissu hématopoïétique extramédullaire est occasionnellement signalé comme une découverte fortuite. Le système le plus simple rapporté pour induire pré-cliniquement de la moelle extramédullaire et de l'os ectopique était un tube en verre à extrémité ouverte. Cette étude recrée ce rapport précoce pour la première fois et détermine si le tissu induit par ce matériau bioinert avait un potentiel régénératif. **METHODES:** Nous avons mené cette étude pré-clinique en plaçant des tubes ouverts en verre et en silicone sous-cutanément et sous-périostément dans la région crânienne. Nous avons maintenu le périoste soit au-dessus, soit en dessous des implants dans tous les groupes expérimentaux sauf un. Dans ce groupe, le lambeau périosté a été enlevé pour permettre un contact direct entre le tube, la peau et l'os. De plus, pour évaluer l'effet de la décortication, plusieurs trous monocorticaux ont été créés dans l'os calvarial dans l'un des groupes. Les tubes avaient soit 3 mm, soit 6 mm de hauteur et 9 mm de diamètre. Pour évaluer l'efficacité de cette méthode dans la guérison des défauts osseux, nous avons également placé les tubes sur des défauts du crâne de 6 mm de diamètre. Cinq semaines après l'opération, des analyses supplémentaires, y compris un examen macroscopique, une analyse par micro-CT et une évaluation histologique, ont été menées. **RESULTATS:** L'examen macroscopique des spécimens a

révélé un cordon central reliant la peau au tissu conjonctif basal sur le crâne. Ce cordon apparaissait plus fin dans le groupe des tubes en silicone par rapport aux cordons plus courts et plus épais observés dans les autres groupes. L'évaluation par micro-CT a indiqué que des caractéristiques osseuses étaient présentes dans tous les tubes en verre mais pas dans les tubes en silicone placés sous la peau. Parmi les groupes sans défauts osseux, la plus grande quantité de formation osseuse a été trouvée dans les tubes en verre plus courts placés sous le périoste, suivis des implants sous-périostés en verre de 6 mm de hauteur. De manière surprenante, l'ablation du périoste et la décortication n'étaient pas corrélées à une différence significative dans la quantité d'os formé à l'intérieur des tubes. Bien que la plus grande fermeture des défauts ait été observée dans les tubes en verre de 6 mm de hauteur, la différence par rapport au groupe témoin n'était pas statistiquement significative (ANOVA, $p < 0,05$; test post hoc de Tukey). L'examen histologique a confirmé la vascularisation dans les cordons tissulaires centraux de tous les échantillons. Dans le groupe des tubes en silicone sous-cutanés, les tissus basaux comprenaient du tissu adipeux et une distribution de fibroblastes et de cellules inflammatoires, sans preuve de formation osseuse. Les tubes en verre sous-cutanés partageaient le même modèle de formation tissulaire avec des îlots supplémentaires de formation osseuse intramembraneuse. Des lamelles osseuses ectopiques ont été trouvées entourant le cordon central dans les tubes en verre courts, tandis que le cordon ne montrait aucun os périphérique dans les autres groupes. L'os nouvellement formé relié au crâne montrait des signes de tissu hématopoïétique. Treize des quinze échantillons placés sur le défaut montraient une structure osseuse supplémentaire sur le dessus s'étendant jusqu'à la plaque basale. **CONCLUSIONS:** Notre étude suggère que des stimuli physiques seuls, non liés aux propriétés physico-chimiques du biomatériau, pourraient induire la formation

osseuse. Cela est très important car cela suggère qu'une partie de la régénération tissulaire observée dans les biomatériaux peut être en partie attribuée à la réaction aux corps étrangers. La manipulation délibérée de ce phénomène apparaîtrait comme une nouvelle voie sous-estimée pour la régénération tissulaire médiée par les matériaux.

Acknowledgments

Firstly, heartfelt gratitude is extended to Prof. Jake Barralet, whose unwavering guidance and support have been the cornerstone of this research journey.

Deep thanks are due to Dr. Makhoul, Dr. Harvey, and Dr. Tran. As the Research Advisory Committee Members and Chair, their sharp insights and invaluable suggestions have significantly enhanced this project.

Special acknowledgment is given to Yu Ling Zhang, the Lab Manager, for her invaluable assistance and patience with training paperwork and lab experiments.

Appreciation is also extended to the colleagues in the laboratory—Samar, Parsa, Julianna, Kelly, Ayden, and many others—for their support.

Lastly, deepest gratitude goes to Mohammad, the love of my life, whose emotional support and infinite patience have been an anchor throughout this journey. Heartfelt thanks are also extended to my parents and beloved siblings, Sadra and Sahar, for their encouragement.

Contribution of Authors

1. Sabah Oghazian conducted all experimental procedures including scaffold preparations, surgical operations, animal injections, and euthanasia. She performed measurements such as Micro-CT scanning, sample fixation, decalcification, and histological analysis. She also conducted the bibliography review and authored the thesis.
2. Prof. Jake Barralet designed the experiments, oversaw the candidate throughout the research, and provided scientific and technical guidance during the study and thesis preparation.
3. Dr. Oluyomi Ajize and Dr. Kevin Watters reviewed histological slides, offering expert opinions and guidance.
4. The embedding and staining of samples were conducted at the RI-MUHC Histopathology Platform.
5. Animal maintenance and welfare were supported by the RI-MUHC ARD.

Chapter 1. Introduction

1.1. Rationale

The dramatic increase in average lifespan, largely due to improvements in medical and social services has been accompanied by a steep rise in bone disorders and injuries, necessitating repair and rebuilding procedures[1]. The exceedingly high demand for perfect bone substitutes has spurred exponential progress in the field of bone tissue engineering. However, no biomaterial has yet overcome all limitations, and autografts remain the primary choice for surgeons[2]. Current research project focuses on investigating how synthetic and composite materials interact with cells and tissues, elucidating the mechanisms by which growth factors promote osteogenesis, and improving their performance in clinical settings. Despite all advancements in the field of biomaterials, the exact mechanism involved in osteoinduction is still unknown[3]. This ongoing challenge affirms the need for further explore into crucial factors impacting bone formation. In this regard, we found a new and underappreciated route of osteogenesis which first introduced by Hans Selye, which has not yet been replicated to our knowledge. Selye reported that bone induction is possible in rat models solely relying on mechanical factors, independent of the physicochemical characteristics of biomaterials. His histopathological findings of extramedullary hematopoiesis also demonstrate the inducing role of mechanical means on hematopoietic tissue and their interaction with local MSCs to promote and sustain ectopic bony structures. Except for Selye's pioneering study, no other report has demonstrated osteoinduction in small animals without employing biologics; previous studies have shown bone induction in other animals using osteoconductive biomaterials[4]. This study aims to replicate and refine Selye's pioneering work

and evaluate whether bone induction is possible in implants three 3 times smaller than the original study which placed over a different anatomic site. It also explores the impact of both material type and geometry on osteogenesis. Additionally, the research intends to assess the efficacy of this method in bony defect healing.

1.2. Hypotheses and Objectives

It is believed that a material placed heterotopically must meet specific requirements to be capable of inducing bone formation. Soon after BMP was first identified as the primary factor responsible for osteoinduction, calcium phosphates and subsequently other materials were recognized as having the capacity to induce bone. Since then, numerous publications have described what are thought to be necessary structural and chemical characteristics of osteoinductive biomaterials. Although the pivotal role of specific materials in forming a bony microenvironment is now widely accepted, other effectors beyond geometrical or chemical parameters have been overlooked. In this regard, we aimed to eliminate any ionic role by using bioinert glass to explore whether the surgical placement of an implant and the subsequent non-physiological environment created had a role to play.

Most of the osteoinductive biomaterials shown to contain calcium phosphate phases and it has been proposed that ions either released from or absorbed onto these materials interact with tissue responsible for bone induction. Nevertheless, non-containing CaP biomaterials such as titanium and alumina ceramics have also demonstrated osteoinductive potential, undergoing a similar calcification process prior to bone formation. In this study silica glass and food grade

silicone were used which do not inherently contain calcium phosphate. They are known for their biocompatibility, hydrophobicity and chemical stability. They both are considered non-osteoinductive. Silica glass is rigid and provides a solid, stable surface, while silicone is flexible and softer which may influence cellular responses and tissue interactions in different ways. The rigid structure of glass compared to silicon is expected to provide better mechanical support, thereby promoting greater osteogenesis.

Geometrically, scaffolds are often designed to closely resemble the natural physical environment that osteogenic cells interact within the body, and the material is thought to offer a physical support allowing tissue bridging of the defect. In this study, most of the volume occupied by the scaffold was open space inside an open-ended cylinder with solid walls. Such a configuration, separates adjacent tissue planes, leaving an air-filled dead space rather than a supportive environment for tissue integration. This situation can leave several potential outcomes. The air inside the tube and its surroundings may either escape through the gaps between the sutures or diffuse within the biologic tissues to be absorbed into the bloodstream. At the same time, the body produces fluids such as exudate, lymph, blood, or tissue debris due to immediate response to surgical trauma, inflammation, and disruption of local blood and lymphatic vessels which accumulates inside the tube.

It is reported and we observed that, the body initiates the formation of a connective tissue bridge spanning from one opening of the tube to the other to restore continuity and stabilize homeostasis. The bridge formation was observed in Selye's study, where it was termed the "growth cord", apparently as it was not the same tissue that forms during secondary intention healing to fill the gap between two edges of the wound. Selye observed a different process,

probably due to the absence of clot formation and other events that promote the healing cascade involved in filling the gap. This suggests that cellular migration likely occurred instead within the moist fluid environment. According to Selye's observations, the formation of the growth cord is an essential stage of bone development. He found no bone formation in groups with fine, delicate cords, emphasizing the critical role of establishing a robust growth cord in osteogenesis.

To understand the circumstances under which the growth cord forms and how its thickness, pattern, and direction differ, we plan to modify the experimental variables in Selye's study.

The dimension adjustments can alter the surface affected by the stimulus resulting from the tube and consequently the body responses. Reducing the tube dimensions by approximately one-third compared to Selye's experiment, while maintaining the height-to-width ratio, would decrease the overall surface area in contact with surrounding tissue. This reduction in surface area is expected to attenuate the local inflammatory response, minimize tissue interaction, and reduce the mechanical pressure caused by tissue tension around the implant, resulting in less amount of bone formation. Additionally, reducing the height-to-width ratio may accelerate the connection between the two ends via the growth cord, as the distance between tissue types would be reduced. Therefore, growth cord formation is expected to be facilitated in shorter tubes (3mm height) compared to taller tubes (6mm height), provided that the minimum volume required to apply sufficient tension is maintained.

Changing the anatomic site from the subcutaneous plane of the back to the calvaria would also alter the biological responses due to differences in tissue composition and mechanical environment. While the skin with similar characteristics covers the upper opening in both

anatomical locations, the lower opening in Selye's study contacted thick muscular tissue with higher vascularity and flexibility in the back, whereas in this study it contacted with either stiff periosteum, or calvarial bone. Direct contact with calvarial bone provides a stable substrate for applying direct injury and tissue tension, as well as local osteoprogenitor cells. Considering these factors, we expect a higher amount of bone formation in subperiosteal implants compared to subcutaneous implants which may not offer the same level of cellular and mechanical support for bone formation. Placing the implants over a bony defect changes the composition of bedding tissue (dura mater vs bone and periosteum). However, the tube will still be in direct contact with the intact bone around the defect and benefit from the mechanical stability and osteogenic reservoir of bone. If a higher amount of bone formation happens compared to subperiosteal intact bone group, it will demonstrate the importance of surgical injury and the following biologic responses.

By total excision of the periosteum, we can assess whether the local osteoprogenitors in periosteum play a crucial role in the mechanism of bone formation in our experiment. The periosteal flap elevation and suturing it on top of the tube can also provide valuable information about the osteogenic potential of the periosteum. Osteogenesis around the periosteum would indicate localized activation of osteoprogenitors.

On the other hand, placing the tube in direct contact with bone not only provides a stable bedding which enhances mechanical stability, but also stimulates osteogenic cells within the bone, potentially enhancing bone formation within the tube. If the direct injury from tube walls promotes differentiation of osteogenic cells, then decortication of the outer wall of the calvarium—creating monocortical holes, a clinical technique used to enhance bone formation and

graft integration—will further enhance bone formation by supporting angiogenesis and facilitating the migration of progenitor cells.

Horizontal placement of a hemicylindrical tube in direct contact with bone, while both ends and walls are covered by skin tissue, provides a method to examine the influence of cord length on subsequent tissue induction. The total area in contact with the skin remains the same (two half-circular openings), but the area in contact with bone increases by 1.7 times. If this bone contact is crucial, the highest amount of bone formation is expected in this group. However, the volume is less than in the 6mm tubes but more than the 3mm tubes, creating a tissue tension between these groups. If this tension plays a key role, bone formation will fall within the range observed in those groups. Additionally, horizontal placement alters the separation of tissue elements. By removing the physical barriers on the sides, the skin can now contact the bone. If preventing such direct contact is important for tissue formation, this arrangement may lead to its inhibition.

Selye reported that marrow formation preceded bone formation within strands of myeloid tissue located in adipose islands, where osseous tissue was not detected. Additionally, he observed islets of myeloid and lymphoid tissue surrounding blood vessels. Although marrow-derived stromal cells can differentiate into osteoblasts ectopically, and extramedullary hematopoietic cells can be driven by injury and inflammation to influence MSC homeostasis, the lack of confirmed marrow tissue suggests no role of marrow formation in subsequent tissue induction.

Table 1.1. Summary of experimental setup influencing tissue formation and osteogenesis.

	Variable	Variable Description	Rationale	Expected Outcome	Relevant Results
1	**Material Type**	Silicon vs Glass	Neither release ions, silica glass is rigid, and silicone is flexible and soft.	If the volume and shape geometry are identical then tissue formation will be identical regardless of material type.	Fig. 4.4: Micro-CT of silicon/glass tubes; Table 4.1, Figs. 4.5 & 4.6: Bone volume; Figs. 4.12 & 4.13: Histological examination of silicone/glass tubes.
2a	**Implant Geometry**	Height (6mm vs 3mm)	Shorter tubes would induce less skin tension following tissue plane separation and cause less mechanical pressure. Also, the distance would be reduced between tissue types.	Shorter implants (3mm) will have faster tissue connection between two ends This may result in faster Saussure development compared with longer tubes Skin tension would be expected to be lower in shorter implants.	Fig. 4.3: Micro-CT 3D view of bone formation patterns; Fig. 4.4: Sagittal Micro-CT of tubes; Table 4.1, Figs. 4.5 & 4.6: Bone volume; Figs. 4.14 & 4.15: Histological examination of 6mm and 3mm subperiosteal glass tubes.
2b		Design (Cylindrical vs Hemi-cylindrical)	Placing a hemicylindrical tube in direct contact with bone, while both ends and walls are covered by skin tissue, can provide a way to examine the role of cord length in subsequent tissue induction. While the total area in contact with skin was the same (two half circular openings), the area in contact with the bone larger.	If both tissue types are equally important then increasing the area of one and not the other will result in no effect.	Fig. 4.3: Micro-CT 3D view of bone formation patterns; Fig. 4.4: Sagittal Micro-CT of tubes; Table 4.1, Figs. 4.5 & 4.6: Bone volume; Fig. 4.17: Histological examination of subperiosteal hemicylindrical glass tubes.
3a	**Contact Area**	Implant Size	Smaller tube volumes will result in less contact area with the surrounding tissue, which may limit the mechanical stimulus necessary for effective tissue integration and osteogenesis.	A minimum volume is required for tissue formation. Smaller tubes in our study compared to Selye's study will result in less amount of bone formation.	Figs. 4.5 & 4.6: Bone volume in different tube sizes; Figs. 2.6 & 2.7: Selye's experiment with larger tubes.
3b		Implant Orientation	Placing the tube horizontally will alter what elements of tissue are physically separated. essential for promoting tissue intrusion and osteogenesis.	Horizontal orientation removes a physical barrier between the skin and the bone. If this is a requirement tissue formation will be inhibited.	Figs. 4.2.h, 4.3 & 4.4.h: Horizontal tube impact on growth cord and bone formation pattern; Table 4.1, Figs. 4.5 & 4.6: Bone volume; Fig. 4.17: Histological examination.
4	**Implantation Anatomic Site**	Implantation over periosteum, over skull bone, and skull bony defect	To evaluate how different tissue compositions and mechanical environments affect biological responses.	The subcutaneous calvarial site is expected to result in lower osteogenesis. Subperiosteal implantation is anticipated to increase bone formation. If greater bone formation occurs in groups with defects, it will confirm the importance of the substrate structure.	Fig. 4.4: Sagittal Micro-CT of tubes in different sites; Table 4.1, Figs. 4.5 & 4.6: Bone volume; Figs. 4.13 & 4.14: Histological examination of subcutaneous and

					subperiosteal glass tubes.
5a	**Mechanical Injury**	Soft material vs Stiff material	Placing a stiff material over the skull may cause mechanical injury to the periosteum since we observe bone resorption below glass implants, this may result in release of osteoprogenitor cells from the periosteum.	Soft material will result in minimal or no mechanical injury, leading to less osteogenesis.	The tube's compressive effect on bone: macroscopic view in Fig. 4.2; Sagittal Micro-CT view in Fig. 4.4.
5b		Bone Decortication	Bone decortication, through the creation of small monocortical holes, a clinical technique to enhance bone formation.	Bone decortication will lead to increased mechanical injury, and this will result in more bone formation.	Fig. 4.4, e: Sagittal Micro-CT; Table 4.1, Figs. 4.5 & 4.6: Bone volume.
6	**Periosteum**	Presence vs Absence of Periosteum	By removing the periosteum, the main source of osteogenic cells will be eliminated, significantly reducing the bone's ability to regenerate. The absence of periosteum would result in decreased recruitment of osteoprogenitor cells, lower vascularization, and consequently decreased bone formation.	Excision of the periosteum will dramatically decrease osteogenesis compared to groups the periosteum remains intact.	Fig. 4.4, f: Sagittal Micro-CT; Table 4.1, Figs. 4.5 & 4.6: Bone volume; Figs. 4.16: Histological examination of glass tubes after periosteal excision.
7	**Growth Cord**		According the Selye's observation, forming the Growth cord is the essential stage of tissue formation. He observed no bone formation in groups with fine, delicate cords emphasizing the critical role of forming a robust growth cord in osteogenesis.	We expect bone formation to align with the implant's ability to form a viable growth cord, which is anticipated to occur more effectively with stiff implants, shorter heights (facilitating easier tissue connection), and larger contact surfaces.	Figs. 4.1 & 4.2: Growth cord formation in different groups.
8	**Marrow and Hematopoietic Stem Cells (HSCs)**		To evaluate whether Selye's observation of hematopoietic tissue using H&E staining can be confirmed by IHC staining,	Marrow can form ectopically and can differentiate into mesenchymal tissues. A lack of confirmation of marrow tissue indicates no role of marrow formation in subsequent tissue induction	Fig. 2.8: Extramedullary hematopoietic tissue in Selye's specimens. IHC staining confirms bone marrow and hematopoietic tissue in the current study.

Chapter 2. Literature Review

2.1. Bone Marrow Biology

The vertebrate skeleton is a complex structure that houses a variety of cell types, structural extracellular matrix (ECM) proteins, and secreted proteins such as cytokines. Bone tissue is composed of several cell types, including skeletal stem cells, osteoprogenitors, osteoblasts at various stages of differentiation into mature osteocytes, osteoclasts, and chondrocytes found in articular and growth-plate cartilages[5]. The bone marrow (BM) is well recognized for its crucial role in hematopoiesis and contains a complex network of blood vessels, including a specialized fenestrated sinusoidal network that facilitates cellular and molecular exchanges between the blood and the BM compartment[6]. Both bone and BM are innervated by various types of neurons and are structurally supported by different families of ECM proteins. Moreover, BM has been proposed as a reservoir for elusive endothelial stem or progenitor cells, which are believed to play a role in vasculogenesis and neo-angiogenesis. In addition to the diverse hematopoietic cells, BM includes a variety of stromal cells that contribute to different regenerative functions: osteogenesis (osteoprogenitors), hematopoiesis (adventitial reticular cells), and metabolism and the endocrine system (adipocytes)[7].

2.1.1. Bone Marrow Structure and Function

The bone marrow is located within the central cavities of axial and long bones. It comprises hematopoietic tissue islands and adipose cells, which are surrounded by vascular sinuses

interspersed within a meshwork of trabecular bone. In terms of body weight, bone marrow accounts for approximately 3% in adult rats[8], around 2% in dogs[9], and about 5% in humans[10].

Bone marrow is the primary hematopoietic organ and a crucial lymphoid tissue, responsible for the production of erythrocytes, granulocytes, monocytes, lymphocytes, and platelets[11].

2.1.1.1. Endosteal Structure

The inner surface of the bone cavities and the outer surface of the cancellous bone spicules within these cavities are covered by an endosteal lining. This lining consists of a single layer of flat "bone-lining cells," which are supported by a thin layer of reticular connective tissue. Additionally, osteoblasts and osteoclasts are also present within the endosteal lining, contributing to bone formation and resorption, respectively[12].

2.1.1.2. Vascular Supply

In long bones, one or more nutrient canals, each containing a nutrient artery and one or two nutrient veins, penetrate the cortical bone obliquely to access the marrow cavity. In flat bones, numerous blood vessels of varying sizes supply the marrow by entering through both large and small nutrient canals. Upon entering the marrow cavity, the nutrient artery divides into ascending and descending branches, which run parallel to the bone's long axis. These branches coil around the central venous marrow channel, known as the central longitudinal vein[12].

These arterial branches further subdivide into numerous small, thin-walled arterioles, and capillaries that extend outward toward the cortical bone. Near the bone, the arterioles open up and connect with a plexus of venous sinuses. These venous sinuses drain into collecting venules, which direct blood back to the central longitudinal vein. From there, the blood exits through the

nutrient veins. Consequently, the marrow possesses an extensive blood supply, which is vital for its role in hematopoiesis and overall function[13].

Additionally, it appears that nutrient artery-derived capillaries extend into the Haversian canals, then return to the marrow cavity, where they open into the venous sinuses. This creates a circular pattern of blood flow within the marrow cavity, moving from the center toward the periphery and then back to the center. In both long and flat bones, the blood supplies of the bone and bone marrow are interconnected through an endosteal network of vessels. The venous sinuses are thin-walled structures composed of a layer of flat endothelial cells with minimal to no basement membrane (Figure 2.1). Notably, the marrow does not have lymphatic drainage[12].

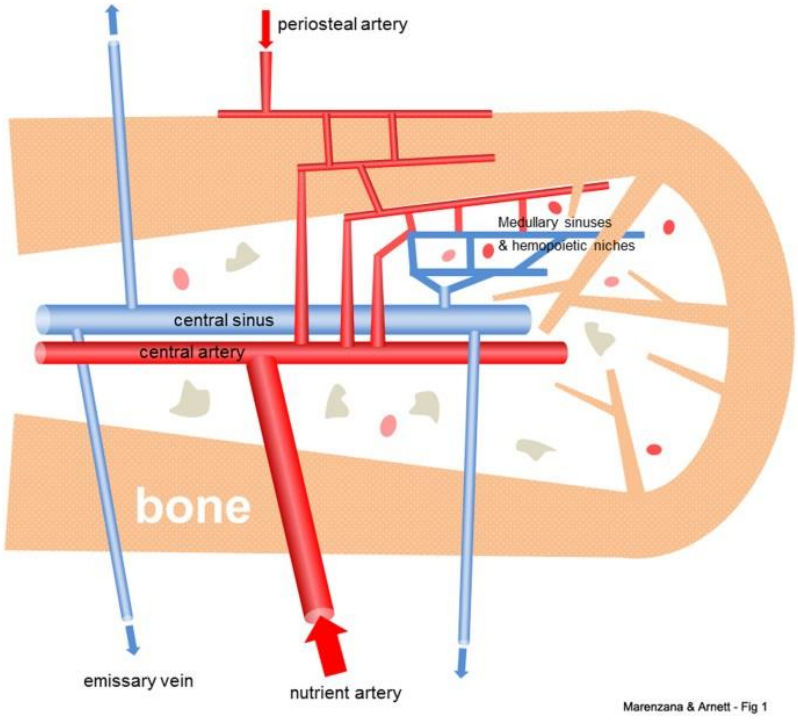

Figure 2.1. The vascular supply of the bone marrow. Reproduced with permission from Marenzana et al, "The Key Role of the Blood Supply to Bone," *Bone Research*, 2013. © 2013 Marenzana et al[14].

2.1.1.3. Innervation of Bone Marrow

Bone marrow receives innervation from both myelinated and non-myelinated nerves, which enter through the nutrient canals. Additionally, some innervation occurs through epiphyseal and metaphyseal foramina. Nerve bundles accompany the arterioles, with branches serving the smooth muscle of the vessels or occasionally terminating within the hematopoietic tissue among hematopoietic cells[12].

2.1.2. Hematopoietic Environment

The hematopoietic tissue is indeed a complex environment crucial for the production and regulation of blood cells. This tissue comprises various cell types, each playing a specific role in supporting hematopoiesis. The organization of these cells within the tissue is not random but rather structured to facilitate the processes of proliferation, differentiation, and maturation of hematopoietic stem cells. At the core of this microenvironment are hematopoietic stem cells, which require a supportive niche to maintain their function and potential. This niche is provided by a combination of cell types, including adventitial reticular cells (barrier cells), endothelial cells, macrophages, adipocytes, and possibly osteoblasts, along with elements of the extracellular matrix. Adventitial reticular cells and endothelial cells create a physical scaffold that helps anchor and organize the hematopoietic stem cells[15]. Macrophages play a crucial role in immune surveillance and clearance of cellular debris, while adipocytes contribute to the regulation of energy metabolism within the tissue. Osteoblasts, if present, likely participate in the regulation of hematopoiesis through interactions with bone marrow cells. Moreover, the microenvironment secretes various factors, such as cytokines, growth factors, and extracellular matrix components,

which regulate the behavior of hematopoietic stem cells, influencing their proliferation, differentiation, and migration[11].

2.1.1.5. Hematopoiesis

Hematopoiesis unfolds as a compartmentalized phenomenon within the hematopoietic tissue. Erythropoiesis specifically transpires within discrete anatomical units known as erythroblastic islands. Granulopoiesis, on the other hand, occurs in less defined concentrations, while megakaryopoiesis takes place in proximity to the sinus endothelium. As the hematopoietic cells mature, they are guided by barrier cells to breach the venous sinus wall, thus gaining entry into the bloodstream. Platelets, meanwhile, are liberated directly into the bloodstream via cytoplasmic extensions of megakaryocytes, which penetrate the sinus wall and access the sinus lumen[12].

Hematopoiesis is an ongoing process, yet it can be delineated into distinct stages. The initial stage involves uncommitted (pluripotent) stem cells located within the bone marrow. These pluripotent cells serve two main functions. Firstly, they sustain their population through self-renewal, and secondly, they possess the capacity to generate all types of hematopoietic cells (erythrocytes, granulocytes, lymphocytes, monocytes, and platelets). They seem to be more abundant in the peripheral regions surrounding the central axis, in close proximity to bone lining cells[12].

Hematopoiesis is generally organized as a hierarchical system that begins with pluripotent stem cells, which differentiate into either lymphoid or multipotent myeloid stem cells. Lymphoid stem cells (CFU-L) generate all types of lymphocytes, whereas myeloid stem cells (CFU-GEMM) produce erythrocytes, granulocytes, platelets, mast cells, and osteoclasts. The immediate descendants of

these lymphoid and myeloid stem cells are known as hematopoietic progenitor cells. These progenitor cells have a limited capacity for self-renewal but can differentiate and produce progeny. Subsequently, these progenitor cells give rise to additional progenitor cells that mature into the most immature morphologically identifiable blood cell precursors (Figure 2.2)[16].

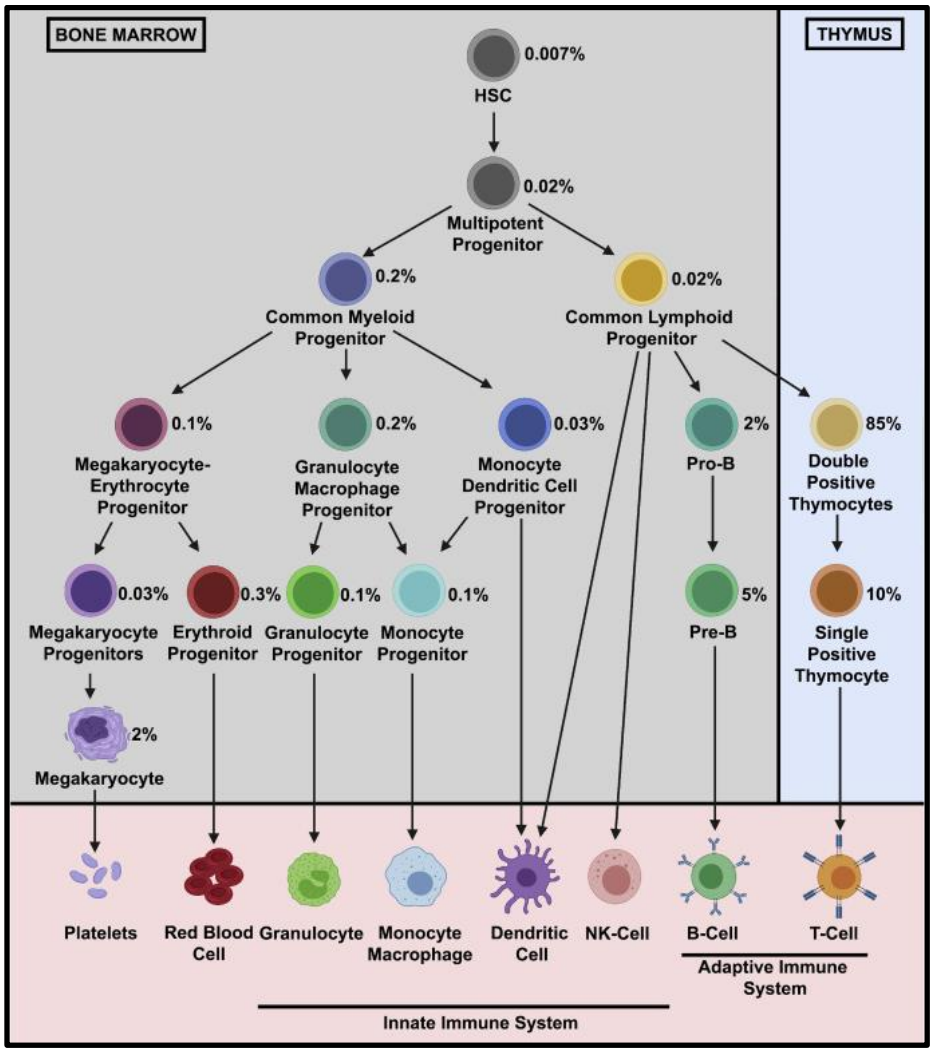

Figure 2.2. The maturation progression of multiple cellular lineages. Reproduced with permission from Comazzetto et al, "Niches that regulate stem cells and hematopoiesis in adult bone marrow," *Developmental Cell*, 2021. © 2021 Elsevier[17].

2.1.3. Osteoprogenitors in Bone Marrow

Bone marrow (BM) stroma is home to self-renewing, multipotent progenitors for skeletal lineages, including cartilage, bone, marrow adipocytes, and fibroblasts. These progenitors, known as skeletal stem cells (SSCs), provide a reservoir of bone-forming cells essential for bone growth during development, bone modeling (shaping of bone and ongoing bone turnover). SSCs also generate adipocytes during growth and BM remodeling, and under specific conditions, they can form cartilage. BM stromal cells (BMSCs), which include SSCs, adventitial reticular cells (ARCs), marrow adipocytes, developing and mature osteogenic cells, and pericytes/mural cells, play a crucial role in shaping and regulating the local microvascular network, influencing the differentiation of osteoclasts, and maintaining the hematopoietic microenvironment necessary for blood cell development and maturation. Furthermore, they may be critical for preserving long-term self-renewing hematopoietic stem cells (HSCs) within their niche[18].

SSCs, which function as skeletal progenitors and organizers and regulators of the local BM microenvironment, physically exist as perivascular cells known as adventitial reticular cells (ARCs). These cells reside adjacent to the endothelial lining of BM sinusoids, characterized by a distinct phenotype and reticular morphology[19]. As Sacchetti et al. reported MCAM/CD146-expressing subendothelial cells in human bone marrow stroma can transfer the hematopoietic microenvironment (HME) to heterotopic sites upon transplantation. These cells also establish themselves within miniature bone structures. In developing heterotopic bone marrow, these subendothelial stromal cells interact dynamically with developing sinusoids. They reside on sinusoidal walls and play a key role in producing Angiopoietin-1, a crucial molecule for the hematopoietic stem cell niche and vascular remodeling (Figure 2.3)[20].

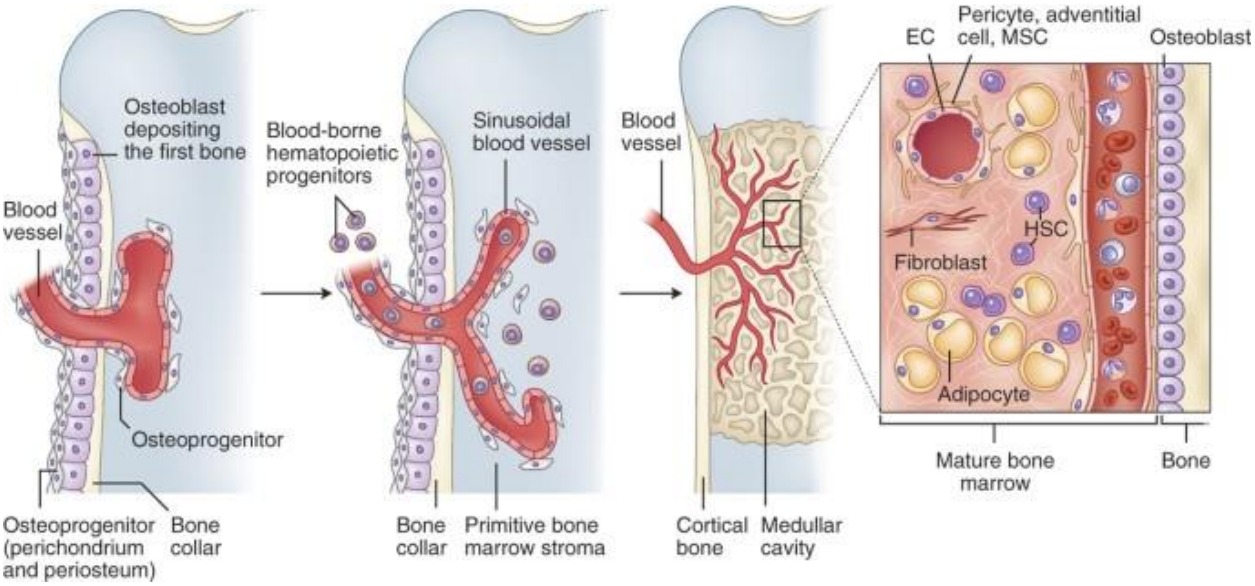

Figure 2.3. The illustration shows skeletal progenitors and MSCs migrating into the bone marrow cavity along blood vessels, mediated by endothelial PDGF-BB signaling. It also highlights Ang-1 production for vascular integrity and TGF-β1-induced quiescence at mural cell-endothelial contacts. Reproduced with permission from Paolo Bianco et al, "The meaning, the sense and the significance: translating the science of mesenchymal stem cells into medicine", Nature Medicine 2013, © 2013, Springer Nature America, Inc[21].

2.1.3.1. Perspectives of Skeletal Stem Cells

The concept of SSCs traces its roots to pioneering experiments conducted by Goujon in the 19th century[18]. The term mesenchymal stem cells (MSCs) was first coined by Caplan, who reported that bone and cartilage formation in embryos, as well as repair and turnover in adults, are mediated by a small population of cells known as mesenchymal stem cells. These cells undergo division, and their progeny commit to specific phenotypic pathways, progressing through distinct lineage stages to eventually form specialized tissue types such as cartilage or bone. Local environmental cues and genetic potential interact at each step of lineage commitment to regulate the rate and characteristics of cell differentiation in the emerging tissue[22].

In 1968, Tavassoli and Crosby conducted experiments where they transplanted autologous fragments of marrow into various extramedullary sites in rats, rabbits, and dogs. The transplanted fragments survived and completely reconstituted the hematopoietic and adventitial structures. They observed that surviving reticular cells proliferated and differentiated into osteoblasts, initiating the formation of trabecular bone. Subsequently, these reticular cells reconstructed the microcirculation within the marrow. Hematopoietic repopulation of the marrow implant occurred only after establishment of its sinusoidal microcirculation[23].

The research by Tavassoli and Crosby in 1968 provided compelling evidence for the osteogenic capabilities inherent in bone marrow (BM). However, they did not definitively identify the specific cell responsible for progenitor differentiation into bone cells and other non-hematopoietic mesenchymal cells[18].

In 1970, Friedenstein et al. demonstrated in monolayer cultures of guinea-pig bone marrow and spleen that discrete fibroblast colonies develop between days 9 and 12. They observed a linear increase in colony numbers with higher numbers of explanted cells, and the distribution of male and female cells in mixed cultures suggested that these fibroblast colonies are clonal in nature. Fibroblasts cultured from bone marrow (but not spleen) exhibited spontaneous bone formation within diffusion chambers. Moreover, fibroblasts from both bone marrow and spleen cultures showed inducibility to osteogenesis when exposed to transitional epithelium within diffusion chambers[24]. Their work not only established bone marrow stroma as the crucial environment for locating these elusive cells but also provided a breakthrough in isolating and characterizing mesenchymal progenitor cells[18].

In his 1990 review, Friedenstein discussed how grafting multicolony-derived rabbit marrow fibroblast cultures heterotopically resulted in the development of bone marrow organs. These findings closely resembled outcomes seen with the transplantation of marrow fragments, suggesting that marrow CFU-Fs (or some of them) may serve as cells capable of transferring the hematopoietic microenvironment (HME). Additionally, when single CFU-F colonies from primary cultures of murine marrow cells were heterotopically transplanted, ossicles formed with marrow cavities containing hematopoietic cells in 10% of cases[25].

Many people began to perceive mesenchymal stem cells (MSCs) as a type of postnatal human stem cell with a broader differentiation potential than initially thought, possibly even comparable to that of embryonic stem cells. This belief, supported by subsequent studies claiming the transgermal potential ("plasticity") of postnatal stem cells, including MSCs, garnered significant attention but also caused confusion and remains highly controversial[18].

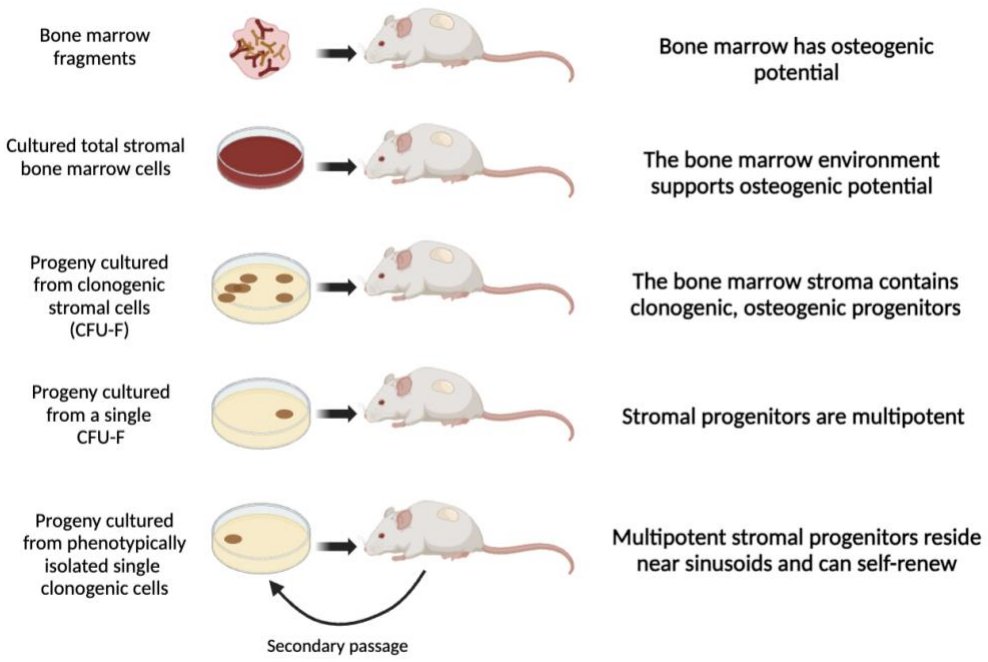

Figure 2.4. The sequential series of experiments to identify multipotent, self-renewing bone marrow–derived MSCs. Reproduced with permission from Paolo Bianco et al, "The meaning, the sense and the significance: translating the science of mesenchymal stem cells into medicine", Nature Medicine 2013, © 2013, Springer Nature America, Inc[21].

2.1.3.2. Bone Marrow Establishment

Bone tissue develops prior to the establishment of a bone marrow cavity, indicating that bone cells emerge before bone marrow osteoprogenitors. The outer layer of the perichondrium/periosteum is populated by proliferating progenitors of bone-forming cells. These progenitors give rise to osteoblasts, which are responsible for depositing the 'bony collar' during the initial stages of ossification[19].

Arai et al. purified perichondrial cells and examined their involvement in hematopoietic bone marrow formation. Their analysis revealed ALCAM expression within the perichondrium. ALCAM is known to facilitate cell adhesion in various cell types, including hematopoietic cells, endothelial

cells, bone marrow stromal cells, and mesenchymal stem cells. Perichondrial cells positive for ALCAM, exhibited mesenchymal stem cell characteristics and demonstrated the ability to differentiate into osteoblasts, adipocytes, chondrocytes, and stromal cells, which can support osteoclastogenesis, hematopoiesis, and angiogenesis. They concluded that the perichondrium may act as BM stromal osteoprogenitors and play a critical role in the early stages of bone and bone marrow development[26].

As osteoclasts resorb bone by perforating the bony collar and the underlying hypertrophic chondrocytes, blood vessels from the osteogenic perichondrium/periosteum infiltrate the forming marrow cavity. Osteoprogenitors from the periosteum are then recruited to a perivascular location and migrate into the developing bone marrow[19]. The primitive, pre-hematopoietic bone marrow consists of large-caliber sinusoidal blood vessels surrounded by osteogenic cells, with some of these cells located on the abluminal surface of the blood vessels. This environment is subsequently seeded by blood-borne hematopoietic progenitors[27].

The growth of bone marrow stroma is regulated by parathyroid hormone (PTH) and PTH-related protein (PTHrP), both of which are crucial in bone development and postnatal physiology. As bones lengthen, the site-specific downregulation of the PTH1 receptor (PTH1R) may be essential to prevent local ossification, thereby creating space for continuous hematopoiesis[28].

2.1.3.3. The influence of HSPCs on the osteogenic differentiation of MSCs

In the bone marrow niche, mesenchymal stem cells (MSCs) are typically regarded as supportive cells for hematopoiesis, and their crucial role in regulating hematopoiesis has been extensively studied. Research has demonstrated that hematopoietic stem/progenitor cells (HSPCs) can also

influence the regeneration of niches that sustain them, suggesting a reciprocal signaling relationship between different cells in the bone marrow niche[29].

However, the understanding of how hematopoietic cells influence MSC homeostasis remains limited. Recent findings indicate that MSCs and HSPCs are located in close proximity and work in cooperation with each other. They identified mesenchymal stem cells (MSCs) expressing nestin as important components of the HSC niche in bone marrow. Nestin+ MSCs, associated with HSCs and adrenergic nerve fibers, express HSC maintenance genes and form self-renewing 'mesenspheres'[30].

The heterozygous loss of the Pten gene (a potent tumor suppressor gene, and its loss in hematopoietic stem/progenitor cells (HSPCs) leads to leukemogenesis) in hematopoietic cells causes MSCs to have reduced osteogenic and increased adipogenic differentiation. Co-culturing MSCs with normal hematopoietic cells corrects this abnormal differentiation, while co-culturing with Pten-deficient hematopoietic cells maintains the abnormal differentiation[31].

The findings of another study suggested that under normal conditions, HSCs can direct mesenchymal differentiation towards the osteoblastic lineage. HSCs isolated from animals subjected to acute stress were significantly more effective at promoting osteoblastic differentiation both in vitro and in vivo compared to those from control animals. Notably, HSC-derived bone morphogenic protein 2 (BMP-2) and BMP-6 were identified as key factors responsible for these activities[32].

It has also been suggested that co-culturing a low dose of HSPCs with MSCs, combined with dexamethasone treatment, accelerates the osteogenic progression of MSCs. Additionally, they

observed a longer persistence of functional primitive hematopoietic stem and progenitor cells in the population treated with dexamethasone, which positively correlated with the enhanced osteogenic differentiation of MSCs[33].

These findings suggest that both hematopoietic cells and MSCs are important components of the bone marrow entity, contributing to the maintenance of niche stability through reciprocal regulation[31].

2.2. Extramedullary Hematopoiesis

The hematopoietic microenvironment undergoes significant changes throughout development, with hematopoietic sites varying even under physiological conditions. Initially, during embryonic development, hematopoiesis begins in the yolk sac. In the second trimester, the primary hematopoietic sites shift to the fetal liver and spleen. By the third trimester, the main site of hematopoiesis transitions to the bone marrow. Hematopoiesis occurring outside the bone marrow during this period is known as physiological extramedullary hematopoiesis (EMH). After birth, the bone marrow establishes itself as the primary hematopoietic organ[34].

In neonatal mice, humans, dogs, cats, cattle, and pigs, residual sites of fetal hematopoiesis, primarily in the spleen but also in the liver and lymph nodes, persist and then regress before adulthood. In mice, and to a lesser extent in rats and hamsters, the spleen remains active in hematopoiesis throughout adulthood. This shift of hematopoietic activity to the spleen late in fetal development, with minor residual activity in other hemic organs such as the liver and lymph nodes, aligns with the distribution of extramedullary hematopoiesis (EMH) in adult animals[35].

2.2.1. Mechanisms of Development of EMH

Conceptually, extramedullary hematopoiesis (EMH) can develop anywhere and anytime a stem cell niche emerges outside of the bone marrow. This can occur due to the mobilization and stimulation of hematopoietic stem cells (HSCs) and mesenchymal stem cells (MSCs), stromal proliferation, or the activation of cytoadhesive and chemokine signaling pathways that induce stem cell homing and activation. The interaction among stromal cells, humoral factors, and stem cells is a complex process, reliant on more than just physical space. A residual fetal niche environment persists in hemic tissues of neonates and can be reactivated in various disease states[36].

While the full reasons for extramedullary hematopoiesis (EMH) in various disorders are not yet completely understood, some major theories cover most of the pathophysiological causes: bone marrow failure; bone marrow stimulation (myelostimulation); tissue inflammation, injury, and repair; and abnormal systemic or local chemokine production. Although EMH is typically trilineage, reflecting the multilineage potential of embryonic hematopoiesis and HSCs, one or two cell types may predominate depending on the specific underlying pathogenesis[36].

2.2.1.1. HSCs and EMH in Tissue Inflammation, Injury, and Repair

The findings in parabiotic mice suggest that HSC engraftment in unconditioned bone marrow does not require large numbers of cells in the bloodstream. This implies that the turnover of HSCs in bone marrow niches is higher than previously thought. HSC migration within the bone marrow may help maintain hematopoietic homeostasis by ensuring that niches are not left unoccupied

after HSC death or differentiation. Migratory HSCs may also serve as a readily available pool for rapid recruitment in response to catastrophic blood loss[37].

The cellular and stromal elements present in granulation tissue, resolving hematomas, areas of ischemia, neovascularization, and sites of inflammation can create a niche environment that supports extramedullary hematopoiesis (EMH). This emerging concept suggests that molecular changes associated with local inflammation, injury, and tissue repair can mimic those involved in hematopoiesis. Various cytokines and inflammatory mediators can increase the number of hematopoietic stem cells (HSCs) and mesenchymal stem cells (MSCs) in peripheral circulation, which then home to affected organs and tissues, participating in local regenerative or inflammatory responses[36].

In one study, EMH was observed in 15 out of 207 cardiac biopsy specimens (7.2%) and 22 out of 598 autopsy specimens (3.7%), which was more than expected. Most instances (24 out of 37, 65%) were found in hearts with infarcts older than 72 hours, characterized by abundant granulation tissue and large numbers of fibroblasts and macrophages. The investigators concluded that the presence of EMH in healing, but not in acute stages of infarction, indicates that EMH is driven by inflammation- or repair-associated trophic factors rather than ischemia itself. This suggests that the healing infarct provides both the structural environment (loose connective tissue with neovascularization) and the cellular components necessary for circulating hematopoietic cells to home and proliferate. It appears that tissue EMH originates from circulating peripheral blood stem cells attracted to the injury site, likely due to the local effects of chemical mediators[38].

Another study reported that EMH in cardiac specimens is relatively common. They identified EMH in 4 out of 11 cases with severe myocardial infarction (MI). The researchers suggested that the previous lack of description might be due to pathologists misidentifying EMH foci as chronic inflammation. They proposed that one potential mechanism for EMH in these cases could be a response to tissue, such as in chronic anemia or hypoxemia[39].

Trilineage extramedullary hematopoiesis (EMH) was identified in the anterior and posterior uvea of enucleated eyes from 3 out of 6 cats with ocular disease. These cats had a history of neonatal corneal degeneration leading to corneal destruction and extensive prolapse of uveal tissue, suggesting that EMH resulted from tissue trauma and repair, accompanied by mild lymphoplasmacytic inflammation. Histologically, EMH was observed mainly in the iris, with some involvement in the adjacent ciliary body and choroid, showing clusters of precursor cells with mature granulocytes, predominantly eosinophils[40].

Resolving hematomas or hemorrhages in various tissues can create a microenvironment conducive to hematopoiesis. EMH in the spinal and cranial dura mater has been associated with subdural hematomas. Additionally, adrenal EMH has been observed in conjunction with hemorrhage. The hypoxic environment of a resolving hematoma promotes the homing of hematopoietic stem cells (HSCs) and hematopoietic progenitor cells (HPCs). Activated macrophages play a supportive role in the development of EMH in tissues affected by hemorrhage, tissue injury, repair, histiocytic hyperplasia, and histiocytic sarcoma. This role warrants further investigation[41].

2.2.1.2. EMH and alternative hypotheses

The potential mechanisms behind idiopathic extramedullary hematopoiesis (EMH) primarily involve the release and migration of stem cells. One theory suggests that bone fractures, such as sacral fractures, may release hematopoietic stem cells from the bone marrow into the presacral space, leading to the formation of EMH masses. This is supported by cases where patients with a history of spinal pathologies developed EMH following fractures[42].

Another hypothesis involves the release of mesenchymal stem cells (MSCs) following hysterectomies. MSCs, which are found in various organs including the uterine endometrium and menstrual blood, retain the potential to differentiate into different tissue types. Surgical manipulation of the female reproductive organs may release these MSCs, which then migrate to the presacral area and interact with hemocytoblast niches outside the bone marrow to form EMH. This theory is supported by cases where patients developed presacral EMH following hysterectomies. Both theories highlight unique complications related to sacral fractures and hysterectomies in the context of idiopathic EMH[43].

2.2.2. Cases with Ectopic Bone Formation and EMH

Several documents report cases of ectopic bone formation and extramedullary hematopoiesis (EMH) in specimens from various organs. Although no specific mechanism has been identified, the frequency of these cases suggests that, while rare, they are not merely incidental.

An observation of a case of endometrial osseous metaplasia with EMH was reported. The patient presented no hematologic disorder. They believed that the presence of mature bone with active hematopoietic marrow could be explained by the bone residing within the endometrial cavity for

an extended period, allowing circulating hematopoietic stem cells to colonize the tissue and initiate marrow formation[44].

A comprehensive literature review summarized a total of 47 cases of extramedullary hematopoiesis (EMH) and/or ectopic bone formation (EBF) in the thyroid gland from the English literature spanning 1985 to 2021. Among these cases, only 5 had a history of hematological disorders. EMH was reported in 32 cases, EBF in 19 cases, and 28 cases showed evidence of calcification. Additionally, they evaluated 3,100 thyroidectomy cases and found 16 cases with EBF, of which 1 was accompanied by EMH[45].

The factors leading to the formation of bone and extramedullary hematopoiesis (EMH) in the thyroid gland remain unclear. Several theories have been proposed, but none have definitively shown the exact mechanism. One suggestion is that mesenchymal cells and capillaries within thyroid nodules create a favorable microenvironment that supports differentiation into hematopoietic tissue and bone tissue formation. Additionally, fibroblasts may differentiate into osteoblasts. These osteoblasts, influenced by local factors, produce collagen and other substances that stimulate the formation of hydroxyapatite, ultimately leading to bone formation[46].

2.3. Engineering the hematopoietic stem cell niche

Hematopoiesis, the process of generating blood cells from hematopoietic stem cells (HSCs), follows a hierarchical structure. The multitude of factors within the HSC niche poses significant challenges in creating biomaterial-based artificial niches. Nevertheless, the potential of such

platforms has piqued the interest of numerous research groups, as they offer opportunities to explore the mechanisms involved in maintaining a healthy niche and the pathophysiology of bone marrow diseases[47].

2.3.1. The importance and applications of BM niche models

BM niche models are crucial for studying HSC biology and disease pathology. They overcome limitations of mouse models by providing an accurate platform for investigating HSC regulation and cellular interactions. Regarding the high demand in transfusion medicine, they can facilitate the ex vivo production of mature blood cells like erythrocytes and platelets. These models also offer advanced platforms for drug screening. They can predict the drug efficacy and toxicity more accurately than traditional methods and reduce the reliance on animal studies. Additionally, BM niche models enhance gene therapy by improving ex vivo culture conditions for gene-modified HSCs, increasing therapeutic success rates and expanding healthy HSC populations for transplantation. This multifaceted approach contributes to better understanding and treatment of blood-related diseases and bone marrow disorders[48].

2.3.2. Ex-vivo Bioengineering of the bone marrow niche

Hematopoietic stem cells (HSCs) cannot be effectively expanded in vitro due to their rapid differentiation and loss of self-renewal capacity once removed from the bone marrow (BM) niche microenvironment. This limitation is attributed to the absence of biophysical and biochemical cues from the native niche present in standard synthetic culture conditions. Recently, biomaterial and bioengineering strategies have emerged as promising approaches to recreate an in vivo-like niche environment for HSCs in laboratory or ex vivo settings, aiming to support clinical

applications. These strategies typically involve constructing a 2D or 3D environment using materials such as scaffolds or hydrogels, along with essential niche components like cytokines, matrix stiffness, extracellular matrix (ECM) components, and specific cell types[49].

In conventional systems, hematopoietic stem cells (HSCs) are typically cultured in media supplemented with various cytokines and growth factors, on substrates functionalized with extracellular matrix (ECM) proteins or using feeder layers. In 3D cultures, HSCs can be cultured alone or in co-culture with supporting cells within spheroids, embedded in polymer matrices or the cavities of polymer scaffolds, or within decellularized ECM or natural and synthetic hydrogels. More advanced systems include perfusion bioreactors that mimic blood flow, shear stress, and facilitate nutrient delivery and waste removal. Organ-on-a-chip models represent even more sophisticated platforms that integrate various ECM compositions, stiffnesses, cell types, soluble factors, and vascular systems into a single multi-parameter model (Figure 2.5)[49].

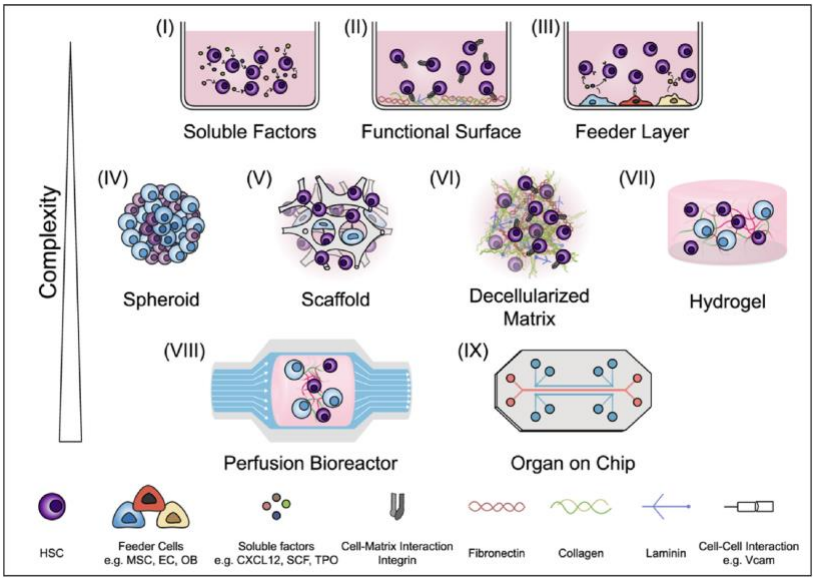

Figure 2.5. Development of BM niche models. Reproduced with permission from Xiao et al., "Current insights into the bone marrow niche: From biology in vivo to bioengineering ex vivo," *Biomaterials*, July 2022. © 2022 Xiao et al. Published by Elsevier Ltd[49].

2.4. Heterotopic ossification

The human skeleton is a complex organ system comprising over 200 articulated bones of various shapes and sizes. During embryogenesis, the skeleton develops from undifferentiated mesenchyme following a genetic plan that dictates its precise temporal and spatial formation. After birth, the initiation of new skeletal elements is generally limited to bone regeneration at fracture sites[50].

Heterotopic ossification is the formation of normal bone in abnormal soft tissue locations due to disrupted regulation of skeletogenesis. This unwanted bone formation ranges from clinically insignificant radiographic findings to severe conditions that significantly impact quality of life. Causes include soft-tissue trauma, central nervous system injury, and vasculopathies (Table 2.1)[51].

Table 2.1. Etiology of Heterotopic ossification[50].

Acquired Forms		
Injury	***Vascular***	***Arthropathy***
Central nervous system Brain Closed head trauma/coma Cerebrovascular accident Spinal cord Paraplegia Quadriplegia Lower motor neuron (poliomyelitis) Soft tissue Blunt trauma Muscle hematoma Joint dislocation Postsurgical Following total hip arthroplasty Surgical scars	Atherosclerosis Valvular heart disease	Ankylosing spondylitis Psoriatic arthritis Seronegative arthropathies Diffuse idiopathic skeletal hyperostosis
Genetic and developmental forms		
Fibrodysplasia ossificans progressiva Progressive osseous heteroplasia		

2.4.1. The Role of Inflammation and HO

In a simplified view, inflammation is a crucial niche factor for the development of heterotopic ossification (HO) and a common element across various conditions that predispose to its formation. HO is observed in autoimmune diseases such as limited cutaneous systemic sclerosis, dermatomyositis, and inflammatory arthritis. Autoimmune diseases affecting the nervous system, like anti-NMDA receptor encephalitis and Guillain-Barré syndrome, have also been reported as predisposing factors to HO. The logical connection between trauma-induced inflammation and bone formation stems from the inflammatory nature of the early stages of fracture repair. The use of NSAIDs for preventing traumatic HO and steroids for treating fibrodysplasia ossificans progressiva (FOP) is based on the theory that reducing postoperative inflammation will similarly reduce HO formation. Animal studies have started to uncover the complex and multifaceted role of the immune system in the genesis and propagation of HO[52].

2.4.1.1. Macrophages and HO

Macrophages play a crucial role in endochondral ossification and fracture repair. Research indicates their involvement in various mouse models of heterotopic ossification (HO) and in human HO as well. In a BMP4 overexpression model, macrophage depletion significantly reduces HO formation, highlighting their essential role. Similarly, in a mouse model of neurogenic HO involving spinal cord injury combined with muscle injury, macrophages were identified in HO tissue, and their depletion resulted in a marked reduction in HO formation[53].

Macrophage accumulation has also been observed in FOP patient samples. More specific depletion methods and characterization of the monocyte subpopulations that migrate to injury

sites are required. The paracrine activity and cargo delivered by macrophages in an HO setting are beginning to be examined. For instance, in a mouse model of neurogenic HO induced by spinal cord injury, macrophage-derived Oncostatin M was found to promote osteoblastic differentiation of precursor cells. Therefore, while macrophage infiltration and paracrine stimulation of HO formation are consistent across genetic, traumatic, and neurogenic HO models, further studies are needed to validate these findings and fully understand the macrophage's role in HO formation[54].

2.4.1.2. Mast Cells and HO

Mast cells may also play a significant role in the pathogenesis of heterotopic ossification (HO). Increased numbers of mast cells have been observed in nongenetic HO cases, often located near sites of ectopic bone formation. This increase in mast cell density is even more pronounced in fibrodysplasia ossificans progressiva (FOP), where it can be up to 150 times higher at the periphery of FOP lesions compared to other inflammatory myopathies[55]. Cromolyn, an FDA-approved drug for asthma, inhibits mast cell degranulation and has been shown to significantly reduce ectopic bone formation in both BMP2-induced and Acvr1 Q207D transgenic mouse models of HO and FOP, respectively[56].

Additionally, Imatinib, a c-kit tyrosine kinase inhibitor that induces mast cell apoptosis, has been found to decrease HO in a mouse model of traumatic HO (Achilles tenotomy)[56]. There is also evidence suggesting that mast cells and macrophages may synergize in inducing HO formation. Studies have shown that depleting both macrophages and mast cells reduces HO formation more effectively than depleting either cell population alone in the Acvr1 R206H knock-in mouse model

of FOP. This indicates that targeting both cell types might be a more effective strategy for reducing HO formation[57].

2.4.1.3. Lymphocytes and HO

The precise mechanisms behind heterotopic ossification (HO) are not well understood. Lymphocytic inflammation is a common histological feature of HO, particularly perivascular lymphocytic inflammation in peri-articular, nongenetic human HO. In HO associated with cardiac valves, a polyclonal chronic inflammatory infiltrate, including lymphocytes, mast cells, and plasma cells, is commonly found[58]. Similarly, lymphocyte accumulation is observed in the early stages of fibrodysplasia ossificans progressiva (FOP) lesions. Clinical and experimental evidence suggests that modulating lymphocytic inflammation may reduce HO formation. For instance, immunocompromised Rag1 mice, which lack B and T lymphocytes, show reduced HO formation after trauma[59]. Corticosteroids, which are used in experimental models of HO in mice, also inhibit HO formation. Clinically, immunosuppressive corticosteroids are employed during FOP flare-ups to reduce HO formation. Additionally, preoperative radiation in patients undergoing hip arthroplasty may alter the inflammatory environment, decreasing HO formation. A study on hematoma fluid from patients undergoing total hip arthroplasty found that those who received preoperative radiation as HO prophylaxis had decreased numbers of T regulatory cells, increased frequency of cytotoxic T cells, and changes in B-cell maturation[60].

2.4.1.4. Inflammation Induced by Trauma and HO

Traumatic injuries, as well as burn and blast injuries, are well-known causes of increased systemic inflammation and are predisposing factors to heterotopic ossification (HO) formation. These

associations have been confirmed experimentally. For instance, a study showed greater heterotopic bone formation when adipose-derived stem/stromal cells were implanted in mice subjected to 30% body surface area burns[61]. Conversely, traumatic HO has been reduced in experimental models by the application of apyrase at the injury site, which causes ATP hydrolysis and thereby reduces inflammation. Another study demonstrated that traumatic HO formation can be mitigated by the administration of rapamycin, which inhibits mTOR signaling and thereby alters the production of several inflammatory signals among other changes. Interestingly, targeting mTOR was also effective in preventing HO formation in a fibrodysplasia ossificans progressive (FOP) model[62].

2.5. Approaches to Osteogenesis

Although autologous bone grafts fulfill many criteria for effective bone regeneration, their use is accompanied by significant drawbacks, including complications related to harvesting, post-operative issues, and limited availability[63]. Unlike autologous bone, allogeneic and xenogeneic grafts are readily available and do not necessitate additional surgery on the patient. However, the processing techniques employed to eliminate the risk of immunogenic reactions negatively impact their osteoinductive and osteoconductive potential[64]. To address these limitations, a wide range of synthetic materials and strategies have been developed.

2.5.1. BMP- and Biomaterial-Induced Osteogenesis

Synthetic bone grafts can be categorized into four main groups based on their chemical composition: metallic implants (e.g., titanium and its alloys, stainless steel, and cobalt–chromium

alloys); ceramics (e.g., calcium phosphate, alumina, carbon, and glass ceramics); polymers (e.g., poly(methyl methacrylate), poly(urethane), ultra-high molecular weight polyethylene, silicon, and polylactide); and composites of the first three groups (e.g., calcium phosphate–ceramic coatings on metallic implants and polymer–ceramic composites)[3].

Osteoinduction, or bone formation at ectopic sites, was observed following the implantation of devitalized tissue and tissue extracts back in the early 20th century. In 1965, Urist conducted an experiment involving the intramuscular implantation of decalcified bone matrix treated with different chemicals into 250 rabbits, 20 rats, 10 mice, and 5 guinea pigs. New bone deposits began to appear at 4 to 6 weeks from osteoprogenitor cells. Between 8 and 16 weeks, bone formation was observed, characterized by vascularization, calcification, and the replacement of cartilage. The new bone never extended beyond the implant area. Urist reported that wandering histiocytes, foreign body giant cells, and inflammatory connective tissue cells, stimulated by degradation products of the dead matrix, repopulated the implant area. This process led to new bone formation through autoinduction, where both the inducer and induced cells originated from the host's ingrowing cells. The inducer cell was identified as a descendant of a wandering histiocyte (circulating macrophage), while the induced cell was a fixed histiocyte (stationary histiocytes) or a perivascular young connective tissue cell[65]. Subsequent work by Urist and Strates concluded that a specific protein, named bone morphogenetic protein (BMP), plays a crucial role in the cascade of events leading to bone formation[66].

In 1973, de Groot explained that bone induction occurs when the concentration of BMP, which is positively charged and present in vivo, reaches a sufficiently high level. Both in vivo calcification and the presence of a negative surface charge were identified as possible causes for this

concentration, thereby enabling bone induction[67]. Since then, numerous publications have demonstrated osteoinduction using various calcium phosphate biomaterials.

In 1995, Ripamonti conducted a study on heterotopic bone formation in different animal species using coral-derived porous hydroxyapatite. The constructs were implanted in the rectus abdominis muscles of adult rabbits, dogs, and baboons. Specimens harvested 90 days post implantation. The study found minimal bone formation in rabbits and dogs, while substantial bone differentiation occurred in baboons. Ripamonti discussed that bone induction in porous hydroxyapatites depends on three critical parameters. Firstly, the animal model plays a significant role, as minimal osseous formation was observed in rabbits and dogs, and it has been reported that intramuscular or subcutaneous implantation of porous hydroxyapatite in rats does not result in bone formation. Secondly, the chemical and surface characteristics of the hydroxyapatite substrata are crucial, with resorbable hydroxyapatite calcium carbonate implants failing to induce bone differentiation. Thirdly, the geometry of the hydroxyapatite is essential, as bone formation was observed only in porous hydroxyapatite with a block configuration, not in identical hydroxyapatite in granular configuration. Ripamonti suggested that porous hydroxyapatites might act as a solid-state matrix for the adsorption, storage, and controlled release of bone morphogenetic proteins (BMPs), which locally initiate bone formation. Different concentrations of putative circulating or locally produced BMPs, influenced by the distinct skeletal homeostasis between rodent and primate models, may account for the dramatic morphological differences observed between the species[68].

To compare host tissue responses to ceramic scaffolds across different animal species and implantation site, Yang, et al implanted synthetic porous calcium phosphate ceramics (HA/TCP)

intramuscularly and subcutaneously in dogs, pigs, goats, rabbits, and rats. Specimens were harvested at different intervals post-implantation. In dogs and pigs, bone formation was detected after 45 days of intramuscular and 60 days of subcutaneous implantation. However, no detectable bone formation was observed in goats, rabbits, and rats until 120 days[4].

Yuan et al. demonstrated bone formation in intramuscularly implanted porous glass ceramic for the first time. They implanted porous glass ceramic cylinders (5 mm in diameter and 6 mm in length) into the thigh muscles of dogs for three months. Histologic analysis, backscattered scanning electron microscopy (BSE), and energy dispersive X-ray microanalysis (EDX) confirmed bone formation in all implants[69].

The exact mechanism of osteoinduction by biomaterials remains unknown. In a review by Habibovic et al. it is reported that endogenous BMPs are collected on the biomaterial surface, leading to ectopic bone formation. There are three notable differences between osteoinduction by BMPs and biomaterials: (a) bone induced by biomaterials is always intramembranous, whereas BMP-induced bone typically forms via the endochondral pathway; (b) in small animals such as rodents, bone is rarely induced by biomaterials but readily induced by BMPs; and (c) while bone formation by biomaterials occurs inside their pores and never on the periphery, BMP-induced bone is often observed on the outside of the carrier and even in the soft tissue distant from the carrier surface[3].

2.5.2. Diaphragm-Mediated Osteogenesis

Selye et al. designed cylinders in different shapes and materials such as glass, plastic, metal, etc., and reported tissue growth with a predictable shape and structure if subcutaneously implanted

in rats. They explained that upon subcutaneous insertion of simple glass tubes with two openings, 10 mm in diameter and 30 mm in length, the two ends are closed by connective tissue and become connected by a central fibrinous bridge. This bridge is replaced by a vascularized cord consisting of collagen fibers and fibroblasts surrounded by yellow protein-rich fluid. They called these cylinders “tissue diaphragms” as they allow tissue growth only in one desired direction. This direction can be modified by changing the geometry of the tube; for example, by adding a hole in the tube wall, an anastomosis occurs, and the central cords connect in a Y- or T-shaped fashion, while a new basal plate forms in the additional opening. After about two months, the constructs tend to degenerate. The appearance of histiocytes containing lipid or iron appear and giant cells leads to the disintegration of vessels and then the cord into a hemorrhagic mass. They interpreted this degeneration as a result of metabolic isolation of the central cord by the wall of the diaphragm and surrounding tissues[70].

They also implied that a spiral-shaped scaffold, which is able to fix water, results in a similar effect albeit at a slower rate. Additionally, they found applying pressure or suction to the construct, another crucial factor in the quality and quantity of induced tissue[71].

To establish the most favorable condition for bone induction, they conducted another experiment[72]. They explained a wide but comparatively short glass cylinder serves best. Therefore, they placed Pyrex glass cylinders (20 mm in length and 30 mm in diameter) with dorso-ventrally orientation subcutaneously in their lower thoracic and upper lumbar fascia of the back of rats (Figure 2.6)[72].

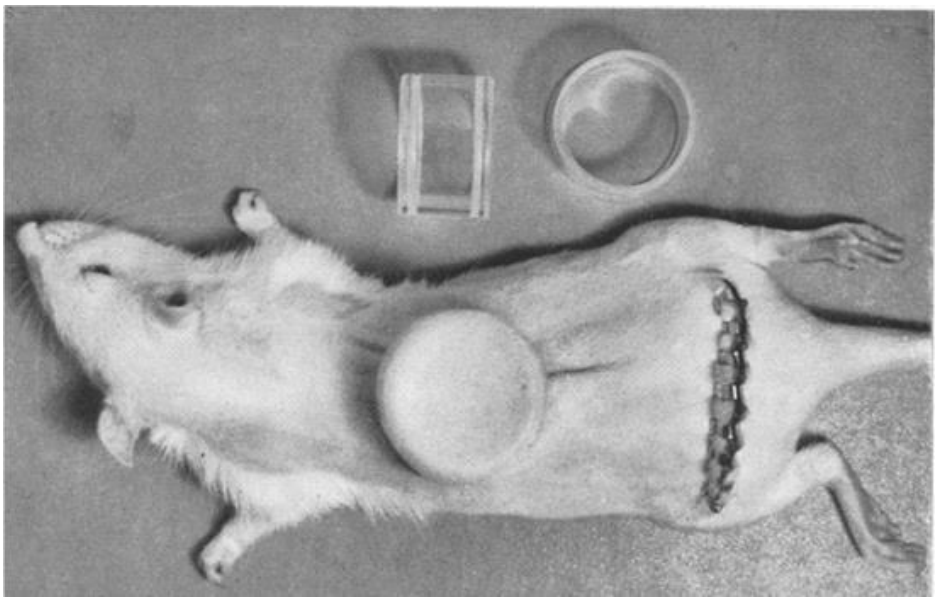

Figure 2.6. A photograph showing Selye's tissue diaphragm implanted subcutaneously. Reproduced with permission from Hans Selye et al., "Induction of bone, cartilage and hemopoietic tissue by subcutaneously implanted tissue diaphragms," *Wilhelm Roux' Archiv für Entwicklungsmechanik der Organismen*, December 31, 1969. © 1969 Springer-Verlag.[72].

They sorted animals into two groups, one was injected India ink into the lumen of the cylinder to block the phagocytic system but left the other one with no further intervention. They observed after a while, that air absorption leads to deep drawing of the skin and sealing the openings of the cylinder. To preserve the cavity of the cylinder, they stretched the overlying skin and cut out the excess skin over the abdomen. They kept the animals 60 days post operatively. They found the same growth cords of 3-4 mm in diameter along the axis of the tube in all animals. They identified bony and cartilaginous structures in the hard areas of the cord and in the basal plates at a distance from the cord insertion in 7 rats out of 10 in group 1. Two rats in this group showed small ossification areas, and no detected bone in one rat. None of animals in the India ink group showed ossified areas. In this group, carbon granules were observed only in central cord not basal plates except in the insertions. They believed the earliest sign of the impending ossification was

the appearance of calcium-salt granules in the histiocytes. These cells were found in an arranged rows surrounded by collagen fibers in the cord and randomly scattered in the connective and adipose tissue of basal plates. They observed encapsulated adipose tissue with calcium granules within the capsule, developed at the insertion points. Moreover, solid bone shells were found around the adipose tissue, apparently following the granular calcification in connective tissue. Interestingly, the ossified structures were found in both types of solid or filled with bone marrow, resembling flat cranial bones and tubular bones with a central marrow cavity, and cartilaginous plates (Figure2.7). Some of these long bones were comparable in size and shape to the tibiae of rats. Interestingly, they observed marrow formation preceded bone formation in strands of myeloid tissue in adipose islands where osseous tissue could not be detected. They also found islets of myeloid and lymphoid tissue around the blood vessels (Figure 2.8). In the India ink group, they detected carbon-phagocytic histiocytes in the cords and basal plates. They also found some histiocytes free on carbon in the periphery of the cord which they thought were formed after completion of the adipose islets. Hematopoietic elements mostly lymphoid cells were also present within the adipose tissue and the carbon-containing histiocytes layers[72].

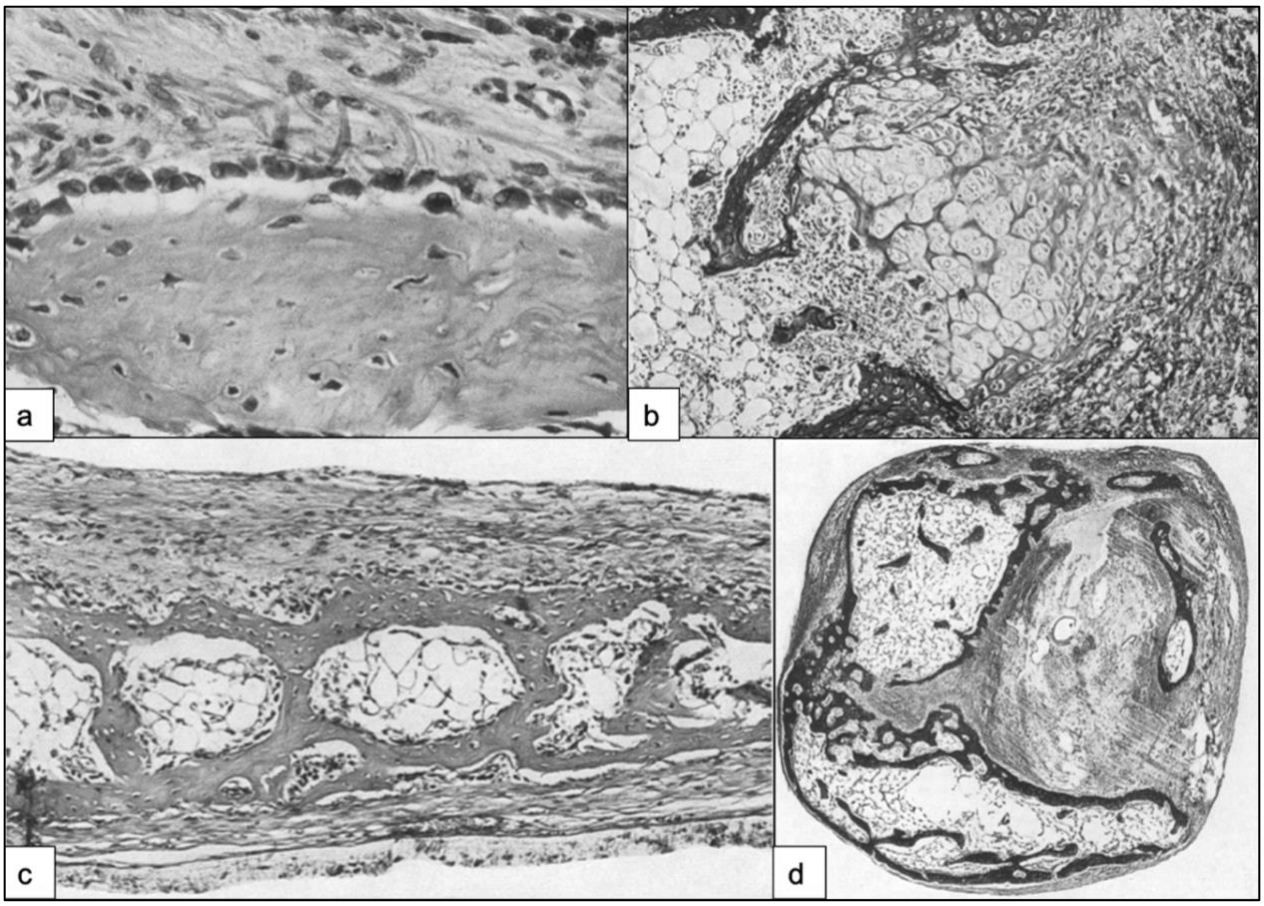

Figure 2.7. Histologic examination of Selye's specimens: a. Intramembranous ossification of a bone spicule lined by a row of osteoblasts, b. Endochondral ossification with a junction plate in the center separated from the bone marrow on the left, c. Squamous bone in the basal plate with marrow cavities and surrounded by periosteum, d. Cross-section of a growth cord near the insertion, showing both flat and tubular bones representing the transition area from flat bone in the basal plate to tubular bone in the growth cord. Reproduced with permission from Hans Selye et al., "Induction of bone, cartilage and hemopoietic tissue by subcutaneously implanted tissue diaphragms," *Wilhelm Roux' Archiv für Entwicklungsmechanik der Organismen*, December 31, 1969. © 1969 Springer-Verlag.[72].

They concluded that inducing ectopic bone formation is achievable through purely mechanical means. They also noted that the degenerative sequestration, which occurs after two months in thin and fragile growth cords developing within narrower cylinders, does not occur in short and wide cylinders with shorter and broader cords. They did not determine whether the tension following the additional skin stretching was a responsible factor for the observed conditions. They

mentioned, the formation of adipose tissue, bone marrow and lymphatic tissue, but not bone in India ink group, would suggest that forced phagocytosis can block specific morphologic responses to local stress situations selectively[72].

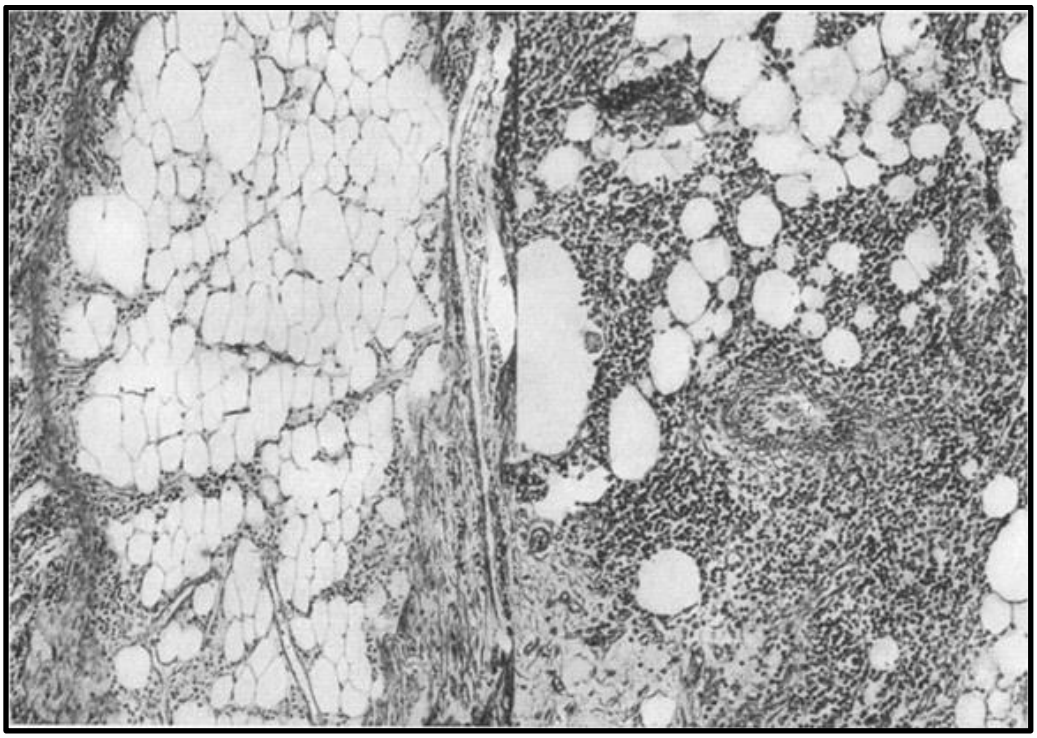

Figure 2.8. Histologic examination of Selye's specimens: Left - Extramedullary hematopoietic tissue with predominant adipose tissue, encapsulated by connective tissue without ossification; Right - Extramedullary hematopoietic tissue around a central artery with few fat cells. Reproduced with permission from Hans Selye et al., "Induction of bone, cartilage and hemopoietic tissue by subcutaneously implanted tissue diaphragms," *Wilhelm Roux' Archiv für Entwicklungsmechanik der Organismen*, December 31, 1969. © 1969 Springer-Verlag[72].

Selye believed that by inducing local stress, these scaffolds initially trigger nonspecific topical stress reactions, such as inflammation and wound healing. However, specific responses can be achieved, the nature of which can be largely controlled by altering the time (duration of the experiment), site (the spatial configuration of the scaffolds), and the intensity (the dimensions of the diaphragm and the stretching of the skin)[72].

2.5.3. Bone Marrow-Induced Osteogenesis

Osteogenesis capacity of bone marrow after transplantation in soft tissue sites was recognized through various studies that demonstrated its osteogenic properties. Building on this foundational knowledge, several studies explored bone formation in marrow-enriched composite materials.

Salama. et al, compared sheep and calf cancellous bone grafts impregnated with autologous red marrow from Wistar rats and implanted intramuscularly as composite xenograft-autografts for two to twelve weeks. Only one out of 223 devitalized bone xenografts implanted without autologous marrow formed new bone, while 216 out of 223 xenografts transplanted with marrow successfully formed new bone. The new bone primarily originated from the rat's marrow, with no observed bone-inducing effect from the different types of xenografts used. Grafts from fully deproteinized sheep iliac bone had the highest new bone formation scores, likely because they were less likely to provoke an immune response, allowing marrow cells to differentiate into bone cells more effectively. In contrast, grafts from intact or partially treated sheep bone and calf bone showed lower new bone formation[73].

In addition to the aforementioned study on xenogenic bone, various types of carrier matrices have been examined in other studies. In 1979 Nade reviewed on recombinants of allogenic cancellous bone and autologous bone marrow and explained the importance of “bone bank” in combination with living cells. He suggested that surgeons should use the capacity of bone marrow to reach the desired results[74].

Ohgushi. et al, reported that bone formation in subcutaneous or intramuscular implantation of porous calcium phosphate ceramics combined with marrow cells while only fibrovascular tissue growth was observed in untreated ceramics. They indicated that intramembranous osteogenesis began at week three after surgery[75].

The effectiveness of alternative grafting materials, such as bone marrow and bone marrow composites, has been evaluated in comminuted fractures, long bone nonunions, and critical-sized segmental defects in various animal models. Analysis of orthotopic bone regeneration by marrow in rat models revealed that by adding a sufficient amount of bone marrow in a fresh femoral defect showed a union bone formation comparable with autologous bone grafts. After injecting marrow in femoral nonunions, significant bone formation occurred, although union and remodeling did not happen. Dead bone marrow resulted in minimal cellular infiltration and bone formation[76].

Using whole bone marrow alone has shown mixed results regarding its ability to support sufficient bone formation within defects for successful bony union. The fluid consistency of whole bone marrow makes it challenging to retain at the defect site long enough to support osteogenesis. This fluidic nature also hinders its capacity to provide the mechanical stabilization needed for cortical bridging and bony continuity. It has been suggested that larger volumes of marrow, potentially exceeding the size of the defect, might be necessary to ensure proper healing[77].

Chapter 3. Methodology

In this chapter, the methods used to replicate Selye's work will first be described. Then, the methods used to assess outcomes will be reported.

3.1. Implant Design and Characteristics

The space-preserving diaphragms were made of two materials with different stiffness. To make hard tubes, ultra-high-temperature quartz glass tubes (McMaster-Carr, USA, product number 4100N22) were used. The tubes had an outer diameter (OD) of 9 mm, a length of 12 inches, and a wall thickness of 1 mm. These quartz glass tubes were cut using an electric drill operated at a speed of 8000 RPM and a diamond cutting disc made of carbon steel, with a diameter of 25 mm, and a thickness of 0.60 mm. Bullet-shaped sanding heads were used to polish the freshly cut edges. The final tubes were categorized into two groups with 6 mm and 3 mm heights, both sharing the outer diameter of 9 mm (Figures 3.1.c,d).

The same instruments were used to create hemi-cylinders out of quartz glass with diameter (the distance across the base) of 9 mm, Height (The vertical distance from the base to the top of the curved surface) of 6 mm, and Length (The distance from one side of the base to the opposite side) of 9 mm (Figure 3.1.e).

To create nonrigid tubes, we used flexible, clear, food-grade silicone tubes with an outer diameter of 9.5 mm and a wall thickness of 1.6 mm. The tubes were cut using a razor blade into tubes measuring 6 mm and 3 mm in height, leaving smooth edges without the need for further trimming (Figures 3.1.a,b).

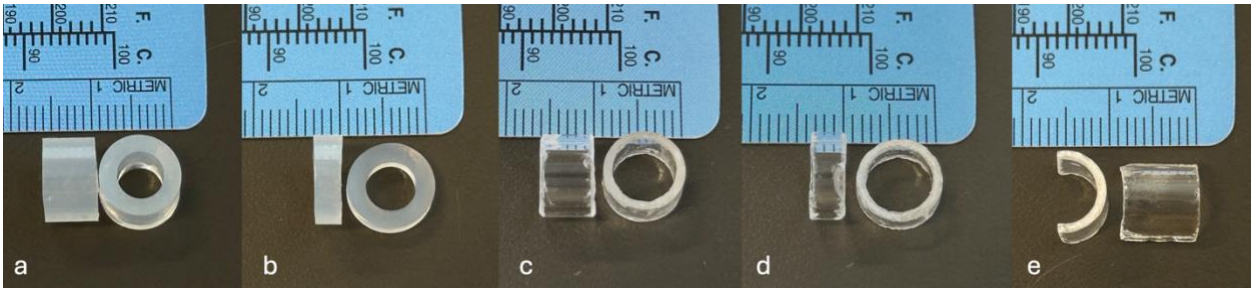

Figure 3.1. Photograph of a,b. Silicone tubes, c,d. Glass tubes, e. Hemi-cylindrical glass tubes used in experiments.

3.2. Experiment Design and Surgical Procedure

All procedures of this pre-clinical study were started after approval at McGill University Animal Care Committee (AUP 7660). 46 adult male Wistar rats (35-40 days old, weighing 300-350g) were purchased from Charles River Laboratories (Montreal, Canada). They were kept in spacious, well-ventilated cages, at anonrigi controlled temperature (20-24°C) and humidity (40-70%) at the Animal Resources Division (ARD) at the Research Institute of the McGill University Health Centre (RI-MUHC). The animals were allowed a one-week acclimation period prior the procedures. All animals were anesthetized using isoflurane gas by placing them in the induction chamber, then maintaining anesthesia with a lower concentration (1-3%) during the procedure. Post-surgery, isoflurane was discontinued, and the animals were given 100% oxygen until recovery. To achieve analgesia, 1 mg/kg slow-release buprenorphine was injected subcutaneously before surgery and 5 mg/kg carprofen 30 minutes prior, continuing daily carprofen treatment for two more days post-surgery.

3.2.1. Experimental and Control Groups

3.2.1.1. Subcutaneous Implantation of Glass Tubes

In the first group, two animals (N=2) underwent implantation surgery. After shaving and cleansing the surgical field with antiseptic solution, a 2 cm incision was made deep to the subcutaneous layer in the nuchal area. A fascial pocket was created over the skull using a blunt haemostat. A glass tube (6 mm height, 9 mm outer diameter) was inserted into the pocket. The incision was closed in two layers: absorbable 4-0 Vicryl® sutures were used for the subcutaneous layer, and non-absorbable 4-0 Prolene® sutures were used for the skin (Figure 3.2). The animals were kept for 8 weeks postoperatively.

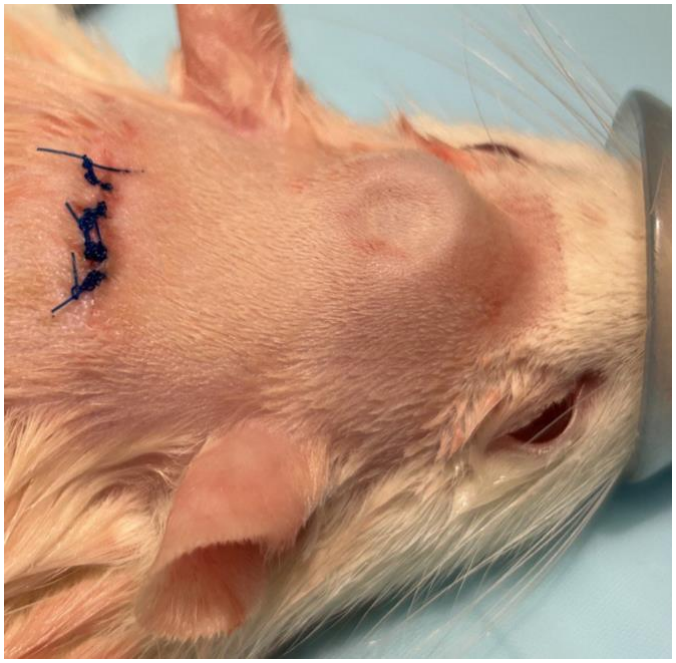

Figure 3.2. Photograph showing subcutaneous insertion of the glass tube.

3.2.1.2. Subcutaneous Implantation of Silicone Tubes

Eight animals (N=8) were assigned to the second group, and Silicone tubes (6 mm height, 9.5 mm outer diameter) were inserted using the same procedure as in the first group. They were also maintained for a similar duration (8 weeks) post-surgery.

3.2.1.3. Subperiosteal Implantation of Glass Tubes

The third group comprised three animals (N=3). After administering anesthesia, the surgical site was shaved and sterilized with an antiseptic solution. A 2 cm incision was made along the midline, extending from the frontonasal suture to just caudal to the middle sagittal crest or bregma, deep to the subcutaneous layer. Using a scalpel, a full-thickness incision was carefully created, starting at the anterior edge and moving towards the posterior base within the temporal ridges on both sides. The rectangular periosteal flap was then lifted from the underlying bone using a periosteal elevator. Subsequently, a glass tube (6 mm height, 9 mm outer diameter) was placed over the intact calvarial bone, and the flap was secured around the tube using absorbable 4-0 Vicryl® sutures. Finally, the skin incision was closed with non-absorbable 4-0 Prolene® sutures (Figure 3.3). All animals were maintained for 8 weeks after surgery.

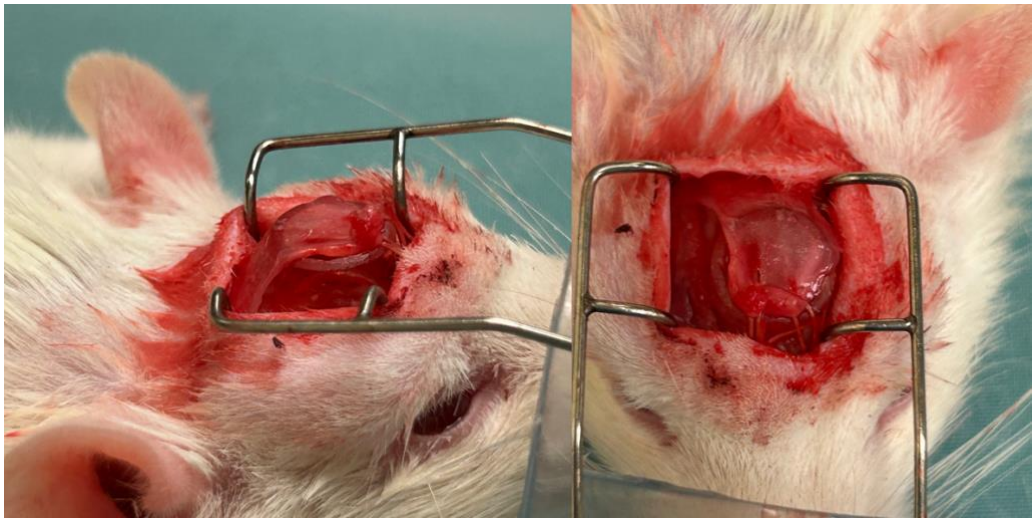

Figure 3.3. Photograph showing subperiosteal insertion of the glass tube.

3.2.1.4. Subperiosteal Implantation of Silicone Tubes

For the fourth group (N=3), the same procedure as the third group was performed using silicone tubes (6 mm height, 9.5 mm outer diameter). Animals were kept for 5 weeks postoperatively.

3.2.1.5. Bone Decortication and Subperiosteal Implantation of Glass Tubes

Following the same procedure of incision and periosteal elevation mentioned above, the fifth group (N=2) underwent a bone decortication procedure by creating several mono-cortical holes through the calvarial bone. These holes were made using a carbide round-shaped #1/4 surgical bur (Patterson Dental, US) with head dimensions: diameter of 0.5 mm and length of 0.5 mm. A glass tube (6 mm height, 9 mm outer diameter) was placed over the decorticated bone, and the periosteum was replaced over the tube before closing the incision (Figure 3.4). Animals were housed for 5 weeks postoperatively.

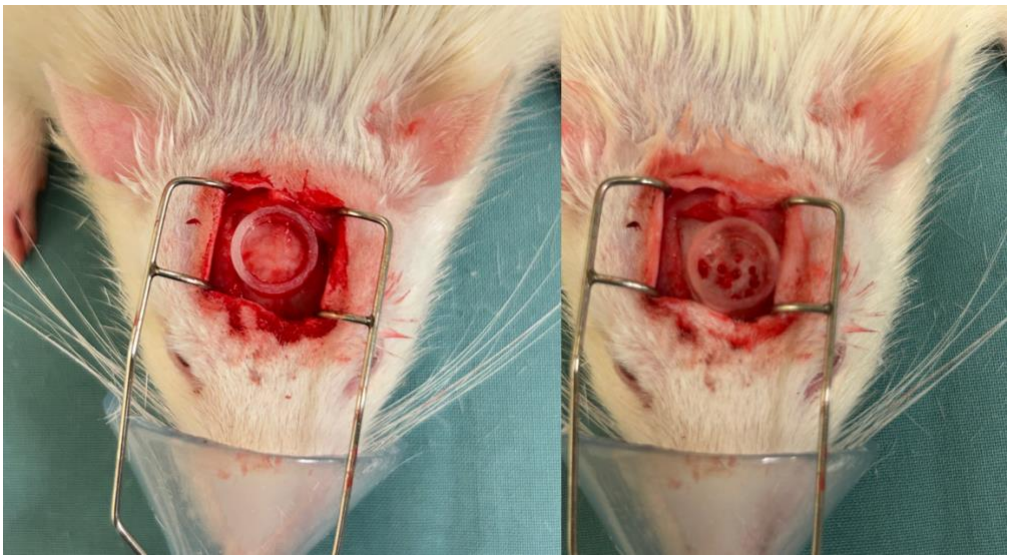

Figure 3.4. Photograph showing bone Decortication and insertion of the glass Tube.

3.2.1.6. Periosteum Excision Following the Implantation of Glass Tubes

After incision and periosteal elevation in the sixth group (N=2), the periosteum was excised, and the glass tube (6 mm height, 9 mm outer diameter) was covered solely with skin. Animals in this group were monitored for 5 weeks post-surgery.

3.2.1.7. Subperiosteal Implantation of Short Glass Tubes

The procedure similar to that performed on the third group was repeated in the seventh group (N=2) using short glass tubes (3 mm height, 9 mm outer diameter). These animals were housed for 5 weeks following surgery.

3.2.1.8. Subperiosteal Implantation of Hemi-cylindrical Glass Tubes

The eighth group (N=2) underwent subperiosteal implantation of hemi-cylindrical glass tubes (9 mm diameter, 6 mm height, and 9 mm length), following a procedure similar to that described for the third group. Animals were monitored for 5 weeks postoperatively.

3.2.1.9. Subperiosteal Implantation of Glass Tubes over the Calvarial Defects

Six male Wistar rats were assigned to the ninth group (N=6). Following a vertical skin incision over the midsagittal skull, the periosteal flap was elevated, and a bicortical calvarial defect (diameter: 6mm) was created using a trephine bur (TPL-4) with an internal diameter of 4.0mm. A glass tube (6 mm height, 9 mm outer diameter) was then placed over the defect and fixed with sutures. The periosteum was replaced, and the overlying skin was closed using non-absorbable sutures (Figure 3.5). Animals in this group were monitored for 5 weeks.

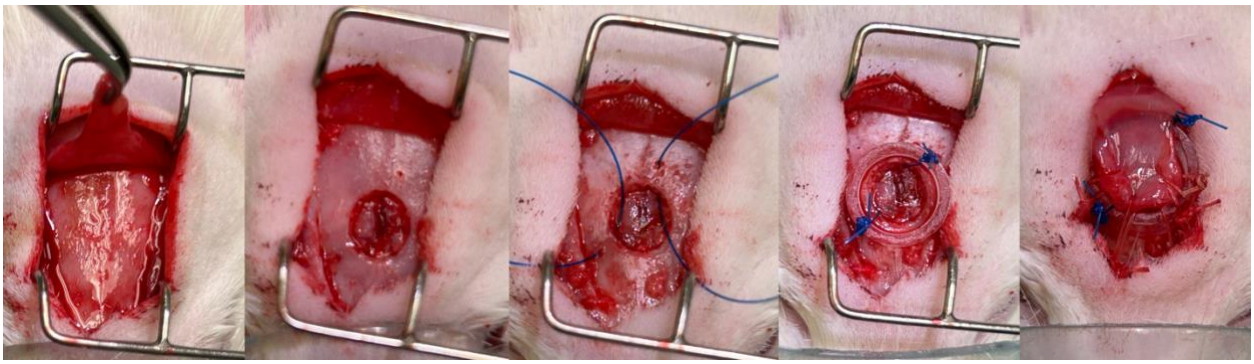

Figure 3.5. Photograph showing the step-by-step surgical procedure of insertion of the glass tubes over the calvarial defect.

3.2.1.10. Subperiosteal Implantation of Short Glass Tubes over the Calvarial Defects

The same procedure as performed in the ninth group was carried out in the tenth group (N=6) using shorter glass tubes (height: 3 mm, outer diameter: 9 mm). These animals were kept under observation for 5 weeks after the surgery.

3.2.1.11. Subperiosteal Implantation of Silicone Tubes over the Calvarial Defects

A similar procedure to that used in the previous two groups was performed on the eleventh group (N=1) using silicone tubes (height: 6 mm, outer diameter: 9.5 mm). The animal was monitored for 5 weeks post-intervention.

3.2.1.12. Subperiosteal Implantation of Short Silicone Tubes over the Calvarial Defects

The twelfth group consisted of 2 animals (N=2) in which silicone tubes (height: 3 mm, outer diameter: 9.5 mm) were inserted subperiosteally over the calvarial defects using the same procedure described above. The postoperative duration for this group was 5 weeks.

3.2.1.13. Control Empty Calvarial Defects

The control group (N=6) underwent the surgical procedure of creating calvarial defects with a diameter of 6 mm, leaving the defect empty with no further intervention. The elevated periosteum was replaced over the skull, and the dermal incision was closed in the same manner as in the experimental groups. The control group was monitored for 5 weeks after surgery.

The schematic summary of all experimental groups is shown in Figure 3.6 and Figure 3.7.

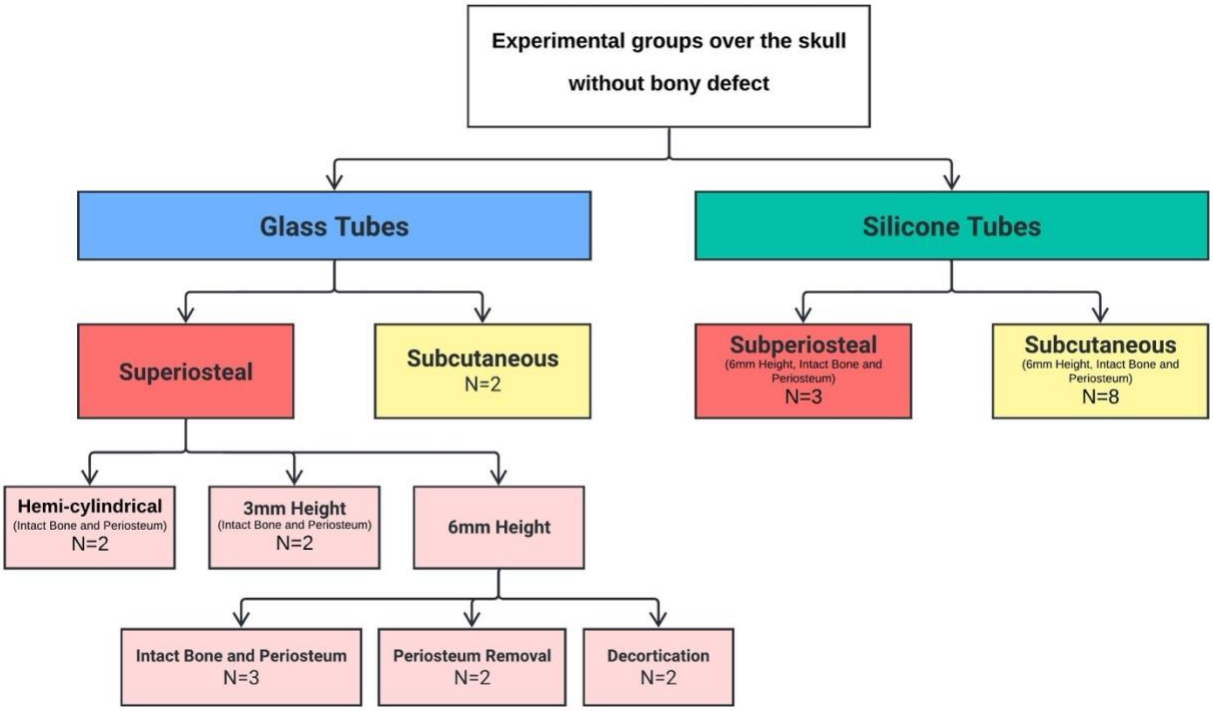

Figure 3.6. Schematic summarizing of experimental groups over the skull without bony defect.

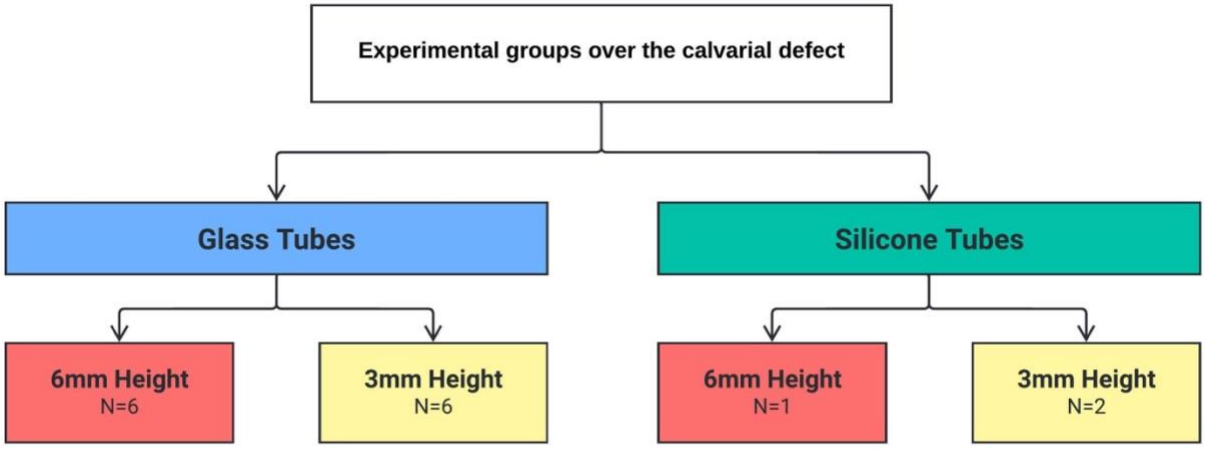

Figure 3.7. Schematic summarizing of experimental groups over the defect.

3.2.3. Euthanasia and Explantation

Euthanasia was performed after the 5-week postoperative period for all groups except the first three groups, which were kept for a longer period of 8 weeks. The animals were euthanized following established protocols to minimize suffering. Isoflurane 5% was used in combination with oxygen to deeply anesthetize the animals, after which CO_2 was administered at a rate of 12 L/min. Once the animals stopped breathing and death was confirmed, the calvarial region including skin and bone were carefully explanted for further analyses.

3.3. Evaluation

After explantation, the calvarial specimens were fixed in 4% paraformaldehyde (PFA) for 48 hours at 4°C. Following the fixation period, the specimens were rinsed with phosphate-buffered saline (PBS) to remove excess PFA and prevent over-fixation. At this step, the specimens were ready for micro-computed tomography (micro-CT). Following the micro-CT analysis, the samples were decalcified in 10% ethylenediaminetetraacetic acid (EDTA) solution for 4-5 weeks at room temperature on an orbital shaker set to 50 rpm. Throughout this period, the solution was changed regularly to ensure complete decalcification. Decalcification was confirmed through micro-CT images when no high-contrast structures remained. Once decalcification was complete, the specimens were transferred into 70% ethanol and kept at 4°C before histological analysis.

3.3.1. Macroscopic Assessment

To evaluate the structures formed inside the tubes, the specimens were either bisected or a window was created in the walls. For the removal of the glass tube, the specimen was frozen at -20°C. A circumferential full-thickness incision using a No. 11 surgical blade was made through the skin to reach the glass tube. While the tube was being pulled out, liquid HistoGel™ was injected into the void to preserve the shape and integrity of the fine structures. Once the glass tube was removed, the specimen was refrozen and bisected.

The silicone tubes did not require removal. In the subperiosteal group, the tubes were bisected, while in the subcutaneous group, a window was created in the tube wall. Liquid HistoGel™ was then injected into the voids. This procedure was performed after decalcification in the subperiosteal group. In the subcutaneous group, the tubes, along with their surrounding capsule and periosteum, were separated from the underlying bone and other tissues before starting the decalcification process.

3.3.2. Micro-CT Analysis

Calvarial explants were placed vertically in a tube with the nasal bone positioned superiorly. The tubes were mounted in a µ-CT scanner (SkyScan 1172; SkyScan, Kontich, Belgium) and scanned at 50 kV, 200 µA, using a 0.5 mm aluminum filter, a voxel size of 13 µm, and a rotation step of 0.6 mm. The images were reconstructed using NRecon software (Version 1.6.2.0; SkyScan) with a smoothing factor of 1, an artifact ring correction of 10, a beam-hardening correction of 20%, and an image-conversion range from 0.007 to 0.061.

Using Data Viewer software (Version: 1.7.0.1, 64-bit, Bruker), the images were loaded for 3D viewing and observed on three planes: Coronal (X-Z), Sagittal (Z-Y), and Transaxial (X-Y). Minimal rotation was applied for further alignment and analysis accuracy, and each plane was saved as a dataset. Using the Sagittal and Transaxial planes, the inferior border of the skull was defined, and the corresponding coronal image was identified (Figure 3.8). The coronal dataset was loaded into CTAn software (Version: 1.32.0.2, 64-bit, Bruker), and the image matching the inferior border was set as the top of selection (Figure 3.9). The same method was applied to set the bottom of selection at the superior border of the skull. A round interpolated region of interest (ROI) with a diameter of 6 mm, indicating the defect dimension, was selected. The grayscale histogram range was set from 50 to 255, to include higher intensity values and reduce noise from lower-intensity regions. To compare defect healing and evaluate the newly formed bone within the defect, the parameters of Bone Volume (BV), Bone Volume Fraction (BV/TV) were measured. The definition of these parameters is shown in Table 3.1[78].

Table 3.1. Parameters measured by micro-computed tomography (CT) analysis.

Parameter	Abbreviation	Description	Standard Unit
Bone Volume	BV	Total bone volume	mm^3
Bone volume Fraction	BV/TV	Ratio of the segmented newly formed bone volume to the total volume of the region of interest	%

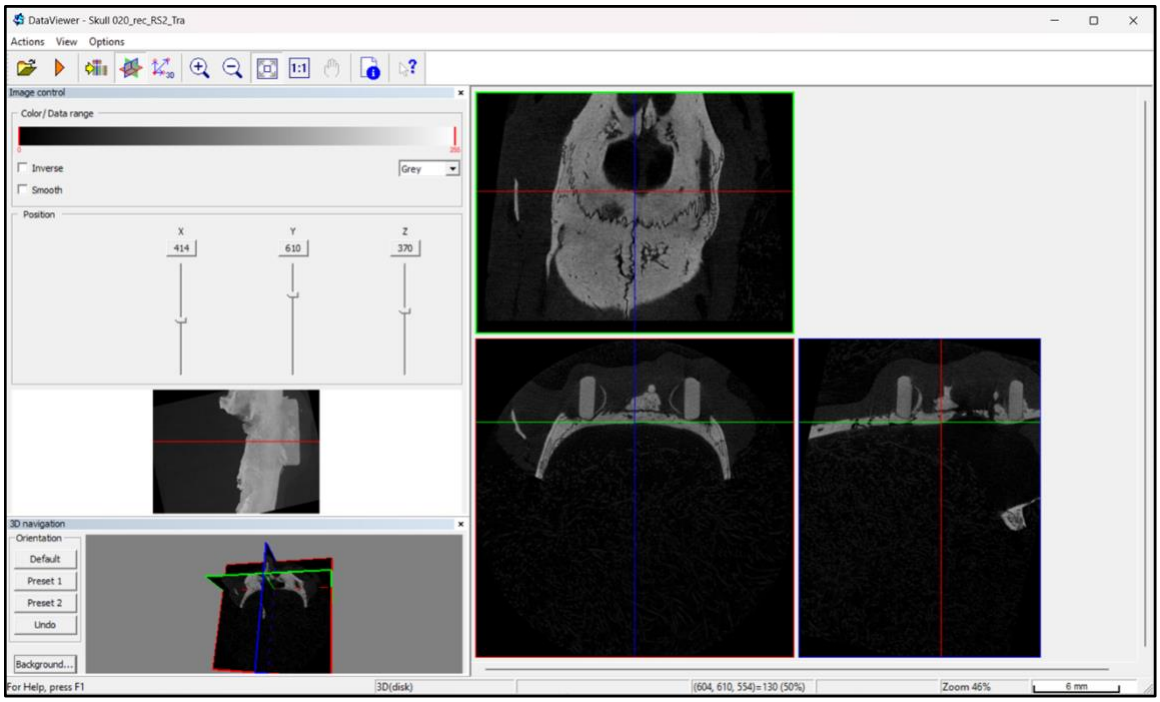

Figure 3.8. Screenshot of Data Viewer Software. The image displays three planes aligned into the desired position with minimal rotation. The inferior border of the skull is marked by a green line in the transaxial and sagittal views (bottom right), while the corresponding coronal view is displayed in the upper right image.

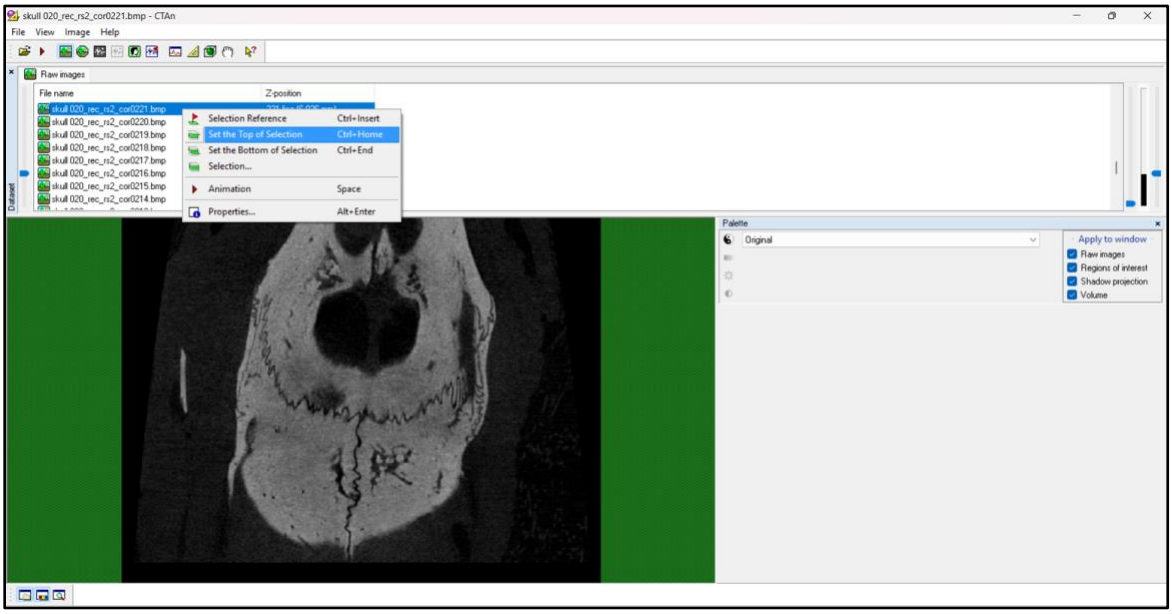

Figure 3.9. Screenshot of CTAn Software. The coronal dataset was loaded into CTAn software. The image matching the selected inferior border in Data Viewer was identified, and the option 'Set as the top of the selection' was chosen using the right-click menu.

To evaluate total bone formation within the tubes placed over the defect, the bottom of the selection was adjusted to the uppermost layer of the tube, and the ROI dimension from the superior border of the skull was extended to encompass the inner space of the tube.

To define the ROI in specimens without a defect, the entire inner space was manually selected in the transaxial dataset (Figure 3.10).

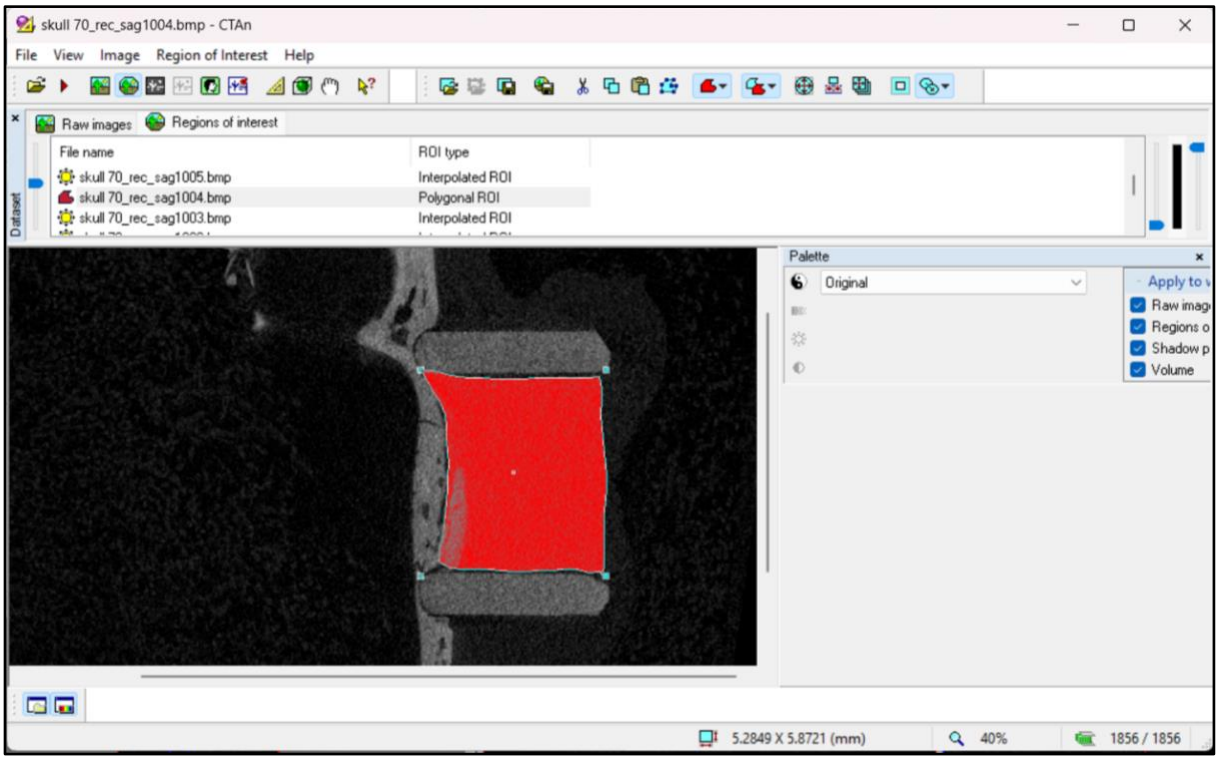

Figure 3.10. Screenshot of CTAn Software. The transaxial dataset of the samples without bony defect was loaded into CTAn software. The entire inner space of the tube was manually selected to define the region of interest (ROI).

3.3.3. Histology

After micro-CT analysis, as mentioned earlier, the samples containing bone were decalcified in 10% EDTA at room temperature for 4-5 weeks with regular solution changes. Following decalcification, the specimens were bisected and embedded in paraffin using standard protocols. Longitudinal sections, 4 µm-thick, were prepared using a microtome. These sections were stained with Hematoxylin and Eosin (H&E). The stained slides were examined under a light microscope at magnifications of 4x, 10x, 20x, 40x to assess the tissues formed inside the tubes.

3.3.5. Statistical Analysis

Data were described using count, mean, standard deviation (SD), minimum, and maximum values. Statistical analysis was performed using R 4.4.1 and RStudio (Version 2024.04.2+764), with one-way analysis of variance (ANOVA) followed by Tukey's HSD test. A p-value of < 0.05 was defined as indicating statistical significance. Box plots were used to display the minimal and maximal values, the 1st and 3rd quartiles, the median value, and the mean value.

Chapter 4. Results

4.1. Macroscopic Evaluation

4.1.1. Silicone Tubes

Gross examination of silicone tubes after explantation showed the formation of one central narrow cord connecting skin to the basal connective tissue in subcutaneous and subperiosteal implantation of tubes with 6mm height placed over the intact skulls. By placement of this tube over the defect, several cords yet narrow formed. However, a thick and short tissue in the placement of short silicone tubes formed over the calvarial defects (Figure 4.1).

The compressive effect of tubes on the skulls, indicated by bone thinning at the points of contact was evident in all categories except the subcutaneous implants.

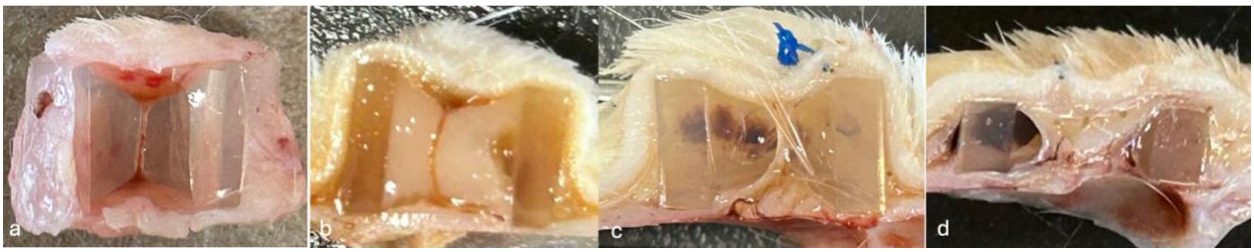

Figure 4.1. Photographs of cross-sectional views of silicone tubes in different categories: a. Subcutaneous implantation of a silicone tube, b. Subperiosteal implantation of a silicone tube, c. A silicone tube over the defect, d. A short silicone tube over the defect. Note that in the subcutaneous category, the tube is separated from the underlying periosteum and bone, whereas in the other groups, bone is attached to the tube and surrounding tissues.

4.1.2. Glass Tubes

The central cords in all these groups were short and thick. Among them, the short tubes, had the greatest volume and thickness of the central tissue (Figure 4.2.e,g). However, it had the least width in the group where periosteum was excised, followed by the subcutaneous implants. This

connection from top to bottom of the group without periosteum was too fragile to withstand the pulling force during the removal of the glass tube, resulting in tearing. In this group, red discoloration, indicating excessive hemorrhage due to surgical periosteum removal and instability of the tube without fixation over the skull, was observed at the base (Figure 4.2.c).

In groups with defects, bone formation within the cord was evident except in two specimens with regular-sized glass tubes.

The pattern of the skin-base connector cord was different in the hemi-cylindrical implants. This cord consisted of two strands two inserting into the skin at the upper edges on both sides, merging at the base to form an inverted C-shape pattern in mid-sagittal cross-sections (Figure 4.2.h).

Bone thinning due to the tube compression was observed in all samples.

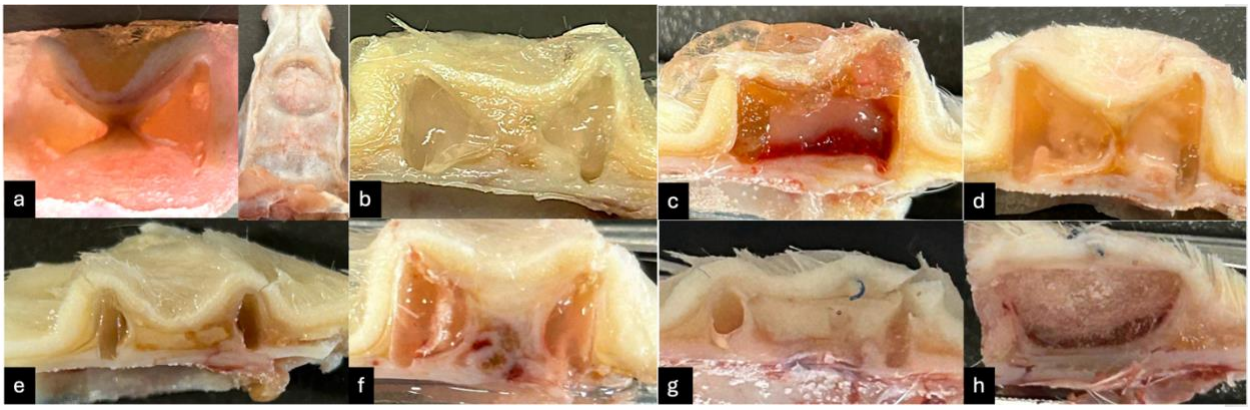

Figure 4.2. Photographs of cross-sectional views of Glass tubes in different categories: a(left). Subcutaneous implantation of a glass tube, a(right). Skull after periosteal separation demonstrating the tube's compressive effect over time, b. Subperiosteal implantation of a glass tube, c. Periosteal removal after implantation of a glass tube, d. Subperiosteal implantation of a glass tube and decortication, e. Subperiosteal implantation of a short glass tube, f. A glass tube over the defect, g. A short glass tube over the defect, h. Subperiosteal implantation of a hemi-cylindrical glass tube.

4.2. Micro-CT Analysis

Micro-CT analyses provided detailed three-dimensional information, including measurements of bone quantity using Bone Volume and Bone Volume Fraction (BV/TV) parameters, as well as bone quality using Trabecular Thickness and Trabecular Separation parameters. Microarchitectural pattern and spatial distribution of bone within the samples were also evident in the Micro-CT images.

4.2.1. Experimental Groups without bony defects

Bone formation inside the 6 mm high tubes, regardless of the material or their implantation beds, consisted of lamellae of newly formed bone at the base. These bony spicules extended from the inferior edges of the walls, with or without connection to the skull bone, towards the center to varying extents. Within the 3 mm high tubes, new bone structures formed from the basal edges and extended towards the upper edges in a C-shaped pattern, covering the perimeter of the central core. The hemi-cylindrical tubes exhibited a different pattern with basal coverage and minimal attachment to the underlying bone, extending towards the superior edges (Figure 4.3. and Figure 4.4).

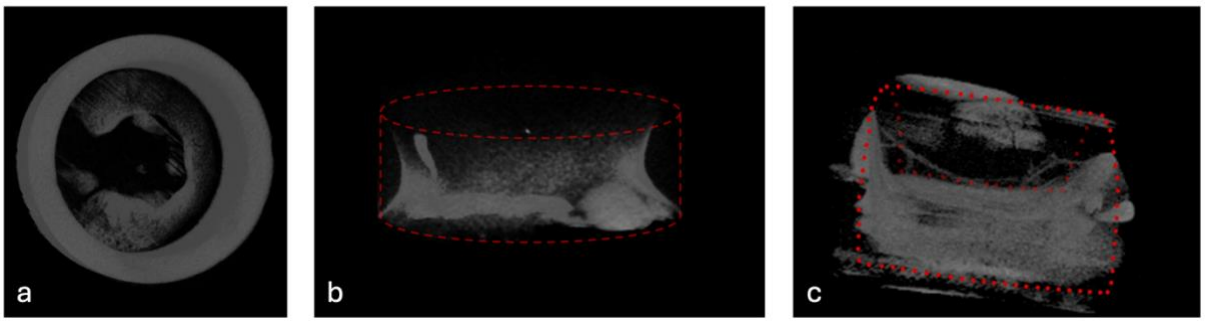

Figure 4.3. Micro-CT 3D view of different patterns of bone formation in experimental groups without bony defects; a. 6 mm high tube, b. 3 mm high tube, c. Hemi-cylindrical tube.

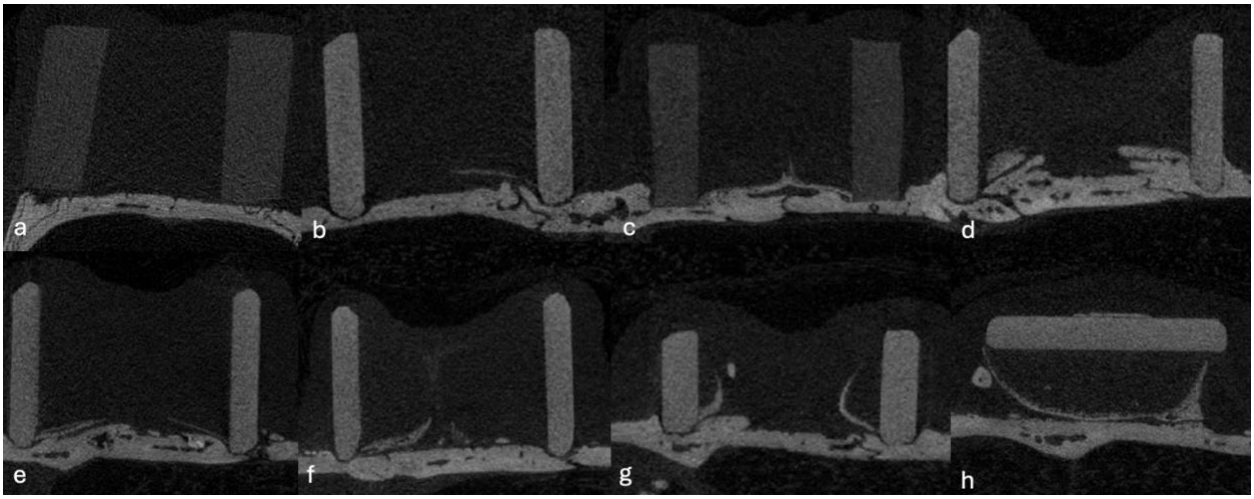

Figure 4.4. Sagittal Micro-CT view of experimental groups without defects: a. Subcutaneous Silicon Tube, b. Subcutaneous Glass tube, c. Subperiosteal Silicone Tube, d. Subperiosteal Glass Tube, e. Subperiosteal Glass tube and Decortication, f. Glass Tube and Periosteum Excision, g. Subperiosteal Short Glass Tube, h. Subperiosteal Hemi-Cylindrical Tube.

The amount of newly formed bone in different groups is presented by Bone Volume statistics in Table 4.1.

While no new bone was found in subcutaneous silicone tubes, subcutaneous glass had an average bone volume of 1.08 mm^3. Subperiosteal tubes showed higher amounts of bone formation, with an average of 4.34 mm^3 in silicone tubes and 8.28 mm^3 in glass tubes. Decortication and periosteal excision in subperiosteal glass tubes resulted in lower averages of 4.73 mm^3 and 3.67 mm^3, respectively. The highest bone formation was observed in subperiosteal hemi-cylindrical tubes at 11.81 mm^3 and subperiosteal short glass tubes at 9.59 mm^3.

Table. 4.3. Color-scaled table of Trabecular Separation statistics for experimental groups without bony defect.

Trabecular Separation					
Experimental Groups Without Bony Defects	Count	Average	Standard Deviation	Min	Max
Subcutaneous Silicone	8	0	0	0	0
Subcutaneous Glass	2	0.31	0.35	0.06	0.56
Subperiosteal Silicone	3	0.53	0.01	0.52	0.54
Subperiosteal Glass	3	0.06	0.02	0.04	0.08
Glass + Decortication	2	0.71	0.27	0.52	0.9
Glass + Periosteal Excision	2	0.5	0.14	0.4	0.6
Subperiosteal Short Glass	2	0.43	0.06	0.38	0.47
Subperiosteal Hemi-Cylindrical	2	1.64	1.02	0.92	2.36

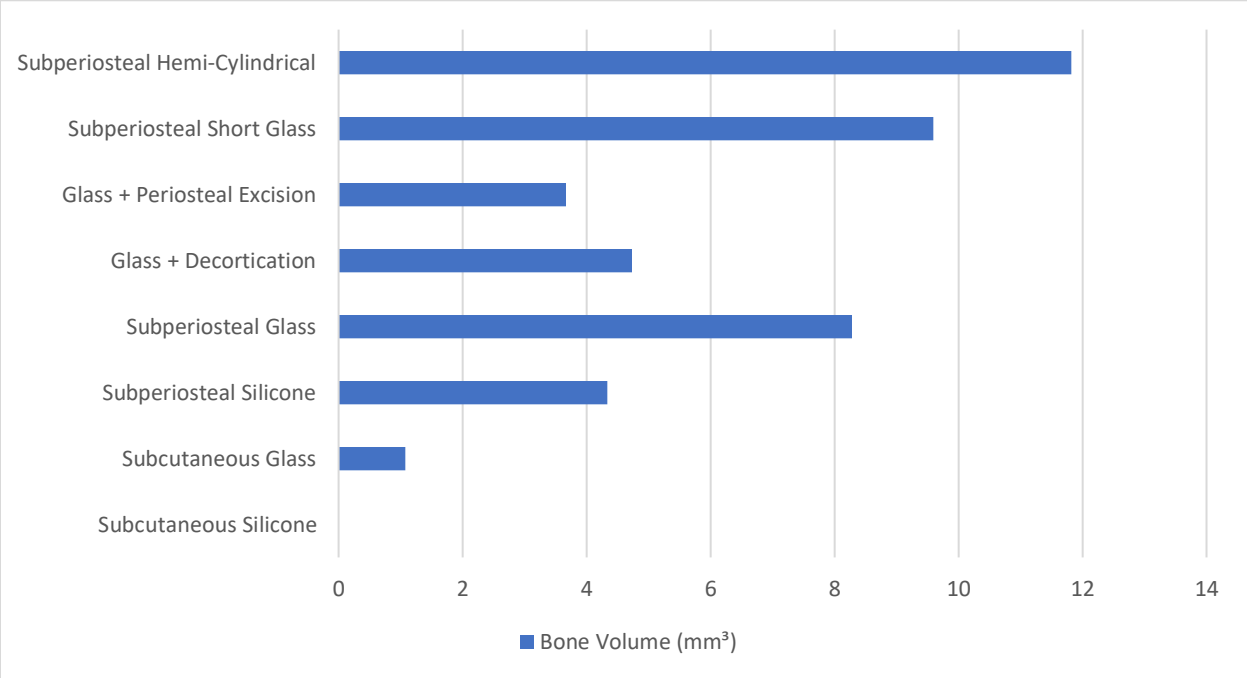

Figure 4.5. Bar chart with standard error of average Bone volume in experimental groups without bony defects.

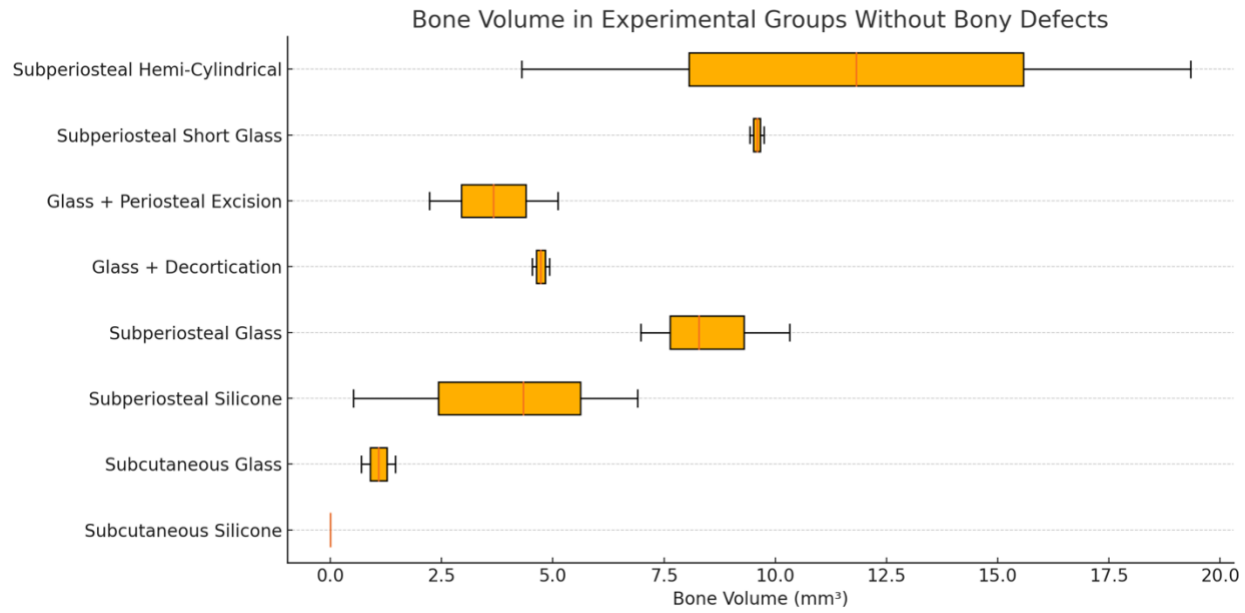

Figure 4.6. Box plot of average Bone Volume in experimental groups without bony defects.

4.2.2. Experimental Groups with bony defects

The pattern of bone formation followed the scenarios without defects, with the addition of central ectopic bone formation, except in 2 samples in the 6 mm high glass tubes. This central bone displayed a range of attachment to the basal bone, from strong attachments covering the defect to minimal or no attachment (Fig. 4.5).

Total amount of bone formation, including the bone formed inside the tube and within the defect, was calculated and is shown in Table 4.6. The highest percentage for this parameter is related to the 6mm high tubes. Defect coverage was assessed by the Bone Volume Fraction parameter, which is shown in Table 4.3. Considering average amounts of BV/TV, the 6 mm Silicone Tubes and 6 mm Glass Tubes showed higher BV/TV at 41.9% and 42.53%, respectively. This indicates more

bone formation within the defects compared to other groups like the Control group, which had an average BV/TV of 28.25%.

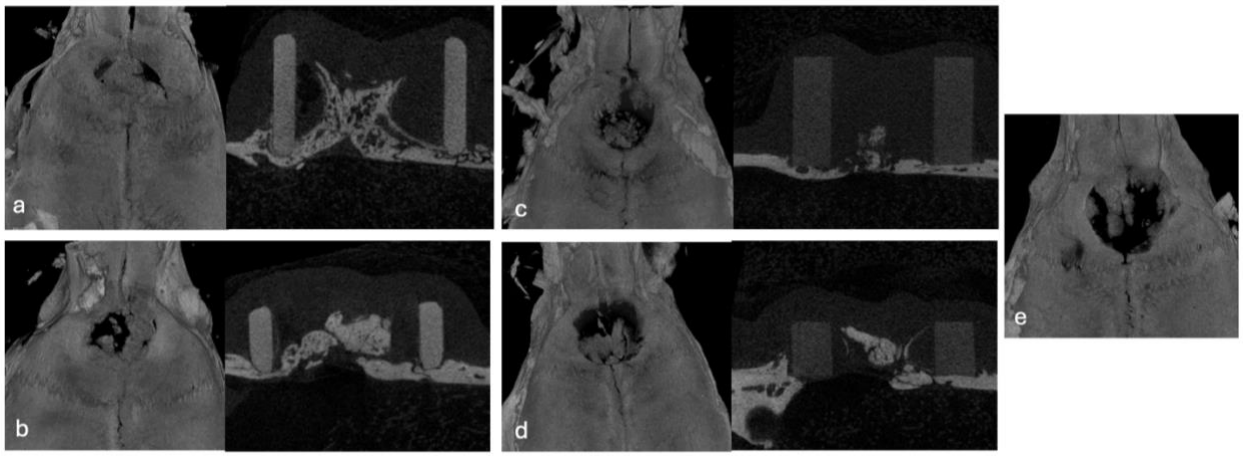

Figure 4.7. Axial and sagittal Micro-CT view of calvarial defects 5 weeks post-implantation: a. 6mm Glass Tube, b. 3mm Glass Tube, c. 6mm Silicone Tube, d. 3mm Silicone Tube, e. Control Group.

Table. 4.2. Color-scaled table of Total Bone Volume (including bone formed within both defect and tube space) statistics for experimental groups with bony defects.

Total Bone Volume (mm^3)					
Experimental Groups with Bony Defects	Count	Average	Standard Deviation	Min	Max
6 mm Silicone Tubes	1	9.56		9.56	9.56
3 mm Silicone Tubes	2	8.11	4.89	4.65	11.56
6 mm Glass Tubes	6	21.58	9.14	11.4	36.61
3 mm Glass Tubes	6	19.45	5.56	11.33	28.54

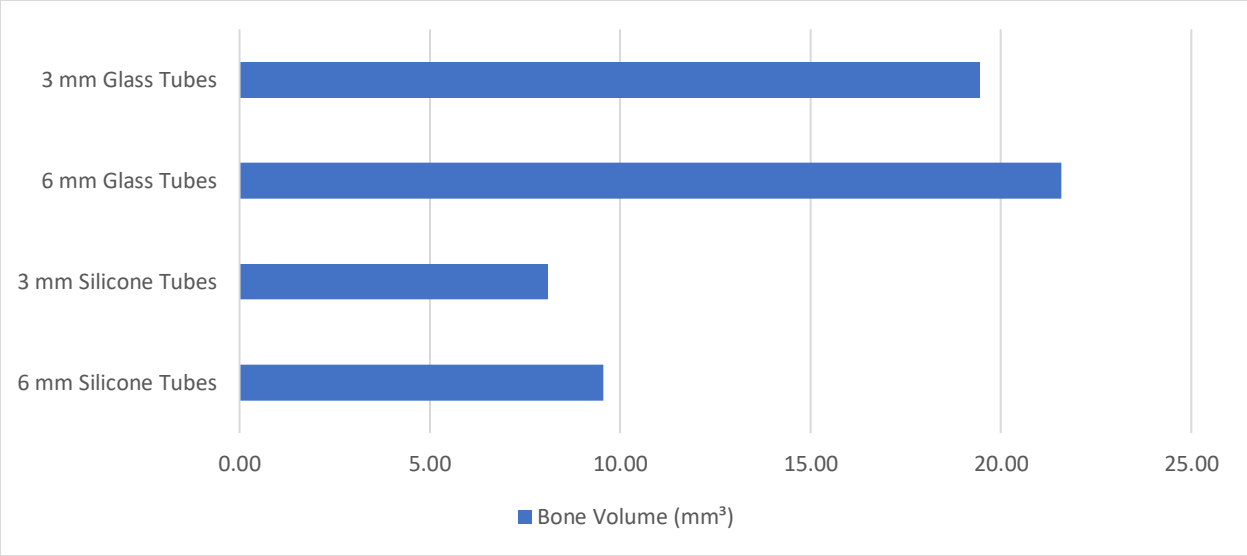

Figure 4.8. Bar chart with standard error of average Total Bone Volume in experimental groups with bony defects.

Table 4.3 Color-scaled table of defect Bone Volume Fraction (BV/TV) statistics for experimental groups with bony defects.

Defect Bone Volume Fraction (BV/TV)					
Experimental Groups with Bony Defects	Count	Average	Standard Deviation	Min	Max
6 mm Silicone Tubes	1	41.9%		41.9%	41.9%
3 mm Silicone Tubes	2	16.66%	1.57	15.55%	17.77%
6 mm Glass Tubes	6	42.53%	11.57	19.33%	51.04%
3 mm Glass Tubes	6	41.29%	10.80	30.76%	54.73%
Control	6	28.25%	5.89	19.67%	35.08%

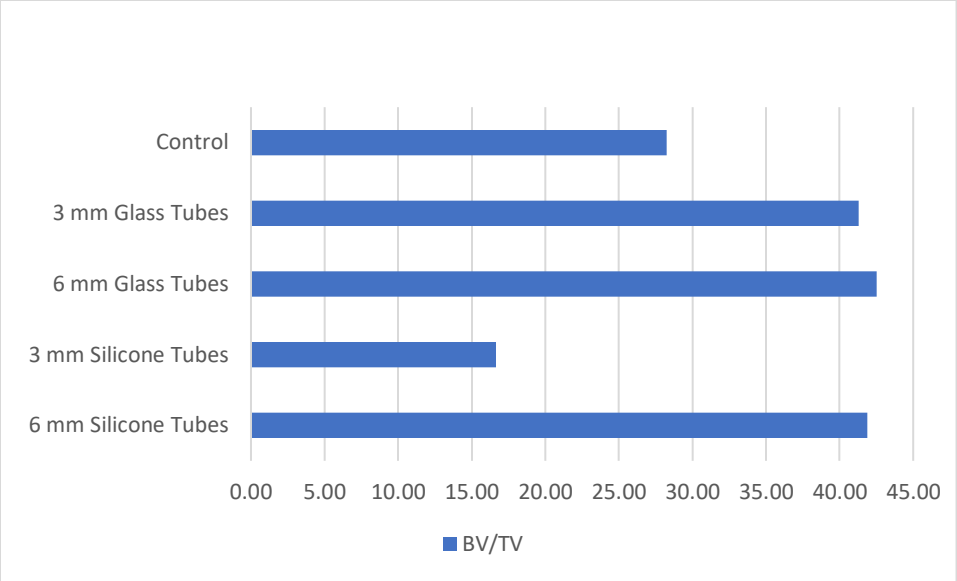

Figure 4.10. Bar chart with standard error of defect average Bone Volume Fraction (BV/TV).

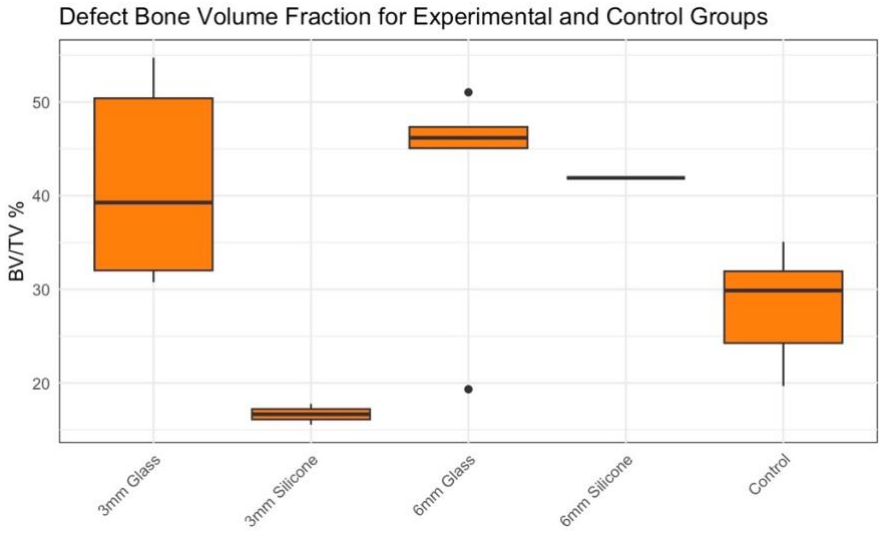

Figure 4.11. Box plot of defect average Bone Volume Fraction (BV/TV).

ANOVA test showed a p-value< 0.05 for defect BV/TV data, indicating a statistically significant difference among the groups. Tukey's HSD Test revealed 6mm Glass is significantly different from 3mm Silicone. 6mm Glass, 6mm Silicone, 3mm Glass, and Control are not significantly different from each other in terms of BV/TV.

4.3. Histology

In this chapter, we present the microscopical assessments of experimental samples mainly using Hematoxylin and Eosin (H&E) staining to provide a detailed understanding of the histological changes occurring within the samples under different experimental conditions. The samples include subcutaneous and subperiosteal implants of silicone and glass tubes, both with and without bony defects.

4.3.1. Subcutaneous Tubes

4.3.1.1. Silicone Tubes

A fibrous capsule composed of parallel collagen bundles and an abundance of fibroblasts and blood vessels was evident around the silicone implant. Inflammatory cells, including lymphocytes and macrophages, were diffusely distributed throughout the capsule, while occasional focal aggregations of these cells were observed at the interface of the capsule and implant. The surrounding connective tissue was more vascularized and was accompanied by strands of adipocytes in the basal plate, where loose connective tissue and an irregular network of collagen and elastic fibers were formed. At the insertion of the loosely arranged collagen fibers of the basal plate and growth cord, hemosiderin-laden macrophages were predominant. These macrophages were surrounded by fibro-collagenous tissue, myeloid cells, reactive lymphocytes, and giant cells, which were observed around foreign bodies. The growth cord was a thin tissue, with its superior two-thirds missing during the sectioning. It was well-vascularized and consisted of dense collagen fibers, fibroblasts, and peripheral inflammatory cells. No evidence of bone formation was found (Figure 4.12).

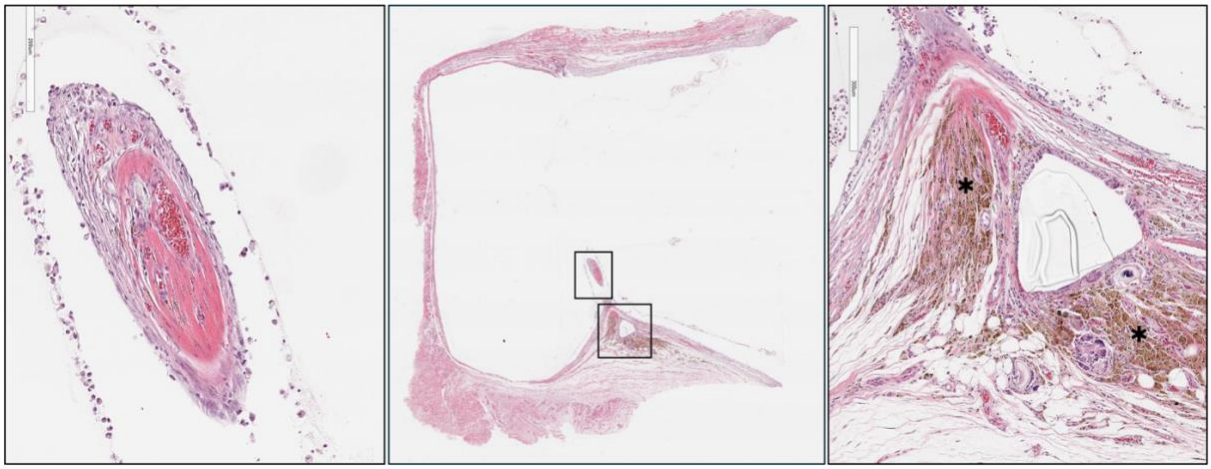

Figure 4.12. Histological examination of subcutaneous silicone tubes; Middle: an overview of the sample shows the remains of the central cord at the center, Left: central cord is shown under higher magnification. Vascular lumens are encircled by endothelial cells, surrounded by fibroblasts and collagen fibers, Right: lymphocytes and macrophages are observed in the periphery. In the base, loose fibro-collagenous tissue and adipocytes are observed. Foreign bodies (silicone) are surrounded by reactive lymphocytes and giant cells and left shifted myeloids. An aggregation of hemosiderin-laden macrophages (∗) are also evident.

4.3.1.2. Glass Tubes

Fibrous tissue exhibited a cellular pattern similar to that observed in silicone tubes. The overlying skin was drawn into the tube space, and a thick tissue attachment (growth cord) extending from superior to inferior was visible. Although fibroelastic tissue and reactive lymphocytes were evident in the basal plate, the sample was predominantly composed of fatty tissue, which extended from the basal plate to the superior one-third of the growth cord. Occasional findings included hemosiderin-laden macrophages and giant cells, mostly located on top of well-vascularized adipocyte islets within the growth cord. Fibroelastic tissue covered the periphery of the growth cord. Newly formed bony structures, characterized by inferior lamellar bone and superior woven bone, were observed on the superior and distal aspects of the basal plate. These bony spicules were surrounded by a layer of osteoblasts, while multinucleated osteoclasts were

located within resorption lacunae. Embedded osteocytes within a bony matrix without medullary cavities were also characteristics of these bony pieces (Figure 4.13).

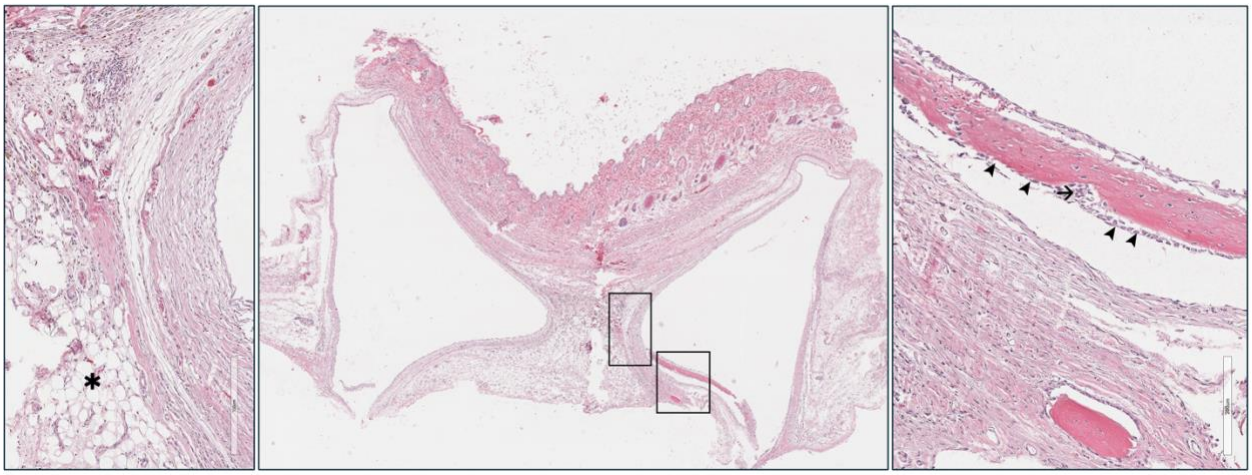

Figure 4.13. Histological examination of subcutaneous glass tubes; Middle: An overview of the sample shows a thick cord connecting the skin to the basal connective tissue. Left: Fibroblasts and collagen fibers line the border of the central tissue. Shifting to the center, there is a transition from fatty tissue (∗) at the base to inflammatory cells consisting of lymphocytes and histiocytes surrounded by fibro-collagenous tissue. Right: Intramembranous bone formation is observed at the top and bottom of the image, embedded in a matrix of connective tissue. A line of osteoblasts (arrowhead), with a few osteoclasts (arrow) within the resorption lacunae at the periphery of the bone spicules, is evident. Lymphocytes and macrophages are observed in the periphery.

4.3.2. Subperiosteal Tubes without Defect

4.3.2.1. 6mm High Tubes

The sample included the underlying calvarial bone, and the effect of the glass tube on the bone was evident by two depressed points observed under the microscope. The glass tube was separated from the skull by the periosteum and from the adjacent tissue by a fibrous capsule. The growth cord in these specimens was thicker than in the subcutaneous group and consisted of connective tissue with irregular patten and scattered inflammatory cells, with aggregations of

reactive lymphocytes and giant cells around foreign bodies (suture remnants). A mild distribution of hemosiderin-laden macrophages was also evident, scattered mostly in the inferior part of the growth cord. The growth cord showed a rich vascular network, and adipocytes were not observed in this group. Newly formed bone was attached to the skull bone and found in distal ends of the basal plate. Cuboidal osteoblasts with prominent nuclei were found in the periphery of these bone pieces. Additionally, high cellular medullary cavities with megakaryocytes were observed within these bony structures (Figure 4.14).

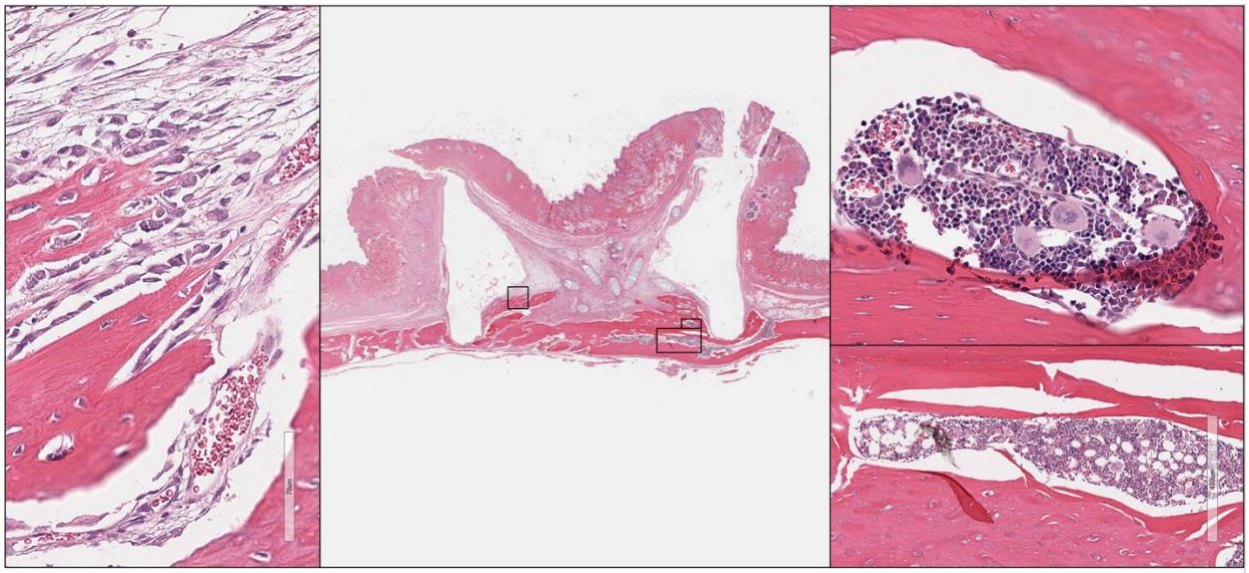

Figure 4.14. Histological examination of subperiosteal glass tubes: Middle: An overview of the sample shows a thicker central cord compared to subcutaneous tubes. Foreign bodies (sutures) are visible at the center. Newly formed bone attached to the cranium is demonstrated. Left: Developing bone with peripheral osteoblasts and osteoclasts is shown. Right, bottom: The original calvarial bone exhibits normal bone and bone marrow structure containing normal trilineage cell lines. Right, top: Newly formed bone and hypercellular bone marrow with increased myeloid elements. Cells with distinctive morphology of megakaryocyte are also evident in this image.

4.3.2.2. Short Tubes

Tubes in this group formed a broad growth cord, with both ends matching the internal diameter of the tube. The connective tissue at both ends was dense and contained scattered histiocytes, plasma cells, and lymphocytes. Centrally, a considerable amount of fatty tissue was observed, interspersed with strands of collagen bundles, fibroblasts, and arteriolar lumens surrounded by endothelial cells. In contrast to other samples where the periphery of the growth cord was covered by dense fibrous tissue, in this group, it was covered by bony lamellae. These bony structures were attached to the basal bone in some sections and woven bone with ongoing deposition was evident in the outer layers. Within these structures, osteogenic units and medullary cavities were identified (Figure 4.15).

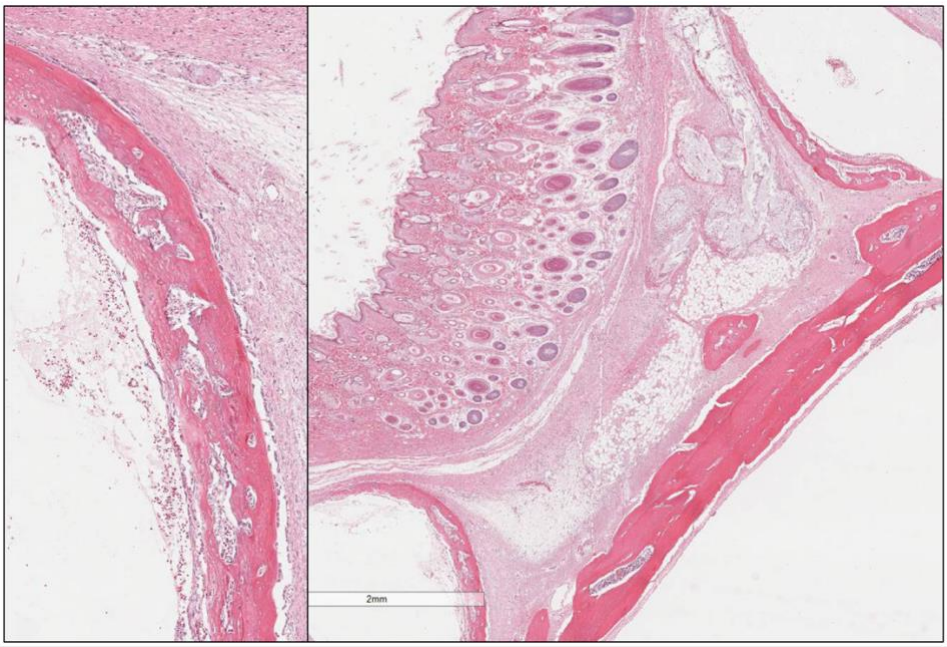

Figure 4.15. Histological examination of subperiosteal short glass tubes: Right: An overview of the sample showing a thick central tissue containing fatty and fibro-collagenous tissue, Left: Intramembranous bone formation with central osteogenic units.

4.3.2.3. Periosteal Removal

In this group, the growth cord was thinner than in the group with preserved periosteum and was partially missed during sectioning. A considerable amount of red blood cells (RBCs) was present within the tube space, indicating hemorrhage due to periosteal excision. A notable observation was the abundance of hemosiderin-laden macrophages along with other inflammatory cells in the basal plate extending to its insertion point in the growth cord. Additionally, acellular calcified elements surrounded by giant cells were evident. Bone formation in this group was observed as bony spicules extending from the basal plate to the growth cord insertion point, containing osteogenic units and medullary cavities. Additionally, vertical bone augmentation over the skull was noted. Similar to the samples with preserved periosteum, no fatty tissue was found in this group (Figure 4.16).

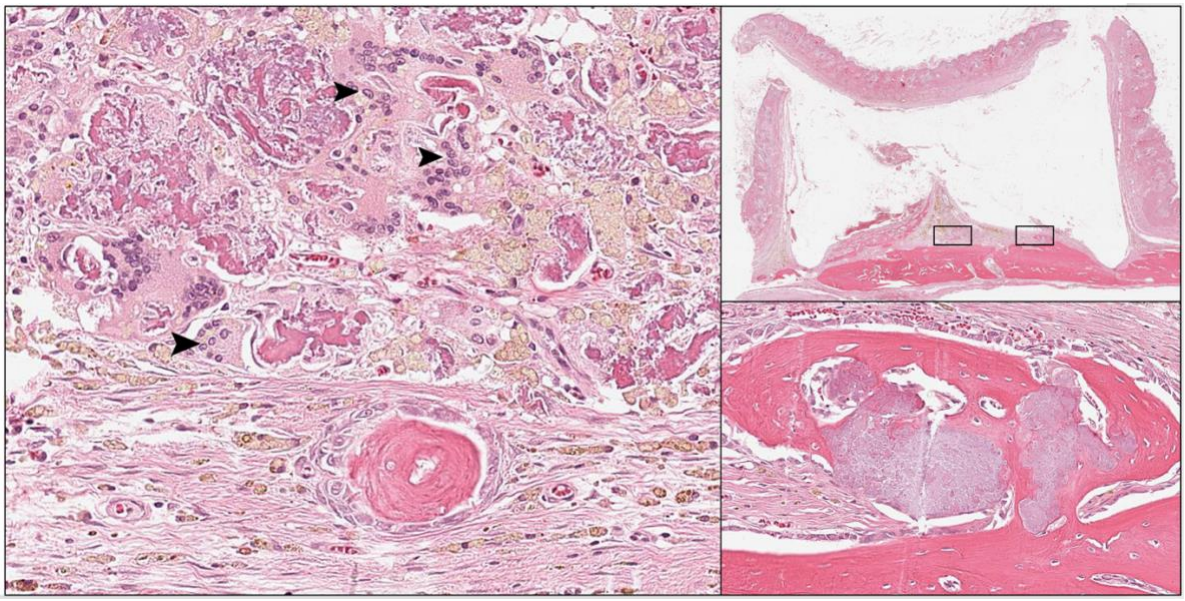

Figure 4.16. Histological examination of glass tubes with periosteal excision: Right top: An overview of the sample showing a relatively thin cord with ectopic bone formation at the base. Right bottom: Bone spicule with patchy, acellular calcified areas. Left: Macrophage-derived multinucleated giant cells (arrowheads), along with lymphocytes and plasma cells, surrounding scattered bone islands and irregular calcifications.

4.3.2.4. Hemi-cylindrical Tubes

The growth cord in this group was formed horizontally, connecting both side plates. These plates contained islets of adipocytes interspersed with strands of collagen fibers, fibroblasts, and blood vessels. Adjacent to the fatty tissue, dense connective tissue and periosteum surrounding the bony structures were present. Newly formed bone lamellae spanned around the periphery of the growth cord, with dense fibrous tissue separating these bony spicules from the basal bone, although there were some attachment points to the basal bone. Bony structures contained hypercellular medullary cavities and developing irregular arranged bone around the sinusoids in the outer layer was observed. A distinct encapsulation between the end plates and adjacent tissue was not evident (Figure 4.17).

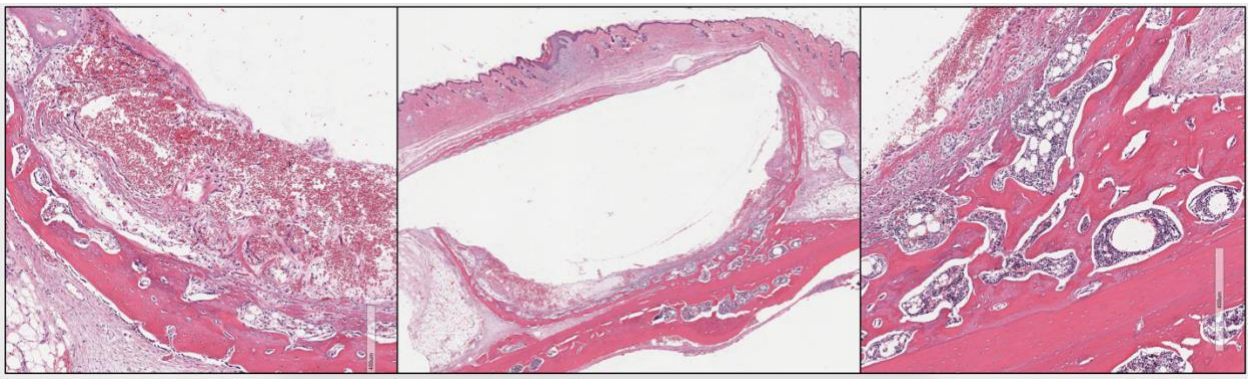

Figure 4.17. Histological examination of subperiosteal Hemi-cylindrical glass tubes: Center: Overview of the sample, Left. Bone formation around a sinusoid, Right, Membranous bone attached to the skull with medullary cavities, predominantly containing hematopoietic tissue.

4.3.3. Subperiosteal Tubes with Defect

The width of the growth cord formed in the tubes placed over the defect was similar to that of their counterparts placed over intact bone. However, unlike the intact bone, fatty tissue was

present in all samples, and additional bone tissue was observed within the growth cord, either inferiorly or adjacent to the adipocyte islets. In some sections, these bony structures were attached to the basal bone and contained medullary cavities, while in others, they were ectopic bones lacking bone marrow. Notably, strands of extramedullary hematopoietic tissue, predominantly lymphoid, were found within the fatty tissue, although no megakaryocyte has yet to be confirmed.

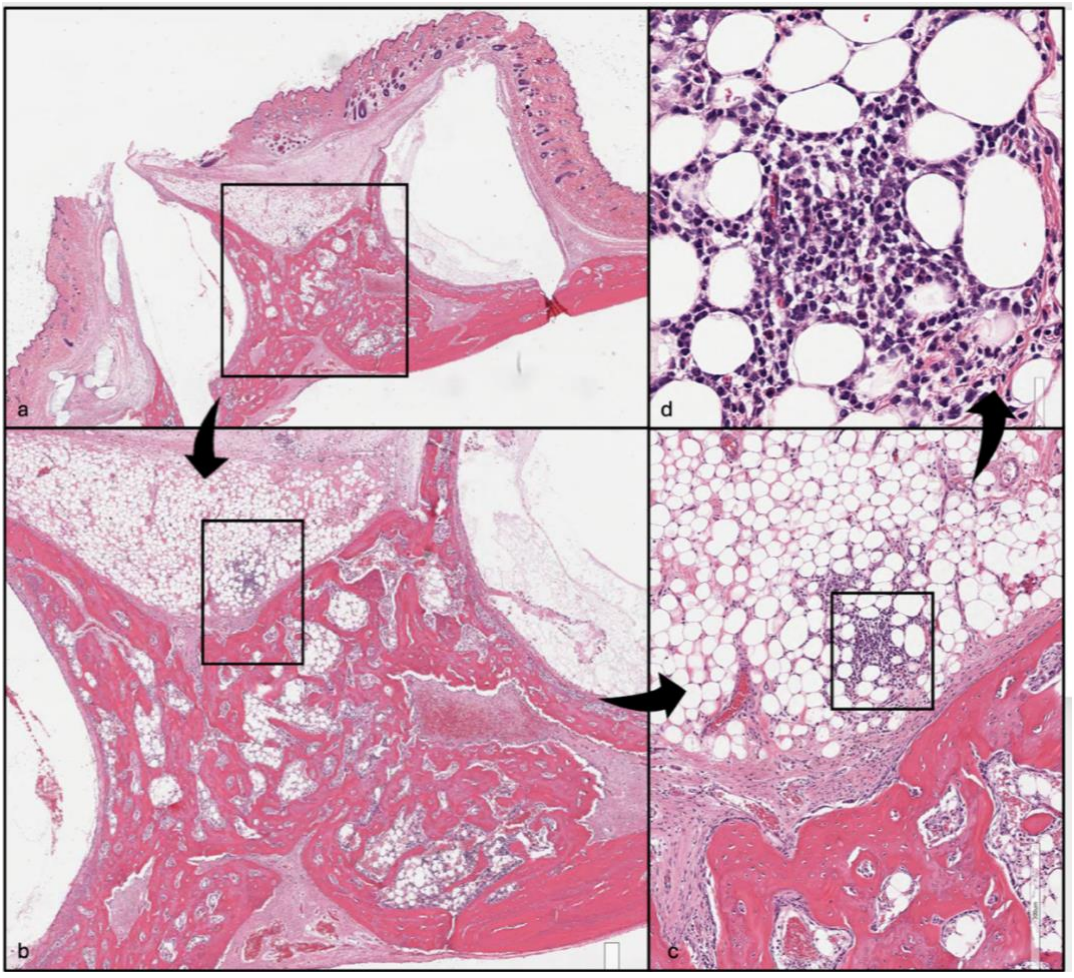

Fig. 4.18. Histological examination of subperiosteal glass tubes over the bony defect: a. Overview of the sample showing a thick ossicle of bone, b. Significant central bone formation attached to the basal bone with bone marrow cavities, c. Presence of adipose tissue around the newly formed bone, d. Hematopoietic tissue within the adipocytes.

Chapter 5. Discussion

This research was designed and conducted to identify factors, beyond bioactive ions and biological components, that contribute to osteogenesis. We were inspired by Selye's reports[70-72,79] who showed inflammatory responses to local stressors such as pressure can be modified by various factors to induce desired tissue formation[72]. Selye indicated that controlling factors include the duration of the experiment, the spatial configuration of the scaffold, and factors influencing the intensity of stressors, such as diaphragm dimensions and skin stretch[72]. Among these, we assessed the outcomes by varying the scaffold's dimensions and architecture, as well as the material itself, using quartz glass and silicone. While the original study did not recognize material type as a controlling factor[72], we found it to be effective in modifying the intensity of the stressors. To assess the efficacy of this method in healing bony defects in rat's cranium and potentially in oral and facial augmentation, we used tubes with smaller dimensions while maintaining a 2/3 proportion in the 6mm height groups.

Table 5.1. The differences in study design between the current study and Selye's study.

Characteristic	**Selye's Study**	**Current Study**
Scaffold Dimensions	30mm×10mm Cylinder	9mm×6mm Cylinder 9mm×3mm Cylinder 9mm×6mm×9mm Hemi-cylinder
Scaffold Material	Glass	Glass Silicone
Surgical Site	Over dorsal muscles	Over periosteum Over calvarial bone
Surgical Technique	Skin stretch on 5th day postoperatively	No skin stretch postoperatively

5.1. Experimental Groups without bony defects

Silicone tubes resulted in little to no bone formation in our experiment. Gross and histological examination of these specimens showed a fine growth cord which was probably incompetent in maintaining tension between two insertions, as well as forming and supporting a sufficient vascular network to transport oxygen and nutrients and remove the wastes. The presence of an abundance of hemosiderin-laden macrophages can be a sign of tissue degeneration following the metabolic isolation of the growth cord. Our observation suggests that, to form and support an adequate amount of pressure to end result of bone formation, a stiff and steady structure is necessary. This finding is in agreement with the conclusions drawn by previous studies, which indicate that scaffold stiffness should ideally match the stiffness of the bony tissue to promote cell differentiation. They also emphasized that scaffold stiffness can influence various other processes, such as cell growth and migration[80,81]. Yi et al, also supported the notion that substrate stiffness is an important physical cue in controlling cell fate at the microscale and tissue remodeling at the macroscale[82].

The results showed a greater extent of osteogenesis in subperiosteal specimens than the subcutaneous group. In subperiosteal groups, new ossicles seemed to form as radiated bone spicules initiated from the tightly adapted walls of the tube into the bony cortex. This observation led us to test whether this mechanical injury to the endosteum played an important role in ossification. Therefore, we examined the effect of bone decortication by creating several mono-cortical holes in the bony field of interest. Removing the outer cortex in order to enhance graft integration and survival has been practiced among surgeons[83]. Bone decortication is encouraged in clinical practice, probably because it enhances the healing process by promoting bleeding and

blood clot formation[84]. It has also been suggested that cortical removal can facilitate the migration of progenitor cells and blood vessels to the bone graft site, which support angiogenesis[85]. Considering the great release of bone proteins at the site of bone perforations, Alberius et al, used the term “explosive bone production” to describe the outcomes[83]. Surprisingly, the extent of bone formation in our specimens did not increase after bone decortication, indicating that the injury to the bone was not the primary driver of osteogenesis in the secluded space. Additionally, to assess the essential role of the periosteum in our experiment, we maintained the periosteum over the tubes in subperiosteal specimens and kept it untouched in the underlying layer of subcutaneous groups, except in one group where the periosteum was completely excised. The periosteum cell population is a mixed population comprising fibroblasts, osteoblasts, MSCs, and pericytes and osteogenesis potential of periosteum has been shown in several studies[86]. Breitbart et al, showed the successful use of cultured periosteal cells on scaffolds to enhance bone formation in experimental rabbit models[87]. Perka et al, also demonstrated the effectiveness of isolated periosteal cells seeded into biodegradable PGLA polymer for healing ulna defects in rabbits[88]. Interestingly, even in the absence of bone matrix, periosteum has the ability to generate bone de novo[89]. Given the fact that periosteal excision did not cease osteogenesis, implies that the other sources also play in the osteogenic process. This finding aligns with Selye’s observation, where ectopic bone formed separated by a thick connective tissue from the host vertebral column[72]. One possible reason for the increased osteogenesis in the subperiosteal specimens is that the placement of the tube over a solid base can support the implant’s stability, as evidenced by the adaptation of the walls into the cranium. This firm foundation can bear the pressure from the stretched skin. To achieve such stability, Selye

designed two grooves close to both margins to facilitate encapsulation and the formation of stabilizing bands[72]. Additionally, another contributing factor might be mechanical loading-triggered osteogenic differentiation, which enhances bone formation and remodeling[90].

By modifying the size and the shape of cylinders, we changed the spatial form of growth cords and consequently pattern and amount of bone formation. The highest amount of bone formation was observed in hemi-cylindrical and 3 mm high tubes. In both cases, osteogenesis occurred at the periphery of growth cords and end plates.

Selye reported strands of myeloid tissue within adipose islands and clusters of myeloid and lymphoid tissue around the blood vessels[72]. However, to confirm the presence of these cells in the current study, further IHC staining is needed. This observation can be attributed to the response of migratory hematopoietic stem cells (HSCs) triggered by inflammation and trauma induced by constant pressure within the tube. In response to these stimuli, HSCs migrate and accumulate around blood vessels, in form of extramedullary hematopoiesis that occurs outside the bone marrow. Here, HSCs interact with local mesenchymal stem cells (MSCs), which are abundant in the perivascular niche. The presence of HSCs and their associated factors induce MSCs to undergo osteogenic differentiation.

Although we demonstrated the feasibility of bone induction by physical stimuli, we did not fully replicate Selye's experiment, as we did not observe cartilage, endochondral ossification, or hematopoietic tissue. The implants in the original study were about three times larger than those in the current study and were placed over the dorsal muscles. Additionally, skin stretch on the

fifth postoperative day prevented the formation of a broad growth cord. These differences may have influenced the outcomes.

5.2. Experimental Groups with bony defects

Cranioplasty has been practiced for a long time, and the techniques for reconstruction are continually evolving[91]. Currently, the optimal graft for small-to-medium cranial defects is an autologous graft harvested from various donor sites, with a preference for splitting calvarial grafts[92]. The primary options for larger defects in adults are titanium mesh and polymethylmethacrylate[93], while in pediatrics, inlay particulate autografts are preferred[94]. Although it is reported that the risk of infection in bioceramic custom-made porous HA, is comparable with titanium and slightly better than PMMA[95], this is difficult to confirm, as infection rates for cranioplasty reported in the literature vary widely, from 0% to 26%[96]. Therefore, the perfect cranioplasty material still remains elusive. Acknowledging the ongoing challenges, our observations showed bone formation in the base of tubes suggesting their potential for covering bony defects.

In these groups, osteogenesis was not limited to the basal plates and the periphery of the growth cord; additional bone formation also occurred on top, extending downward within the growth cord. The specimens in which the additional central bone could attach to the newly formed bone in the defect, showed the greatest BV/TV percentage indicating the highest defect healing capacity. The average BV/TV in 6mm high glass tubes was higher than in shorter glass tubes, but this difference was not statistically significant. While both categories of glass tubes showed a higher BV/TV for defect coverage compared to the control group, the difference was not

statistically significant. Future experiments should consider using critical-sized defects that do not heal without intervention to assess the actual efficacy. It comes as no surprise that silicone tubes were again found to be less effective compared to glass tubes in this experiment.

Considering these additional ossicles, placing tubes over the bony defect increased the total amount of bone formation compared to groups without defects. However, these new bony pieces in some cases were not efficient in covering the defects, it underscores the potential of osteogenesis through mechanical stimuli. The observation in the presence of defects can be contributed to available inflammatory cells, vasculature, and MSCs within the defect necessary to initiate and support osteogenesis.

5.3. Evaluation of Experimental Hypotheses

The hypotheses developed during this work are shown in Table 1.1. Here, we summarize whether our data support, disprove or are ambiguous regarding the role of the parameters examined.

1. Material Type

Expected outcome: tissue formation will be identical regardless of material type.

Figure 4.4. clearly showed that bone volume in silicone tubes was less than that found in glass tubes and so it would appear that material type is indeed an important factor. However, it is not clear whether this is as a result of strain in the overlying skin, resorption

of the tissue under the implant due to high localized stresses, or deformation of the silicone alters the volume and geometry of the space delineated by the implant.

2a. Implant Height

Expected outcome: Shorter implants (3mm) will have faster tissue connection between two ends. Skin tension would be expected to be lower in shorter implants.

Figure 4.4. shows that tissue formation was largely equivalent in terms of formation pattern, regardless of tube length. We did not perform a time series, so cannot say tube formation speed was different; however, bone volume was 1.3 times greater in shorter tubes (Figure 4.5) which may be as a result of beginning to be formed earlier. An earlier time point experiment would be required.

2b. Design

Expected Outcome: If both tissue types are equally important then increasing the area of one and not the other will result in no effect.

Bone pattern formation was altered but there was insufficient power (N=2) to comment on statistically significant differences, but neither were worse than the upright cylinder

configuration. This suggests that the area of the lower tissue layer does not have a strong effect since it was ~2 times greater in the hemispherical implant.

3a. Implant Size

Expected Outcome: A minimum volume is required for tissue formation. Smaller tubes in our study compared to Selye's study will result in less amount of bone formation.

We consistently observed bone formation in all glass tubes which were about one-third the dimensions used by Selye. This suggests that the minimum volume required for osteogenesis is less than the amounts we tested. Although the average bone volume in hemi-cylindrical tubes, which had approximately twice the bone contact area compared to cylindrical ones, was higher than in other groups, the small sample size and high standard deviation make it inconclusive to comment on the direct effect of size on tissue formation.

3b. Implant Orientation

Expected Outcome: Horizontal orientation removes a physical barrier between the skin and the bone. If this is a requirement tissue formation will be inhibited.

Reorienting the tubes from vertical to a horizontal placement, shifted the open ends to sides in hemi-cylindrical design. These side openings removed barriers used to impede soft tissue growth over denuded bone. Histologic evaluation (Figure 4.17) showed two growth cords, merging centrally over the bone, which disproves the need to consider any potential inhibitory effect of soft tissue growth or any absolute requirement to physically separate the two tissue types completely.

4. Anatomic Site

Expected Outcome: The subcutaneous calvarial site is expected to result in lower osteogenesis. Subperiosteal implantation is anticipated to increase bone formation. If greater bone formation occurs in groups with defects, it will confirm the importance of the substrate structure.

Figure 4.6 shows lower bone volume in subcutaneous tubes made of either material compared to subperiosteal groups. This observation implies the role of surrounding tissue in providing biochemical signaling to initiate and accelerate the osteogenesis process or offering a supportive framework. Additionally, the promotion of greater bone formation in groups with defects compared to groups with intact bone (as shown in Table 4.1 and Table 4.2) demonstrates the role of a complex environment containing both structural support and other factors contributing to osteogenesis. Using a bony defect as the tube substrate, which led to higher bone formation compared to the negative control (Figure

4.6), suggests that the capacity for bone formation in such environments can benefit bone healing.

5a. Mechanical Injury associated with Material Type

Expected Outcome: Soft material will result in minimal or no mechanical injury, leading to less osteogenesis.

MicroCT images shown in Figure 4.4 demonstrate the extent of tube accommodation into the underlying bone due to pressure-induced bone remodeling in different groups. Silicone tubes showed no effect (subcutaneous) and minimal effect (subperiosteal) on the subjacent bone, while this effect seemed to be more pronounced in glass tubes, which also exhibited a higher amount of bone formation. Although we did not directly measure the correlation between pressure-induced remodeling and the amount of bone formation, we decided to test this presumption by deliberately causing mechanical injury through the creation of monocortical holes.

5b. Mechanical Injury by Bone Decortication

Expected Outcome: Bone decortication will lead to increased mechanical injury, and this will result in more bone formation.

Creating small monocortical perforations in the skull to induce mechanical injury and enhance progenitor cell migration and support vasculogenesis did not lead to higher osteogenesis (Figure 4.5), disproving the assumption that direct injury would promote bone formation.

6. Periosteum

Expected Outcome: Excision of the periosteum will dramatically decrease osteogenesis compared to groups the periosteum remains intact.

The elevation of the periosteal flap in subperiosteal groups, with the flap placed over the glass tube such that the inner osteogenic layer of the periosteum covered the upper opening, did not result in osteogenesis on top of the tube (Figure 4.4). This observation suggests that the osteogenic capacity of the periosteum did not directly influence bone formation in this experiment. However, total excision of the periosteum led to a lower amount of bone formation (Figure 4.5), indicating a potential supportive role of the periosteum. Nonetheless, the data cannot be considered conclusive due to the small sample size (N=2) and the hematoma formation in one of the samples.

7. Growth Cord

Expected Outcome: We expect bone formation to align with the implant's ability to form a viable growth cord, which is anticipated to occur more effectively with stiff implants, shorter heights (facilitating easier tissue connection), and larger contact surfaces.

Macroscopic evaluation confirmed the presence of growth cords in all specimens, suggesting their potential significance in the outcome (Figures 4.1 and 4.2). In particular, the growth cords in silicone tubes with the lowest amount of bone was the narrowest and longest, while short tubes with the greatest bone formation showed the broadest and shortest growth cords (Figure 4.5).While these data suggest that easier tissue connection leads to more bone formation, the findings in the defect groups were not consistent with this pattern (Figure 4.8), which indicates that factors other than tissue connection could be playing a more dominant role in promoting bone formation. To better understand the role of growth cords in tissue formation, further studies are recommended to focus on isolating growth cords and directly assessing their impact on bone regeneration through in-vivo implantation in different environments.

8. Marrow and Hematopoietic Stem Cells (HSCs)

Expected Outcome: Marrow can form ectopically and can differentiate into mesenchymal tissues. A lack of confirmation of marrow tissue indicates no role of marrow formation in subsequent tissue induction.

Histologic evaluations did not reveal any evidence of bone marrow strands that were not surrounded by bony structures, which contrasts with Selye's findings suggesting marrow formation might not be necessary for inducing osteogenesis. While scattered cells exhibiting characteristics of hematopoietic progenitors were observed within the growth cords, this has yet to be confirmed through immunohistochemical (IHC) staining.

Chapter 6. Conclusion

We demonstrated the feasibility of ectopic bone induction by factors influencing osteogenesis beyond biomaterials and biological components. Deliberate manipulation of this phenomenon would appear a new and underappreciated route to materials mediated tissue regeneration.

Our findings provided significant insights:

1. We demonstrated that the material type, quartz glass vs. silicone, in our study affected osteogenesis. Glass tubes exhibited higher amount of bone formation, highlighting the importance of material stiffness to form and support adequate pressure.
2. The spatial configuration of scaffolds, including dimensions and architecture could change the growth cord structure and subsequently the quantity and distribution of bone formation. This implies that by manipulating scaffold architecture, it is possible to achieve desired tissue outcomes.
3. If the presence of myeloid tissue was confirmed through additional IHC staining as observed in Selye's seminal study, we could confirm triggering EMH by physical stimuli which involved migrating HSCs and their interaction with local MSCs, promoting osteogenic differentiation. The tissue containing marrow components is viable with the potential to enhance bone regeneration.
4. The new bone regeneration route had potential applications in craniofacial augmentation and defect repair. However, additional investigation in critical-sized defects was needed to better understand its translational potential in clinical settings.

This study improved our understanding of osteogenesis and offered a new perspective to explore mechanisms impacting bone formation that were not connected to physicochemical properties of the material.

Chapter 7. Future Directions

1. Conduct additional IHC staining to confirm the presence of myeloid and lymphoid tissue to Investigate the role of inflammation in triggering HSCs and their interaction with MSCs to initiate and support osteogenesis.
2. Test the approach in critical-sized defects to evaluate the potential for clinical translation and applications in craniofacial surgery.
3. Develop and test different scaffold geometry to optimize spatial configuration for bone augmentation and defect healing.
4. Explore the use of biodegradable materials to gradually dissolve after inducing bone formation to remove the need for the second surgery.
5. Investigate the efficacy of growth cord construct in bone induction in animal models.

References

(1) Baroli, B. From Natural Bone Grafts to Tissue Engineering Therapeutics: Brainstorming on Pharmaceutical Formulative Requirements and Challenges. *J. Pharm. Sci.* **2009**, *98* (4), 1317–1375. https://doi.org/10.1002/jps.21528.

(2) Henkel, J.; Woodruff, M. A.; Epari, D. R.; Steck, R.; Glatt, V.; Dickinson, I. C.; Choong, P. F. M.; Schuetz, M. A.; Hutmacher, D. W. Bone Regeneration Based on Tissue Engineering Conceptions — A 21st Century Perspective. *Bone Res.* **2013**, *1* (1), 216–248. https://doi.org/10.4248/BR201303002.

(3) Habibovic, P.; de Groot, K. Osteoinductive Biomaterials—Properties and Relevance in Bone Repair. *J. Tissue Eng. Regen. Med.* **2007**, *1* (1), 25–32. https://doi.org/10.1002/term.5.

(4) Yang, Z.; Yuan, H.; Tong, W.; Zou, P.; Chen, W.; Zhang, X. Osteogenesis in Extraskeletally Implanted Porous Calcium Phosphate Ceramics: Variability among Different Kinds of Animals. *Biomaterials* **1996**, *17* (22), 2131–2137. https://doi.org/10.1016/0142-9612(96)00044-0.

(5) Maes, C.; Kronenberg, H. M. Chapter 4 - Postnatal Bone Growth: Growth Plate Biology, Bone Formation, and Remodeling. In *Pediatric Bone (Second Edition)*; Glorieux, F. H., Pettifor, J. M., Jüppner, H., Eds.; Academic Press: San Diego, 2012; pp 55–82. https://doi.org/10.1016/B978-0-12-382040-2.10004-8.

(6) Tavassoli, M.; Weiss, L. The Structure of Developing Bone Marrow Sinuses in Extramedullary Autotransplant of the Marrow in Rats. *Anat. Rec.* **1971**, *171* (4), 477–493. https://doi.org/10.1002/ar.1091710405.

(7) Coutu, D. L.; Kokkaliaris, K. D.; Kunz, L.; Schroeder, T. Three-Dimensional Map of Nonhematopoietic Bone and Bone-Marrow Cells and Molecules. *Nat. Biotechnol.* **2017**, *35* (12), 1202–1210. https://doi.org/10.1038/nbt.4006.

(8) Schermer, S. The Blood Morphology of Laboratory Animals. *No Title* **1967**.

(9) Jain, N.C. *Schalm's Veterinary Haematology*, 4th edition.; Lea and Febiger: Philadelphia, 1986.

(10) Picker, L. J. Lymphoid Tissues and Organs. In *Fundamental immunology*; 1999.

(11) Hoffman, R.; Benz, E. J.; Silberstein, L. E.; Heslop, H.; Weitz, J.; Salama, M. E.; Abutalib, S. A. *Hematology: Basic Principles and Practice*; Elsevier Health Sciences, 2022.

(12) Travlos, G. S. Normal Structure, Function, and Histology of the Bone Marrow. *Toxicol. Pathol.* **2006**, *34* (5), 548–565. https://doi.org/10.1080/01926230600939856.

(13) Munka, V.; Gregor, A. Lymphatics and Bone Marrow. *Folia Morphologica (Praha)* **1965**, *13* (4), 404–412.

(14) Marenzana, M.; Arnett, T. R. The Key Role of the Blood Supply to Bone. *Bone Res.* **2013**, *1* (1), 203–215. https://doi.org/10.4248/BR201303001.

(15) Weiss, L.; Geduldig, U. Barrier Cells: Stromal Regulation of Hematopoiesis and Blood Cell Release in Normal and Stressed Murine Bone Marrow. *Blood* **1991**, *78* (4), 975–990. https://doi.org/10.1182/blood.V78.4.975.975.

(16) Cora, M. C.; Latimer, K.; Travlos, G. S. Chapter 25 - Bone Marrow. In *Boorman's Pathology of the Rat (Second Edition)*; Suttie, A. W., Ed.; Academic Press: Boston, 2018; pp 495–519. https://doi.org/10.1016/B978-0-12-391448-4.00025-3.

(17) Comazzetto, S.; Shen, B.; Morrison, S. J. Niches That Regulate Stem Cells and Hematopoiesis in Adult Bone Marrow. *Dev. Cell* **2021**, *56* (13), 1848–1860. https://doi.org/10.1016/j.devcel.2021.05.018.

(18) Bianco, P.; Robey, P. G.; Simmons, P. J. Mesenchymal Stem Cells: Revisiting History, Concepts, and Assays. *Cell Stem Cell* **2008**, *2* (4), 313–319. https://doi.org/10.1016/j.stem.2008.03.002.

(19) Bianco, P.; Robey, P. G. Skeletal Stem Cells. *Dev. Camb. Engl.* **2015**, *142* (6), 1023–1027. https://doi.org/10.1242/dev.102210.

(20) Sacchetti, B.; Funari, A.; Michienzi, S.; Cesare, S. D.; Piersanti, S.; Saggio, I.; Tagliafico, E.; Ferrari, S.; Robey, P. G.; Riminucci, M.; Bianco, P. Self-Renewing Osteoprogenitors in Bone Marrow Sinusoids Can Organize a Hematopoietic Microenvironment. *Cell* **2007**, *131* (2), 324–336. https://doi.org/10.1016/j.cell.2007.08.025.

(21) Bianco, P.; Cao, X.; Frenette, P. S.; Mao, J. J.; Robey, P. G.; Simmons, P. J.; Wang, C.-Y. The Meaning, the Sense and the Significance: Translating the Science of Mesenchymal Stem Cells into Medicine. *Nat. Med.* **2013**, *19* (1), 35–42. https://doi.org/10.1038/nm.3028.

(22) Caplan, A. I. Mesenchymal Stem Cells. *J. Orthop. Res.* **1991**, *9* (5), 641–650. https://doi.org/10.1002/jor.1100090504.

(23) Tavassoli, M.; Crosby, W. H. Transplantation of Marrow to Extramedullary Sites. *Science* **1968**, *161* (3836), 54–56. https://doi.org/10.1126/science.161.3836.54.

(24) Friedenstein, A. J.; Chailakhjan, R. K.; Lalykina, K. S. THE DEVELOPMENT OF FIBROBLAST COLONIES IN MONOLAYER CULTURES OF GUINEA-PIG BONE MARROW AND SPLEEN CELLS. *Cell Prolif.* **1970**, *3* (4), 393–403. https://doi.org/10.1111/j.1365-2184.1970.tb00347.x.

(25) Friedenstein, A. J. Osteogenic Stem Cells in the Bone Marrow. In *Bone and Mineral Research*; Heersche, J. N. M., Kanis, J. A., Eds.; Elsevier, 1990; pp 243–272. https://doi.org/10.1016/B978-0-444-81371-8.50012-1.

(26) Arai, F.; Ohneda, O.; Miyamoto, T.; Zhang, X. Q.; Suda, T. Mesenchymal Stem Cells in Perichondrium Express Activated Leukocyte Cell Adhesion Molecule and Participate in Bone Marrow Formation. *J. Exp. Med.* **2002**, *195* (12), 1549–1563. https://doi.org/10.1084/jem.20011700.

(27) Bianco, P.; Riminucci, M.; Kuznetsov, S.; Robey, P. G. Multipotential Cells in the Bone Marrow Stroma: Regulation in the Context of Organ Physiology. *Crit. Rev. Eukaryot. Gene Expr.* **1999**, *9* (2), 159–173. https://doi.org/10.1615/critreveukargeneexpr.v9.i2.30.

(28) Kuznetsov, S. A.; Riminucci, M.; Ziran, N.; Tsutsui, T. W.; Corsi, A.; Calvi, L.; Kronenberg, H. M.; Schipani, E.; Robey, P. G.; Bianco, P. The Interplay of Osteogenesis and Hematopoiesis : Expression of a Constitutively Active PTH/PTHrP Receptor in Osteogenic Cells Perturbs the Establishment of Hematopoiesis in Bone and of Skeletal Stem Cells in the Bone Marrow. *J. Cell Biol.* **2004**, *167* (6), 1113–1122. https://doi.org/10.1083/jcb.200408079.

(29) Zhou, B. O.; Ding, L.; Morrison, S. J. Hematopoietic Stem and Progenitor Cells Regulate the Regeneration of Their Niche by Secreting Angiopoietin-1. *eLife* **2015**, *4*, e05521. https://doi.org/10.7554/eLife.05521.

(30) Méndez-Ferrer, S.; Michurina, T. V.; Ferraro, F.; Mazloom, A. R.; MacArthur, B. D.; Lira, S. A.; Scadden, D. T.; Ma'ayan, A.; Enikolopov, G. N.; Frenette, P. S. Mesenchymal and Haematopoietic Stem Cells Form a Unique Bone Marrow Niche. *Nature* **2010**, *466* (7308), 829–834. https://doi.org/10.1038/nature09262.

(31) Wang, C.; Ning, H.; Gao, J.; Xue, T.; Zhao, M.; Jiang, X.; Zhu, X.; Guo, X.; Li, H.; Wang, X. Disruption of Hematopoiesis Attenuates the Osteogenic Differentiation Capacity of Bone Marrow Stromal Cells. *Stem Cell Res. Ther.* **2022**, *13* (1), 27. https://doi.org/10.1186/s13287-022-02708-3.

(32) Jung, Y.; Song, J.; Shiozawa, Y.; Wang, J.; Wang, Z.; Williams, B.; Havens, A.; Schneider, A.; Ge, C.; Franceschi, R. T.; McCauley, L. K.; Krebsbach, P. H.; Taichman, R. S. Hematopoietic Stem Cells Regulate Mesenchymal Stromal Cell Induction into Osteoblasts Thereby Participating in the Formation of the Stem Cell Niche. *Stem Cells* **2008**, *26* (8), 2042–2051. https://doi.org/10.1634/stemcells.2008-0149.

(33) Liao, J.; Hammerick, K. E.; Challen, G. A.; Goodell, M. A.; Kasper, F. K.; Mikos, A. G. Investigating the Role of Hematopoietic Stem and Progenitor Cells in Regulating the Osteogenic Differentiation of Mesenchymal Stem Cells in Vitro. *J. Orthop. Res.* **2011**, *29* (10), 1544–1553. https://doi.org/10.1002/jor.21436.

(34) Yang, X.; Chen, D.; Long, H.; Zhu, B. The Mechanisms of Pathological Extramedullary Hematopoiesis in Diseases. *Cell. Mol. Life Sci. CMLS* **2020**, *77* (14), 2723–2738. https://doi.org/10.1007/s00018-020-03450-w.

(35) Maxie, G. *Jubb, Kennedy & Palmer's Pathology of Domestic Animals: Volume 3*; Elsevier Health Sciences, 2015.

(36) Johns, J. L.; Christopher, M. M. Extramedullary Hematopoiesis: A New Look at the Underlying Stem Cell Niche, Theories of Development, and Occurrence in Animals. *Vet. Pathol.* **2012**, *49* (3), 508–523. https://doi.org/10.1177/0300985811432344.

(37) Wright, D. E.; Wagers, A. J.; Gulati, A. P.; Johnson, F. L.; Weissman, I. L. Physiological Migration of Hematopoietic Stem and Progenitor Cells. *Science* **2001**, *294* (5548), 1933–1936. https://doi.org/10.1126/science.1064081.

(38) Hill, D. A.; Swanson, P. E. Myocardial Extramedullary Hematopoiesis: A Clinicopathologic Study. *Mod. Pathol. Off. J. U. S. Can. Acad. Pathol. Inc* **2000**, *13* (7), 779–787. https://doi.org/10.1038/modpathol.3880135.

(39) Goldman, B. I.; Wurzel, J. Hematopoiesis/Erythropoiesis in Myocardial Infarcts. *Mod. Pathol. Off. J. U. S. Can. Acad. Pathol. Inc* **2001**, *14* (6), 589–594. https://doi.org/10.1038/modpathol.3880356.

(40) Jacobi, S.; Dubielzig, R. R. Feline Early Life Ocular Disease. *Vet. Ophthalmol.* **2008**, *11* (3), 166–169. https://doi.org/10.1111/j.1463-5224.2008.00615.x.

(41) Firsching, R.; Müller, W.; Thun, F.; Boop, F. Clinical Correlates of Erythropoiesis in Chronic Subdural Hematoma. *Surg. Neurol.* **1990**, *33* (3), 173–177. https://doi.org/10.1016/0090-3019(90)90180-w.

(42) Forster, N.; Schöb, O. Incidental Discovery of Presacral Tumour in a Healthy Patient: Extramedullary Haematopoiesis Caused by a Sacral Fracture? *Br. J. Haematol.* **2006**, *133* (1), 1–1. https://doi.org/10.1111/j.1365-2141.2006.05977.x.

(43) Macki, M.; Bydon, M.; Papademetriou, K.; Gokaslan, Z.; Bydon, A. Presacral Extramedullary Hematopoiesis: An Alternative Hypothesis. *J. Clin. Neurosci.* **2013**, *20* (12), 1664–1668. https://doi.org/10.1016/j.jocn.2013.06.003.

(44) Singh, P.; Kapur, K.; Singla, S.; Naz, N. Endometrial Osseous Metaplasia and Mature Bone Formation with Extramedullary Hematopoiesis. *J. Hum. Reprod. Sci.* **2011**, *4* (1), 56–57. https://doi.org/10.4103/0974-1208.82363.

(45) Rosa, A. D. *Ectopic bone formation in thyroid gland: report of sixteen cases and comprehensive literature review*. European Review. https://www.europeanreview.org/article/31193 (accessed 2024-06-30).

(46) García, J.; Alvarez, M.; Moreno, D.; Acosta, B. Heterotopic Bone Formation with Extramedullary Haematopoiesis in a Thyroid Nodule. *BMJ Case Rep. CP* **2023**, *16* (11), e257200. https://doi.org/10.1136/bcr-2023-257200.

(47) Chatterjee, C.; Schertl, P.; Frommer, M.; Ludwig-Husemann, A.; Mohra, A.; Dilger, N.; Naolou, T.; Meermeyer, S.; Bergmann, T. C.; Alonso Calleja, A.; Lee-Thedieck, C. Rebuilding the Hematopoietic Stem Cell Niche: Recent Developments and Future Prospects. *Acta Biomater.* **2021**, *132*, 129–148. https://doi.org/10.1016/j.actbio.2021.03.061.

(48) Sugimura, R. Bioengineering Hematopoietic Stem Cell Niche toward Regenerative Medicine. *Adv. Drug Deliv. Rev.* **2016**, *99*, 212–220. https://doi.org/10.1016/j.addr.2015.10.010.

(49) Xiao, Y.; McGuinness, C. S.; Doherty-Boyd, W. S.; Salmeron-Sanchez, M.; Donnelly, H.; Dalby, M. J. Current Insights into the Bone Marrow Niche: From Biology in Vivo to Bioengineering Ex Vivo. *Biomaterials* **2022**, *286*, 121568. https://doi.org/10.1016/j.biomaterials.2022.121568.

(50) Kaplan, F. S.; Glaser, D. L.; Hebela, N.; Shore, E. M. Heterotopic Ossification. *JAAOS - J. Am. Acad. Orthop. Surg.* **2004**, *12* (2), 116.

(51) Kaplan, F. S.; Hahn, G. V.; Zasloff, M. A. Heterotopic Ossification: Two Rare Forms and What They Can Teach Us. *JAAOS - J. Am. Acad. Orthop. Surg.* **1994**, *2* (5), 288.

(52) Meyers, C.; Lisiecki, J.; Miller, S.; Levin, A.; Fayad, L.; Ding, C.; Sono, T.; McCarthy, E.; Levi, B.; James, A. W. Heterotopic Ossification: A Comprehensive Review. *JBMR Plus* **2019**, *3* (4), e10172. https://doi.org/10.1002/jbm4.10172.

(53) Kraft, C. T.; Agarwal, S.; Ranganathan, K.; Wong, V. W.; Loder, S.; Li, J.; Delano, M. J.; Levi, B. Trauma-Induced Heterotopic Bone Formation and the Role of the Immune System: A Review. *J. Trauma Acute Care Surg.* **2016**, *80* (1), 156–165. https://doi.org/10.1097/TA.0000000000000883.

(54) Torossian, F.; Guerton, B.; Anginot, A.; Alexander, K. A.; Desterke, C.; Soave, S.; Tseng, H.-W.; Arouche, N.; Boutin, L.; Kulina, I.; Salga, M.; Jose, B.; Pettit, A. R.; Clay, D.; Rochet, N.; Vlachos, E.; Genet, G.; Debaud, C.; Denormandie, P.; Genet, F.; Sims, N. A.; Banzet, S.; Levesque, J.-P.; Lataillade, J.-J.; Le Bousse-Kerdilès, M.-C. Macrophage-Derived Oncostatin M Contributes to Human and Mouse Neurogenic Heterotopic Ossifications. *JCI Insight* **2017**, *2* (21), e96034, 96034. https://doi.org/10.1172/jci.insight.96034.

(55) Gannon, F. H.; Glaser, D.; Caron, R.; Thompson, L. D.; Shore, E. M.; Kaplan, F. S. Mast Cell Involvement in Fibrodysplasia Ossificans Progressiva. *Hum. Pathol.* **2001**, *32* (8), 842–848. https://doi.org/10.1053/hupa.2001.26464.

(56) Convente, M. R.; Wang, H.; Pignolo, R. J.; Kaplan, F. S.; Shore, E. M. The Immunological Contribution to Heterotopic Ossification Disorders. *Curr. Osteoporos. Rep.* **2015**, *13* (2), 116–124. https://doi.org/10.1007/s11914-015-0258-z.

(57) Convente, M. R.; Chakkalakal, S. A.; Yang, E.; Caron, R. J.; Zhang, D.; Kambayashi, T.; Kaplan, F. S.; Shore, E. M. Depletion of Mast Cells and Macrophages Impairs Heterotopic

Ossification in an Acvr1R206H Mouse Model of Fibrodysplasia Ossificans Progressiva. *J. Bone Miner. Res. Off. J. Am. Soc. Bone Miner. Res.* **2018**, *33* (2), 269–282. https://doi.org/10.1002/jbmr.3304.

(58) Steiner, I.; Kasparová, P.; Kohout, A.; Dominik, J. Bone Formation in Cardiac Valves: A Histopathological Study of 128 Cases. *Virchows Arch. Int. J. Pathol.* **2007**, *450* (6), 653–657. https://doi.org/10.1007/s00428-007-0430-7.

(59) Ranganathan, K.; Agarwal, S.; Cholok, D.; Loder, S.; Li, J.; Sung Hsieh, H. H.; Wang, S. C.; Buchman, S. R.; Levi, B. The Role of the Adaptive Immune System in Burn-Induced Heterotopic Ossification and Mesenchymal Cell Osteogenic Differentiation. *J. Surg. Res.* **2016**, *206* (1), 53–61. https://doi.org/10.1016/j.jss.2016.04.040.

(60) Hoff, P.; Rakow, A.; Gaber, T.; Hahne, M.; Sentürk, U.; Strehl, C.; Fangradt, M.; Schmidt-Bleek, K.; Huscher, D.; Winkler, T.; Matziolis, D.; Matziolis, G.; Badakhshi, H.; Burmester, G.-R.; Duda, G. N.; Perka, C.; Buttgereit, F. Preoperative Irradiation for the Prevention of Heterotopic Ossification Induces Local Inflammation in Humans. *Bone* **2013**, *55* (1), 93–101. https://doi.org/10.1016/j.bone.2013.03.020.

(61) Peterson, J. R.; De La Rosa, S.; Sun, H.; Eboda, O.; Cilwa, K. E.; Donneys, A.; Morris, M.; Buchman, S. R.; Cederna, P. S.; Krebsbach, P. H.; Wang, S. C.; Levi, B. Burn Injury Enhances Bone Formation in Heterotopic Ossification Model. *Ann. Surg.* **2014**, *259* (5), 993–998. https://doi.org/10.1097/SLA.0b013e318291da85.

(62) Hino, K.; Horigome, K.; Nishio, M.; Komura, S.; Nagata, S.; Zhao, C.; Jin, Y.; Kawakami, K.; Yamada, Y.; Ohta, A.; Toguchida, J.; Ikeya, M. Activin-A Enhances mTOR Signaling to Promote

Aberrant Chondrogenesis in Fibrodysplasia Ossificans Progressiva. *J. Clin. Invest.* **2017**, *127* (9), 3339–3352. https://doi.org/10.1172/JCI93521.

(63) Damien, C. J.; Parsons, J. R. Bone Graft and Bone Graft Substitutes: A Review of Current Technology and Applications. *J. Appl. Biomater. Off. J. Soc. Biomater.* **1991**, *2* (3), 187–208. https://doi.org/10.1002/jab.770020307.

(64) Lane, J. M.; Sandhu, H. S. Current Approaches to Experimental Bone Grafting. *Orthop. Clin. North Am.* **1987**, *18* (2), 213–225.

(65) Urist, M. R. Bone: Formation by Autoinduction. *Science* **1965**, *150* (3698), 893–899. https://doi.org/10.1126/science.150.3698.893.

(66) Urist, M. R.; Strates, B. S. Bone Morphogenetic Protein. *J. Dent. Res.* **1971**, *50* (6), 1392–1406. https://doi.org/10.1177/00220345710500060601.

(67) de Groot, K. Some Considerations about Bone-Induction. *Calcif. Tissue Res.* **1973**, *13* (1), 335–337. https://doi.org/10.1007/BF02015425.

(68) Ripamonti, U. Osteoinduction in Porous Hydroxyapatite Implanted in Heterotopic Sites of Different Animal Models. *Biomaterials* **1996**, *17* (1), 31–35. https://doi.org/10.1016/0142-9612(96)80752-6.

(69) Yuan, H.; de Bruijn, J. D.; Zhang, X.; van Blitterswijk, C. A.; de Groot, K. Bone Induction by Porous Glass Ceramic Made from Bioglass® (45S5). *J. Biomed. Mater. Res.* **2001**, *58* (3), 270–276. https://doi.org/10.1002/1097-4636(2001)58:3<270::AID-JBM1016>3.0.CO;2-2.

(70) Selye, H. Diaphragms for Analysing the Development of Connective Tissue. *Nature* **1959**, *184* (4687), 701–703. https://doi.org/10.1038/184701a0.

(71) Selye, H.; Prioreschi, P.; Jean, P. Water Fixation as the Ultimate Cause of Tissue Growth. *Growth* **1959**, *23*, 169–187.

(72) Selye, H.; Lemire, Y.; Bajusz, E. Induction of Bone, Cartilage and Hemopoietic Tissue by Subcutaneously Implanted Tissue Diaphragms. *Wilhelm Roux Arch. Entwicklungsmechanik Org.* **1960**, *151* (5), 572–585. https://doi.org/10.1007/BF00577813.

(73) Salama, R.; Burwell, R. D.; Dickson, I. R. Recombined Grafts of Bone and Marrow. The Beneficial Effect upon Osteogenesis of Impregnating Xenograft (Heterograft) Bone with Autologous Red Marrow. *J. Bone Joint Surg. Br.* **1973**, *55* (2), 402–417.

(74) Nade, S. Clinical Implications of Cell Function in Osteogenesis. A Reappraisal of Bone-Graft Surgery. *Ann. R. Coll. Surg. Engl.* **1979**, *61* (3), 189–194.

(75) Ohgushi, H.; Goldberg, V. M.; Caplan, A. I. Heterotopic Osteogenesis in Porous Ceramics Induced by Marrow Cells. *J. Orthop. Res.* **1989**, *7* (4), 568–578. https://doi.org/10.1002/jor.1100070415.

(76) Werntz, J. R.; Lane, J. M.; Burstein, A. H.; Justin, R.; Klein, R.; Tomin, E. Qualitative and Quantitative Analysis of Orthotopic Bone Regeneration by Marrow. *J. Orthop. Res.* **1996**, *14* (1), 85–93. https://doi.org/10.1002/jor.1100140115.

(77) Block, J. E. The Role and Effectiveness of Bone Marrow in Osseous Regeneration. *Med. Hypotheses* **2005**, *65* (4), 740–747. https://doi.org/10.1016/j.mehy.2005.04.026.

(78) Leventis, M.; Fairbairn, P.; Mangham, C.; Galanos, A.; Vasiliadis, O.; Papavasileiou, D.; Horowitz, R. Bone Healing in Rabbit Calvaria Defects Using a Synthetic Bone Substitute: A Histological and Micro-CT Comparative Study. *Materials* **2018**, *11* (10), 2004. https://doi.org/10.3390/ma11102004.

(79) Selye, H. The Part of Inflammation in the Local Adaptation Syndrome. *Rev. Can. Biol.* **1953**, *12* (2), 155–175.

(80) Breuls, R. G. M.; Jiya, T. U.; Smit, T. H. Scaffold Stiffness Influences Cell Behavior: Opportunities for Skeletal Tissue Engineering. *Open Orthop. J.* **2008**, *2*, 103–109. https://doi.org/10.2174/1874325000802010103.

(81) Harley, B. A. C.; Kim, H.-D.; Zaman, M. H.; Yannas, I. V.; Lauffenburger, D. A.; Gibson, L. J. Microarchitecture of Three-Dimensional Scaffolds Influences Cell Migration Behavior via Junction Interactions. *Biophys. J.* **2008**, *95* (8), 4013–4024. https://doi.org/10.1529/biophysj.107.122598.

(82) Yi, B.; Xu, Q.; Liu, W. An Overview of Substrate Stiffness Guided Cellular Response and Its Applications in Tissue Regeneration. *Bioact. Mater.* **2022**, *15*, 82–102. https://doi.org/10.1016/j.bioactmat.2021.12.005.

(83) Alberius, P.; Gordh, M.; Lindberg, L.; Johnell, O. Onlay Bone Graft Behaviour After Marrow Exposure of the Recipient Rat Skull Bone. *Scand. J. Plast. Reconstr. Surg. Hand Surg.* **1996**, *30* (4), 257–266. https://doi.org/10.3109/02844319609056403.

(84) Liu, J.; Kerns, D. G. Mechanisms of Guided Bone Regeneration: A Review. *Open Dent. J.* **2014**, *8*, 56–65. https://doi.org/10.2174/1874210601408010056.

(85) Lundgren, A. K.; Lundgren, D.; Hämmerle, C. H.; Nyman, S.; Sennerby, L. Influence of Decortication of the Donor Bone on Guided Bone Augmentation. An Experimental Study in the Rabbit Skull Bone. *Clin. Oral Implants Res.* **2000**, *11* (2), 99–106.

(86) Chang, H.; Knothe Tate, M. L. Concise Review: The Periosteum: Tapping into a Reservoir of Clinically Useful Progenitor Cells. *Stem Cells Transl. Med.* **2012**, *1* (6), 480–491. https://doi.org/10.5966/sctm.2011-0056.

(87) Breitbart, A. S.; Grande, D. A.; Kessler, R.; Ryaby, J. T.; Fitzsimmons, R. J.; Grant, R. T. Tissue Engineered Bone Repair of Calvarial Defects Using Cultured Periosteal Cells. *Plast. Reconstr. Surg.* **1998**, *101* (3), 567.

(88) Perka, C.; Schultz, O.; Spitzer, R. S.; Lindenhayn, K.; Burmester, G. R.; Sittinger, M. Segmental Bone Repair by Tissue-Engineered Periosteal Cell Transplants with Bioresorbable Fleece and Fibrin Scaffolds in Rabbits. *Biomaterials* **2000**, *21* (11), 1145–1153. https://doi.org/10.1016/s0142-9612(99)00280-x.

(89) Knothe Tate, M. L.; Ritzman, T. F.; Schneider, E.; Knothe, U. R. Testing of a New One-Stage Bone-Transport Surgical Procedure Exploiting the Periosteum for the Repair of Long-Bone Defects. *J. Bone Joint Surg. Am.* **2007**, *89* (2), 307–316. https://doi.org/10.2106/JBJS.E.00512.

(90) Wang, J.; Wang, C. D.; Zhang, N.; Tong, W. X.; Zhang, Y. F.; Shan, S. Z.; Zhang, X. L.; Li, Q. F. Mechanical Stimulation Orchestrates the Osteogenic Differentiation of Human Bone Marrow Stromal Cells by Regulating HDAC1. *Cell Death Dis.* **2016**, *7* (5), e2221–e2221. https://doi.org/10.1038/cddis.2016.112.

(91) Johnston, D. T.; Lohmeier, S. J.; Langdell, H. C.; Pyfer, B. J.; Komisarow, J.; Powers, D. B.; Erdmann, D. Current Concepts in Cranial Reconstruction: Review of Alloplastic Materials. *Plast. Reconstr. Surg. Glob. Open* **2022**, *10* (8), e4466. https://doi.org/10.1097/GOX.0000000000004466.

(92) Cabbad, N. C.; Stalder, M. W.; Arroyave, A.; Wolfe, E. M.; Wolfe, S. A. Autogenous Bone Cranioplasty: Review of a 42-Year Experience by a Single Surgeon. *Plast. Reconstr. Surg.* **2019**, *143* (6), 1713–1723. https://doi.org/10.1097/PRS.0000000000005677.

(93) Goldstein, J. A.; Paliga, J. T.; Bartlett, S. P. Cranioplasty: Indications and Advances. *Curr. Opin. Otolaryngol. Head Neck Surg.* **2013**, *21* (4), 400–409. https://doi.org/10.1097/MOO.0b013e328363003e.

(94) Greene, A. K.; Mulliken, J. B.; Proctor, M. R.; Rogers, G. F. Pediatric Cranioplasty Using Particulate Calvarial Bone Graft. *Plast. Reconstr. Surg.* **2008**, *122* (2), 563–571. https://doi.org/10.1097/PRS.0b013e31817d61c1.

(95) Stefini, R.; Esposito, G.; Zanotti, B.; Iaccarino, C.; Fontanella, M. M.; Servadei, F. Use of "Custom Made" Porous Hydroxyapatite Implants for Cranioplasty: Postoperative Analysis of Complications in 1549 Patients. *Surg. Neurol. Int.* **2013**, *4*, 12. https://doi.org/10.4103/2152-7806.106290.

(96) Zanotti, B.; Zingaretti, N.; Verlicchi, A.; Robiony, M.; Alfieri, A.; Parodi, P. C. Cranioplasty: Review of Materials. *J. Craniofac. Surg.* **2016**, *27* (8), 2061. https://doi.org/10.1097/SCS.0000000000003025.